AALTO UNIVERSITY
School of Engineering
Department of Applied Mechanics

Juhani Antero Hämäläinen

SUBSTRUCTURE TOPOLOGY OPTIMIZATION OF AN ELECTRIC MACHINE

Thesis in partial fulfilment of the requirements for the degree of
Master of Science in Mechanical Engineering

Espoo, Finland on June 3rd, 2013

Supervisor of the Thesis	Professor	Jukka Tuhkuri
Instructor of the Thesis	M.Sc. Tech.	Petteri Kokkonen

AALTO-YLIOPISTO PL 12100, 00076 Aalto http://www.aalto.fi	DIPLOMITYÖN TIIVISTELMÄ

Tekijä: Juhani Hämäläinen

Työn nimi: Sähkökoneen osarakenteen topologian optimointi

Korkeakoulu: Insinööritieteiden korkeakoulu

Laitos: Sovelletun mekaniikan laitos

Professuuri: Lujuusoppi	Koodi: Kul-49

Työn valvoja: Professori Jukka Tuhkuri

Työn ohjaaja: Diplomi-insinööri Petteri Kokkonen

Työssä hyödynnetään rakenneoptimoinnin menetelmää, topologian optimointia, sähkökoneen osarakenteen uudelleensuunnitteluissa. Tavoitteena on lisätä rakenteen jäykkyyttä ennalta määrätyn tilavuusrajoitteen puitteissa. Topologian optimointi suoritetaan kaupallisella OptiStruct ohjelmistolla, joka hyödyntää n.k. SIMP-menetelmää.

Alkuperäinen sähkökoneen osarakenne on hitsattu teräslevyistä, mutta optimointitulos koostuu perusaineesta ja siksi optimoidussa rakenteessa ei ole hitsejä. Tämän vaikutusta rakenteen väsymiskestävyyden nousuun tutkitaan lyhyesti. Topologian optimoinnin teoria esitellään ja käytetty ohjelmisto testataan kolmella alan kirjallisuudesta saadulla optimirakenteella. Topologian optimoinnin käyttöönottoa tuotteen suunnitteluprosessissa käsitellään ja annetaan esimerkkejä prosessista.

Ohjelman validointitulosten mukaan OptiStruct tuottaa optimoituja ja läheisoptimaalisia rakenteita, ja ohjelmaa suositellaan käytettäväksi lopputyössä. Topologian optimointi lineaaristen elementtien malleilla paljasti tunnettuja SIMP-menetelmän ominaisuuksia, kuten n.k. shakkilautarakenteen muodostumisen ratkaisussa.

Osarakenteen optimoinnissa käytetään erilaisia kuormitustapauksia. Reunaehdot annetaan ennalta määrättyinä staattisina siirtyminä, jotka saadaan erillisestä FE-analyysistä. Siirtymät edustavat alirakenteen käyttöympäristössään kokemia kuormia. Aluksi optimointi ratkaistaan jokaisessa kuormitustapauksessa erikseen, hyödyntäen lineaaristen elementtien mallia, ilman optimoinnin lisärajoitteita. Tulosrakenteiden piirteitä ja eroja tutkitaan ja tietoja hyödynnetään myöhemmissä analyyseissä. Tämän jälkeen suoritetaan yhdistetty, monen kuormitustapauksen optimointi, parabolisten elementtien mallilla. Tässä optimoinnissa hyödynnetään lisärajoitteina symmetriaa ja rakenneosien minimipaksuusehtoa.

Uusi osarakenne on modifioitu topologian optimointitulos. Rakenteen staattinen jäykkyys nousi ja rakenteen paino lisääntyi n. 8 % verrattuna alkuperäiseen rakenteeseen. Optimoidun osarakenteen väsymiskestävyys parani, koska hitsit jäivät pois kuormitetuilta alueilta. Topologian optimointia ehdotetaan hyödynnettäväksi konseptivaiheessa, mutta menetelmä soveltuu myös tarkasti määriteltyjen rakenteiden optimointiin.

Päivämäärä: 3.6.2013	Kieli: englanti	Sivumäärä: 101

Avainsanat: topology optimization, SIMP, penalization, substructure, forced displacements

AALTO UNIVERSITY PO Box 12100, FI-00076 AALTO http://www.aalto.fi	ABSTRACT OF THE MASTER'S THESIS

Author: Juhani Hämäläinen

Title: Substructure Topology Optimization of an Electric Machine

School: School of Engineering

Department: Department of Applied Mechanics

Professorship: Mechanics of Materials	Code: Kul-49

Supervisor: Professor Jukka Tuhkuri

Instructor: Petteri Kokkonen, M.Sc. Tech.

In the thesis a structural optimization method called topology optimization is applied to redesign a substructure of an electric machine. The objective is to increase the stiffness of this structure with a prescribed volume constraint. Topology optimization is performed with commercial software OptiStruct. The software utilizes the so called SIMP method.

The initial substructure of the electric machine is welded from steel plates. The optimization result consists of base material, thus no welds are found in the optimized structure. The influence of this to the fatigue life of the structure is briefly studied. Topology optimization theory is outlined and the software is validated with three optimal benchmark cases from the literature. The implementation of topology optimization in a product design process is discussed and examples of the procedure are provided.

According to the software validation, OptiStruct delivers optimized and near optimal topologies. The software is recommended to be used in the thesis. Topology optimization with linear element models revealed known features of the SIMP method, like the formation of the so called checkerboarding in the optimization solution.

In the optimization of the substructure various load cases, with prescribed static displacements, are used. These are extracted from a separate FEA and they represent loadings of the substructure in its operating environment. The topology optimization is initially performed in individual load cases with linear element models. No additional constraints of the software are used in this optimization. Defining features and differences of the resulting structures are studied. Finally a combined optimization of multiple load cases is performed with parabolic element models with symmetry and minimum member size constraints.

The new substructure consists of topology optimization results, with modified features by the author. The stiffness of the structure was multiplied in specific load cases, with around 8% added weight, when compared to the original substructure. The fatigue strength of the structure was increased, as no welds are found in highly stressed regions of the structure. The implementation of the topology optimization method was recommended in the concept phase of product development, but it can be also used in cases where the initial structure is strictly defined.

Date: 3.6.2013	Language: English	Number of pages: 101

Keywords: topology optimization, SIMP, penalization, substructure, forced displacements

Preface

I wish to thank my colleagues at VTT Structural Dynamics team, specialists at ABB Pitäjänmäki and at Altair in Sweden for advising me throughout the thesis. I also want to thank Professor Jukka Tuhkuri for his insightful supervision.

I thank family and relatives for their encouragement; especially my wife Hilkka and my father-in-law Esa were very supportive.

The intensive writing was balanced with hands-on activities on my free-time. For example, I was able to increase the output of the B16A1, 1.6 litre naturally aspirated combustion engine, by 24% to 186hp during the thesis.

Gratefully
Juhani Hämäläinen

Contents

Terminology

Compliance	The inverse of stiffness. C=1/k. Where k: stiffness.
Checkerboarding	Checkerboard-like pattern of elements in the topology optimization solution. Unwanted and virtually over stiff.
Design space	Elements in which the optimum is sought.
Design variable	Variable that is changed in the optimization.
Excitation order	The frequency of the vibration, excitation order 1 being the crank shaft rotating frequency of the diesel engine.
Feasible point/set	The points / a Set that satisfy all constraints of an optimization problem
FE	Finite Element
FEM	Finite Element Method
FEA	Finite Element Analysis
Ground structure	The initial set of nodal points in a FE-mesh, or connections of a truss structure.
Homogenization approach	Using composite material for describing varying material properties.
MMA	Method of Moving Asymptotes. Approximation method used to solve optimization problems.
Non-design Space	Elements that are not affected by the design variable. Typically at boundary condition areas.
Penalty factor	
Relaxation	Replacing integer valued and discrete constraints with a continuous variable.
Relaxed constraint	Discrete constraint functions reformulated to continuous functions.
Relative density	Is used as design variable in SIMP, denoted with ρ.
Sensitivity analysis	Finding gradients of obj./const. functions with respect to the design variable.
State variable	Variable that that is monitored during the optimization process.
SIMP	Solid Isotropic Material with Penalization
Topology optimization	Most general form of structural optimization. Material connectivity and distributions is determined.
Objective function	The function to be minimized/maximized.

List of Symbols

´	Above a symbol, first derivative
´´	Above a symbol, second derivative
T	Upper right corner of a symbol, transpose
I	Upper right corner of a symbol, inverse
Ω	Design Space
σ	Stress
ε	Strain
λ	Lagrange Multiplier
ρ	Density / relative density in SIMP
ν	Poisson coefficient
$\in$	Belongs to
C_i	Compliance of a load case
C_w	The weighted sum of the compliance of each individual load case
$\boldsymbol{E}_{ad}$	Admissible stiffness matrix
E	Young's modulus
$\mathbf{E}_e$	Elemental stiffness matrix
FAT xx	IIW Fatigue class
$\mathbf{F}(\mathbf{x})$	Vector of external global forces
$\mathbf{f}$	Vector of External forces
$\mathbf{f}_i$	Force vector of a load case
$\widehat{g_0}(\boldsymbol{x})$	Nested formulation of the optimization problem
$\hat{g}_i(\boldsymbol{x})$	Subproblem of the approximate objective function
$g_i^{M,k}$MMA	MMA approximation of the objective function
$\mathbf{K}$	Stiffness matrix of an FE-entity
$\mathbf{K}_e$	Elemental stiffness matrix
L_j^k	Moving asymptote
U_j^k	Moving asymptote
$\mathbf{u}$	Displacement vector
$\mathbf{u}_i$	Displacement vector of a load case
V	Specified volume/vol.fraction constraint value
w_i	Weighting factor of a load case
x^k	Design variable at iteration k
x_0	Design variable at iteration 0
$\bar{x}$	New design
$\rho(\boldsymbol{x})$	Relative density
α_i^k	Move limit
β_i^k	Move limit
$\mathcal{L}(\mathbf{x}, \boldsymbol{\lambda})$	Lagrange function
$\varphi(\boldsymbol{\lambda})$	Dual Objective function

1 Introduction

ABB's main areas are power and automation technologies and the company is a global market leader in the branches of industrial motors and drives, wind turbine generators and power grids world-wide. ABB's headquarters is based in Switzerland, and the company employs around 145,000 people and operates in circa 100 countries. The company was created in 1988, but the history of the Helsinki factory dates back to 1883 and 1889 to the Elektriska Aktiebolaget in Sweden and Ab Strömberg Oy in Finland. The abbreviation ABB comes for the words Asea Brown Boveri. [ABB Finland]

This thesis is about the topology optimization of an attachment region of an industrial generator from ABB that is exposed to cyclic loading. The generator is a part of a generator set also called genset. A genset consists of an engine connected to a generator via a flexible coupling. The engine and generator are mounted on a common base frame, which is dynamically isolated from the concrete foundation by steel springs. Generator sets produce electricity for various purposes, e.g. on off-shore facilities, for ship propulsion or as power plants. An example of a generator set is shown in the Figure 1. The generator is attached from its sides by a bolt joint and this area is considered in the thesis. This attachment area is illustrated with the Figure 2, which shows a steel frame similar to the considered generator frame, with the stator winding shown in red. The original structure consists of welded steel plates. Future plans for increasing the electric output require more strength and rigidity of the generator frame. In the thesis topology optimization is used to achieve this. Over the last decade topology optimization has evolved to an important tool for finding optimized connectivity and material distribution of load carrying structures.

The objective of this thesis is to increase the stiffness of the attachment region using topology optimization approach. A Finite Element based topology optimization software called OptiStruct is used for optimization. The loadings of the structure are taken from an earlier computational simulation of the electric device in its operating environment. The theoretical background of topology optimization, and its computational applications, is reviewed. The used software is validated by benchmarking it with optimal topologies found in the literature.

In the optimization a stiffness maximization problem with a prescribed volume constraint is considered. The structure is optimized inside a fixed design space according to loadings, boundary conditions, objectives and constraints. To facilitate the comparison of stiffnesses between the original and optimized structure, the optimization is constrained to have approximately the same amount of material available, as in the original attachment area. The optimized attachment will consist of base material, thus no welds are needed in highly stressed region. Significant fatigue strength increase is expected by removing welds in critically loaded regions.

The outcome of the optimization will be a new material distribution in the optimization area, i.e. a new concept for the generator attachment area. The post-processing of the optimized design to a ready functional part is not in the scope of this thesis. However, the required workflow to achieve this is presented and illustrated.

Figure 1. Wärtsilä 18V50 gensets with ABB generators in a power plant configuration [Wärtsilä Power Plants].

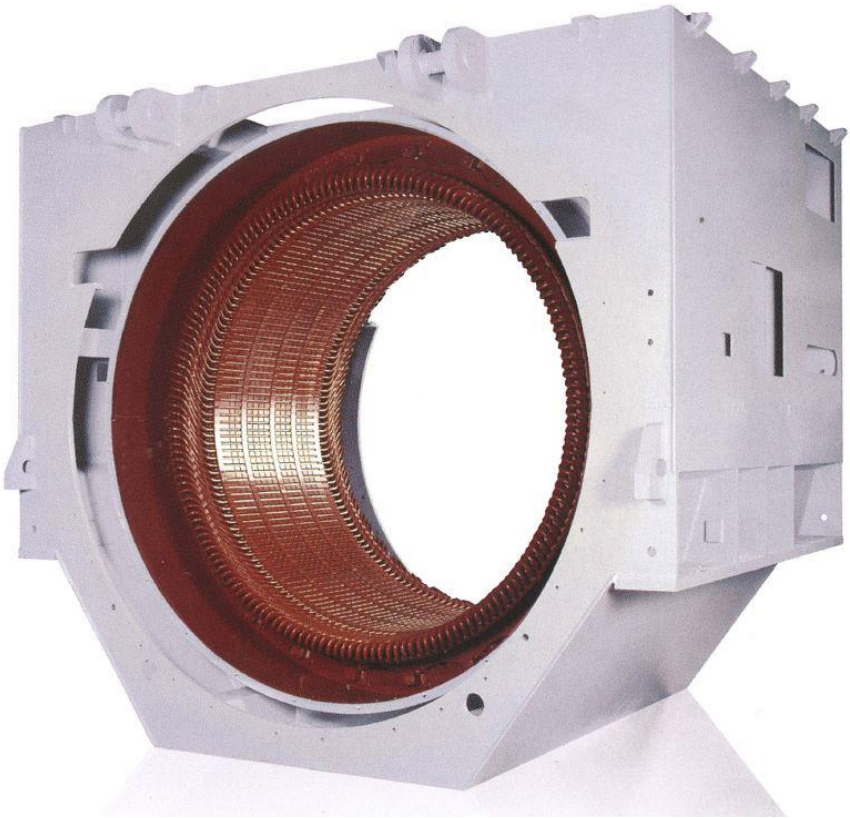

Figure 2. ABB electric machine frame. [ABB Borchure].

2 Optimization

This chapter introduces some basic definitions terminology in optimization. A common separation in optimization is made between linear and nonlinear optimization. In linear optimization the objective function and all constraints are linear, i.e. they can be expressed e.g. in the form A**x**=**b** or A**x**<**b**. This, however, does not restrict the terms in the vector or matrix **x** to be linear, but quadratic or of other order. A benefit of linear optimization problems is that they are always convex. Convexity is explained later on in the text, but in short convex problems are guaranteed to have a global optimum, which otherwise is not so obvious. Nonlinear optimization problems deal with nonlinear constraints and objectives respectively. Nonlinearities, i.e. functions of second order, are common in science and engineering, as many relations can only be described with nonlinear functions, e.g. energy dissipation, force-displacement relations etc. [Griva et al. (2009) p.3-7, 9-15].

In the thesis continuous nonlinear optimization is regarded because *topology optimization* falls into this branch of mathematical optimization and its basic concepts are outlined later in the text. The field is approached with simple equations and a truss example. An example is provided to demonstrate how a nonlinear topology optimization problem is solved utilizing convexity and gradient based algorithms, like the Method of Moving Asymptotes (MMA). Optimization problems involving multiple and complex functions are facilitated for using Lagrangian Duality principle.

From mathematical point of view optimization is a process of finding the maximum or minimum of an objective function and its optimal points are called optima. The minimization or maximization is performed with respect to a design variable and subject to some limiting functions called constraint functions. Optima are either local or global, which is illustrated in the Figure 3, where the function $y(x)$ is evaluated in an interval $[x_1, x_5]$, which is called the *design domain*. For 3D structures like in the scope of this thesis the design domain is called *design space*. The points x_1 and x_5 are the global minimum and maximum, x_4 is a local minimum, x_2 and x_3 are stationary points and not optimal. [Christensen (2008) p.3, 37]

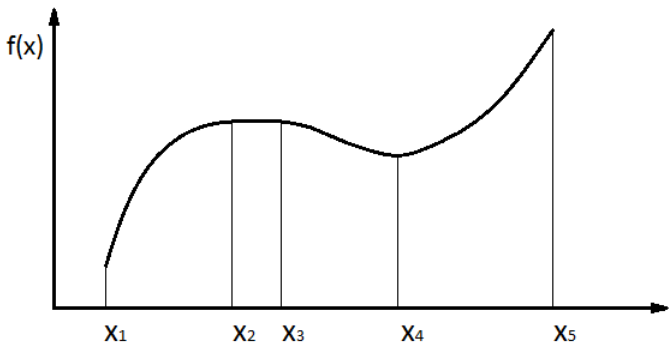

Figure 3. Global and local optima.

Typically global optimum is the most wanted, but hard to find or it might not exists. Especially in nonlinear optimization the non-existence of global optima is a common problem. Thus many optimization methods only seek for local optima and global optima are sought via solutions of sub-problems or with other search methods. Global optima are guaranteed for the convex problems, as for these problems local optima are also global optima. [Griva et al. (2009) p.9-15] In the optimizations of this thesis the following *compliance* and *volume fraction* are central conceptions. Compliance, C, is the inverse of stiffness, k

$$C = \frac{1}{k} \qquad (2.1)$$

and this is often used as objective. Volume faction is a perceptual value of material and it is used as constraint in most of the cases.

2.1 Optimization Problem Formulation

The function to be minimized or maximized is called the *objective function*, and the variable that is changed in the optimization is called the d*esign variable*. The limitations of the optimization are called *constraints*. The response of the optimization system is represented by a *state variable*. In a mechanical structure the response means displacement, stress, strain of force for example. An example of nonlinear optimization problem with one linear constraint function is shown below. The point x_*=(1,1) is the global optimum for this optimization problem. [Griva et. Al. (2009) p. 3-4]

$$\text{min:} \quad f(x) = (x_1 - 2)^2 + (x_2 - 2)^2 \qquad (2.2)$$

Subject to (s.t.):

$$c(x) = x_1 + x_1 = 2 \qquad (2.3)$$

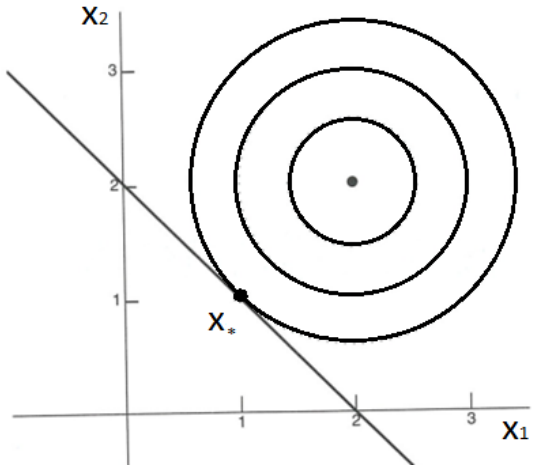

Figure 4. Global optimum of a nonlinear problem with a linear constraint. [Grivat et. al. (2009) p.4.]

Where *f(x)* is the objective function and *c(x)* is the constraint function. Another representation of a nonlinear optimization problem with a constraint on a vector set of design variables:

$$\min g(\boldsymbol{x}), \quad x = [x_1, x_2, x_3 \dots x_n]^T \qquad (2.4)$$

$$c_j(\boldsymbol{x}) \leq 0, \quad j = 1,2, \dots, m \qquad (2.5)$$

$$l_j(\boldsymbol{x}) = 0, \qquad j = 1,2, \dots, p \qquad (2.6)$$

$$x_{n-1} \leq x_n \leq x_{n+1}, \qquad n = 1,2 \dots, i, \qquad (2.7)$$

where: $g(\boldsymbol{x})$ is the objective function of the design variables in x. $c_j(\boldsymbol{x})$ and $l_j(\boldsymbol{x})$ are constraint functions, and the design variables are bound in the last inequality statement [Singresu (2009) p.6]. The points that satisfy all constraints of an optimization problem belong to a feasible set and individual points are called feasible [Grivat et. al. (2009) p.43-44].

2.2 Convexity

Convexity is illustrated in the Figure 5. In the Figure first function is strictly convex, middle one is convex and left one is non-convex. A set defined by a linear system of constraints is a convex set; this is illustrated in the Figure 6. For convex problems local optima are also global optima. An optimization problem is convex if the objective function is convex and the constraints are concave. [Griva et al. (2009) p.7.]

It is sometimes possible to formulate nonconvex constraint or objective functions as convex combinations using approximation methods. Convexity can also be examined by differentiation. A twice differentiable function is convex if

$$f''(\boldsymbol{x}) \geq 0 \text{ for all x } \in S, \qquad (2.8)$$

where $\boldsymbol{x}$ is the design variable. For problems with multiple dimensions the Hessian matrix of second derivatives has to be positive semi definite or all eigenvalues of the Hessian matrix are greater than or equal zero [Griva et al. (2009) p.48-52].

Figure 5. Strictly convex, convex and non-convex functions. [Christensen (2008) p. 38]

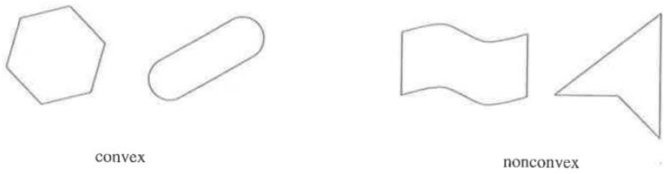

Figure 6. Convex and non-convex sets. [Griva et al. (2009) p. 48]

2.3 Solving Large Optimization Problems

Practical optimization problems of mechanics typically involve many design variables and constraints. In such a case it might be impossible to determine which constraints are active and where in the design domain. Typically in large problems objective and constraint functions cannot be written as explicit functions of the design variables. The remedy is to solve these problems in a sequence of explicit sub-problems that are approximations of the original optimization problem and typically simpler to solve. [Christensen (2008) p.57]

When the optimization deals with simplifications of the objective function, the problem formulation is based on limited information of the original function. In such a case the information is only valid in the vicinity of the approximation and the global optimum is tedious to find. Thus conditions for optimality are typically introduced to facilitate finding the optimum. Especially in nonlinear optimization the optimality constraints are important, as they form the basis of the solution for these problems. On the other hand the type of the optimal points can be validated with derivatives of the objective function. For example stationary points are expressed by first derivatives and second derivatives express maxima or minima. For nonlinear problems the derivation involves multiple techniques such as Karush-Kuhn-Tucker conditions (KKT), with Lagrange multipliers [Griva et. al. (2009) p.44-46, 503-504].

Topology optimization software utilize typically one of the following methods to solve the optimization problem; optimality criteria method involving the so called Karus-Kuhn-Tucker (KKT) conditions or Mathematical programming utilizing sensitivity analysis methods. The latter is also called gradient based optimization in the topology optimization literature. [Bendsøe (2003) p.9-22] Software utilized in the thesis applies a gradient based optimization and thus an approach of this method is reviewed. [Appendix A]

2.4 Gradient Based Optimization

OptiStruct uses a gradient based optimization method to solve the topology optimization problem. The method is called a “local approximation method” in OptiStruct, but it is probably just a reformulation of the so called “*Method of Moving Asymptotes*” (MMA), as move limits of the design variable are used to control the convergence, as in MMA. In general the method is about solving a large scale optimization problem in a sequence of smaller sub-problems that are approximations of the original optimization problem.

Due to the formulation, the MMA leads to a convex optimization problem, even though the original optimization problem is nonconvex. The update of the structure between iterations is generated by solving the MMA approximate problem, which is based on information on the gradients of the objective and constraint functions with respect to the desing variable. The extraction of this information is also called *sensitivity analysis*. The so called “Lagrangian Duality” method is utilized to solve the MMA approximation. The method is highly efficient for design problems involving a very large number of design variables but much less constraints. This is common to topology optimization. [HW Help]

Based on [Christensen (2008) p.57], let us consider a structural optimization of an FE-discretized elastic body, with a finite number of degrees of freedom (dof). Let us minimize deflection $g(\mathbf{u},\boldsymbol{x})$ with constraints on the displacement. $\boldsymbol{x}$ is the design variable, e.g. total length of the structure The solution is bound to a given area of the structure given by bounds on the design variable $\boldsymbol{x}$:

$$\min g(\boldsymbol{x},\boldsymbol{u}) \tag{2.9}$$

$$s.t.\ \boldsymbol{K}(\boldsymbol{x})\boldsymbol{u} = \boldsymbol{F}(\boldsymbol{x}) \tag{2.10}$$

$$g_i(\boldsymbol{x},\boldsymbol{u}) \leq 0, \quad i = 1,\dots,m \tag{2.11}$$

$$\boldsymbol{x} \in X = \{\boldsymbol{x} \in \mathbb{R}^n \ x_j^{min} \leq x_j \leq x_j^{max}, \qquad j = 1,\dots,n\} \tag{2.12}$$

Where $g(\boldsymbol{x},\boldsymbol{u})$ is the objective function, and $g_i(\boldsymbol{x},\boldsymbol{u})$ is the i:th constraint function. $\mathbf{K}(\boldsymbol{x})$ is the stiffness matrix of the structure, $\mathbf{u}$ is the global displacement vector, $\mathbf{F}(\mathbf{x})$ is the vector of external global forces. An Equilibrium equation $\boldsymbol{u}(\boldsymbol{x})=\boldsymbol{K}^{-1}(\boldsymbol{x})\boldsymbol{F}(\boldsymbol{x})$ is used to implicitly define the displacement vector of a given design. It is possible to solve $\boldsymbol{u}(\bar{x})$ numerically using equilibrium equations in FEA for example for any given design $\bar{x}$. Now the optimization problem is rewritten:

$$\min \widehat{g_0}(\boldsymbol{x}) \tag{2.13}$$

$$s.t.\ \widehat{g_i}(\boldsymbol{x}) \leq 0, \quad i = 1,\dots,n, \tag{2.14}$$

where

$$\widehat{g_0}(\boldsymbol{x}) = g_0(\boldsymbol{x},u(\boldsymbol{x})), \tag{2.15}$$

and

$$\widehat{g_i} = g_i\big(\boldsymbol{x},u(\boldsymbol{x})\big), \qquad i = 0,\dots n. \tag{2.16}$$

This is a nested formulation of the optimization problem formulation in (2.9), i.e. all functions are expressed with respect to the design variable. Using MMA it is solved in a sequence involving multiple sub-problems. The procedure for solving the above structural optimization is described as follows [Christensen (2008) p.58]:

1. Initial design $\boldsymbol{x}_0$. Iteration k=0
2. FEA to calculate the displacement vector $\mathbf{u}(\boldsymbol{x}^k)$.
3. For the design $\boldsymbol{x}^k$ calculate the objective function $\widehat{g_0}(\boldsymbol{x}^k)$ and the constraint functions and their gradients, $\nabla g_i(\boldsymbol{x}^k)$ (sensitivity analysis).
4. Formulate an explicit, convex approximation of the nested formulation at x^k.
5. Solve the approximation by nonlinear algorithm to give a new design $\boldsymbol{x}^{k+1}$.
6. Set iteration k+1 and return to step 2 and start a new iteration, unless convergence criterion is satisfied.

FEA is here used as an automated design optimization framework.

Typically used methods to obtain this explicit approximation of the original optimization problem are Sequential Linear Programming (SLP), Sequential Quadratic Programming (SQP), Convex Linearization (COLIN) and Method of Moving Asymptotes (MMA) used in OptiStruct. The introduction of the MMA later on provides an example how the topology optimization problem is solved.

2.4.1 Method of Moving Asymptotes

The Method of Moving Asymptotes (MMA) is an iterative solution first order method for non-linear programming in mathematical optimization. "*In each step of the iterative process, a strictly convex approximating subproblem is generated and solved. The generation of these sub-problems is controlled by so called 'moving asymptotes', which may both stabilize and speed up the convergence of the general process."* [Svanbeg (1987)].

To form the approximating optimization subproblem MMA uses intervening variables, which include the moving asymptotes. The asymptotes are changed during the iterations. An MMA approximation of a function g_i, i=0,…,n at the design x^k at iteration k is [Svanberg (1987)]:

$$g_i^{MMA,k}(\mathbf{x}) = r_i^k + \sum_{j=1}^{n}\left(\frac{p_{i,j}^k}{U_j^k - x_j} + \frac{q_{i,j}^k}{x_j - L_j^k}\right) \qquad (2.17)$$

Where L_j and U_j are the moving asymptotes, i is the index of a function, j is the index of the intervening variables, $p_{i,j}^k$, $q_{i,j}^k$ involve derivatives of the original function $g(\boldsymbol{x})$ with respect to the design variable the term r is:

$$r_i^k = g_i(\boldsymbol{x}^k) - \sum_{j=1}^{n}\left(\frac{p_{i,j}^k}{U_j^k - x_j} + \frac{q_{i,j}^k}{x_j - L_j^k}\right). \qquad (2.18)$$

The moving asymptotes satisfy

$$L_j^k < x_j^k < U_j^k \qquad (2.19)$$

These are presented in more detail in [Svanberg (1987)]. Differentiating $g_i^{M,k}(\mathbf{x})$ twice gives:

$$\frac{\partial g_i^{MMA,k}(\mathbf{x})}{\partial x_j} = \frac{p_{ij}^k}{(U_j^k - x_j)^2} - \frac{q_{ij}^k}{(x_j - L_j^k)^2} \qquad (2.20)$$

$$\frac{\partial^2 g_i^{MMA,k}(\mathbf{x})}{\partial {x_j}^2} = \frac{2p_{ij}^k}{(U_j^k - x_j)^3} - \frac{2q_{ij}^k}{(x_j - L_j^k)^3} \qquad (2.21)$$

$$\frac{\partial^2 g_i^{MMA,k}(\mathbf{x})}{\partial x_j \partial x_p} = 0, \text{ if } j \neq p. \qquad (2.22)$$

The MMA approximation of the original optimization problem (14) at iteration k is:

$$MMA\begin{cases}\min g_0^{MMA,k}(\mathbf{x}) \\ s.t.\, g_i^{MMA,k}(\mathbf{x}) \le 0, \mathrm{i} = 1, \dots, \mathrm{l} \\ \alpha_i^k \le x_j \le \beta_i^k, j = 1, \dots, n.\end{cases} \qquad (2.23)$$

Where α and β are move limits. This problem is solved using Lagrangian duality. The conservatism of the approximation may be controlled by moving the asymptotes during the iteration [Christensen (2008) p.68].

2.4.2 Lagrangian Duality

The duality principle in mathematical optimization states that optimization problems can be considered from viewpoints; the primal problem or the dual problem and they are related. The following relationships facilitate many optimization problems. The dual problem might have a simpler solution than the primal problem. Even an estimation of the solution of the dual problem may facilitate finding a good approximate solution for the primal problem. [Griva et al. (2009) s 522 – 523]. The principle uses the Lagrangian function, which is a function that combines the objective and constraint functions. It is a central concept in structural optimization [Griva et al. (2009) p.484]. The prima dual principle:

(i) If the primal is a minimization problem the dual is a maximization problem and vice versa.
(ii) The dual of the dual problem is the primal problem.
(iii) The objective value for any feasible solution to the dual maximization problem is a lower bound on the objective value for any feasible solution to the primal minimization problem.
(iv) If either optimization problem has an optimal solution then so does the other. These optimal objective values of the two problems are equal.

In the following, the dual problem is used to find the optimum of the primal problem in equation (2.23). Due to the features of the MMA algorithm the objective function of the optimization problem in equation (2.23) is continuously differentiable, strictly convex and the constraint functions are convex and separable. The separability of the constraint functions gives advantages when Lagrangian duality is used.

The Lagrangian function $\mathcal{L}$ of the optimization problem (2.23) at iteration k is

$$\mathcal{L}(x,\lambda) = g_0^{MMA,k}(\boldsymbol{x}) + \sum_{i=1}^{l} \lambda_i g_i^{MMA,k}(\boldsymbol{x}) \quad (2.24)$$

$$= \sum_{i=1}^{l} g_{0j}^{M,k}(\boldsymbol{x_j}) + \sum_{i=1}^{l} \lambda_i \left(\sum_{j=1}^{n} g_{ij}^{M,k}(\boldsymbol{x_j}) \right) \quad (2.25)$$

$$= \sum_{j=1}^{n} \left(g_{0j}^{M,k}(\boldsymbol{x_j}) + \sum_{i=1}^{l} \lambda_i g_{ij}^{M,k}(\boldsymbol{x_j}) \right) \quad (2.26)$$

Where $\lambda_i \leq 0$, i=1,…,l. The dual objective function is

$$\varphi(\lambda) = min_{x\in\chi}\mathcal{L}(\boldsymbol{x},\lambda) = min_{x\in\chi} \sum_{j=1}^{n} \mathcal{L}_j\left(\boldsymbol{x_j},\lambda\right) \quad (2.27)$$

$$\sum_{j=1}^{n} \min_{x_j^{min} \leq x_j \leq x_j^{max}} \mathcal{L}_j(\boldsymbol{x_j},\lambda) = \sum_{j=1}^{n} \min_{\alpha_i^k \leq x_j \leq \beta_i^k} \mathcal{L}_j(\boldsymbol{x_j},\lambda) \quad (2.28)$$

Minimizing the Lagrangian inside the dual objective funtion $\varphi(\boldsymbol{\lambda})$ is straight forward as the optimization is minimizations of functions of a single variable. The solution of the original optimization problem is found by maximizing $\varphi(\boldsymbol{\lambda})$ for $\lambda \leq 0$.

3 Topology Optimization

Structural optimization is commonly divided into three subclasses, which are sizing optimization, shape optimization and topology optimization. Topology optimization is the most general form of structural optimization. The method involves determination of material connectivity and the size and shape of holes in a structure. Known quantities are boundary conditions, applied loads, prescribed restrictions and for example the volume of the end structure. [Bendsøe (2003) p.1]

Figure 7 illustrates the differences of the three optimization classes. Starting from the top most structure the optimized quantities in the figure are sizes of the truss members, the boundary shape and in the last the connectivity of the trusses, i.e. topology. [Christensen (2008) p. 4-7]

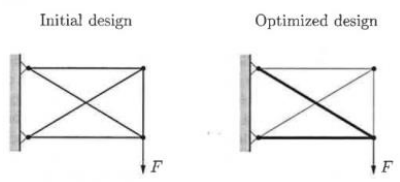

Sizing optimizaition

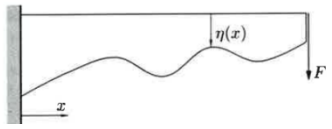

Shape optimization

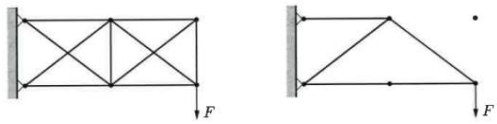

Topology optimization

Figure 7. Classes of structural optimization. [Christensen (2008) p. 5-6]

The first publication in the field of topology optimization considered low volume fractions and appeared in 1904 by A.G.M. Michell. This paper presented optimality criteria for the least weight layout of truss structures, similar to the one in Figure 8.

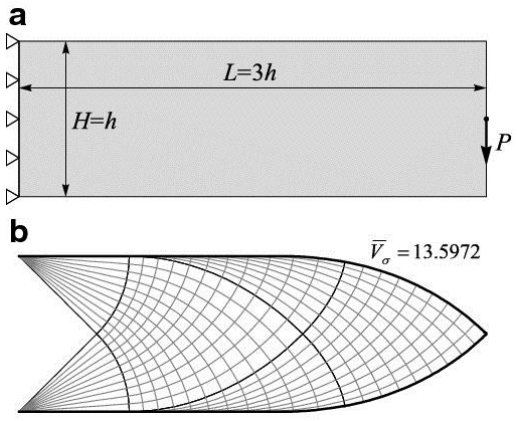

Figure 8. Long cantilever problem and the exact optimal truss layout by Lewiński et. al. [Springer Images]

The structures are often referred to as Mitchell's trusses. [Rozvany (2007) & (2001)]. Mitchell recognized that the theoretically optimal least weight truss structure is an infinitely dense, but discrete system of tension and compression members. The continuous curvature of the truss members is possible, as they are supported by a continuum of connections with other intersecting truss members. The solution is a structure with a dense discrete–continuous network of support members. Michell proved that an optimal truss must follow the orthogonal network of lines of maximum and minimum strain, in a constant-magnitude strain field. This facilitated the optimization problem, as finding optimal node positions of the truss structure was reduced to finding an orthogonal network of layout curves, on which the nodes should lie [Taggart, Dewhurst (2010)].

This theory was extended to grillages, i.e. beam like structures in the 1970's by Rozvany and the first general theory of topology optimization was released in 1977 and it was called "optimal layout theory". [Rozvany (2007)] Topology optimization for higher volume fractions also termed Generalized Shape Optimization (GSO) or Variable Topology Shape Optimization. In GSO the topology and shape of internal boundaries in porous and composite continua is optimized simultaneously.

Development of the numerical finite element (FE) based methods of topology optimization has been intensive since the late 1980's. Bendsøe, Kikuchi, Diaz presented the so called homogenization approach over the decade. The so called Solid Isotropic Microstructure (or Material) with Penalization for intermediate densities-method (SIMP) was presented in the late eighties. The method is sometimes also called material interpolation, artificial material, power law, or density method. The method is most popular at the moment. It was suggested by Bensøe in 1989 and presented for the first time by Zhou and Rozvany in 1990. Xie and Steven presented the Evolutionary Structural Optimization ESO in 1992. The method is also referred to as Sequential Element Rejections and Admissions (SERA) [Rozvany (2001) & (2007)].

Computational topology optimization software uses typically one of the presented methods; the Homogenization Method, Evolutionary Structural Optimization (ESO) or Solid Isotropic Material with Penalization (SIMP). The SIMP topology optimization method is utilized in this thesis.

3.1 Density Method (SIMP) in FEA

The SIMP method is implemented in a finite element formulation in OptiStruct. Basic concept in finite element based SIMP is to relate the elemental stiffness matrix with a continuous variable, which is used as a design variable in the optimization. The design variables are scaled up in regions of high strain energy and down in regions of low strain energy, thus iteratively creating a new distribution of stiffness in the FE-model. [Bendsøe (2003) p.11]

The design variable is interpreted as the density of the material and it is named *relative density*, denoted with ρ. Areas of low density are low in stiffness. A penalty factor p with a penalization scheme is included to make elements with low density values unfavourable in the optimization [Bendsøe (2003) p.4]. The distribution of stiffness in a FE-model is discrete due to the discretion in finite elements. Minimum compliance problem for one element is:

$$\min \ f^T \boldsymbol{u} \tag{3.1}$$

$$s.t.: \boldsymbol{K_e}(\boldsymbol{E_e})\boldsymbol{u} = f \tag{3.2}$$

$$\boldsymbol{E_e} \in E_{ad} \tag{3.3}$$

where **u** and **f** are the displacement and load vectors. Here the stiffness $\mathbf{K_e}$ depends on the elements stiffness $\mathbf{E_e}$. In the total mesh where elements are e=1,…,N, the problem is:

$$\boldsymbol{K} = \sum_{e=1}^{N} \boldsymbol{K_e}(\boldsymbol{E_e}) \tag{3.4}$$

where $\mathbf{K_e}$ is the global element stiffness matrix. In the topology optimization problem, one is interested in material distribution, so in discretised form, in a mesh with voids or solids. In the design domain, this means that we are seeking the admissible stiffness matrices, for which:

$$E_{ijkl} = 1_{\Omega mat} E^0_{ijk}, 1_{\Omega mat} = \begin{cases} 1 \ if \ x \in \Omega mat \\ 0 \ if \ x \ \Omega \backslash \Omega mat \end{cases} \tag{3.5}$$

And the minimum compliance design is sought for a limited volume fraction, i.e. limited amount of material is used as constraint. It follows:

$$\int_{\Omega} 1_{\Omega mat} d\Omega = Volfrac\ (\Omega mat) \leq V. \tag{3.6}$$

This is a distributed discrete valued problem, i.e. intention is to find a structure comprising solid or void elements. The problem is solved by replacing the integer variables with continuous variables, i.e. relaxed. These are then penalized, so that the solution is steered into discrete 0-1 values in individual elements. The stiffness matrix of the problem is then formulated, so that it depends on continuous function, which is interpreted as the density of the material. In SIMP topology optimization this function is the design variable. [Bendsøe (2003) p.4-6]

In SIMP the stiffness depends on the design variable x as follows:

$$E_{ijkl}(\boldsymbol{x}) = \rho(\boldsymbol{x})^p E^0_{ijk}, \qquad p > 1 \tag{3.7}$$

$$\int_\Omega \rho(\boldsymbol{x}) d\Omega \leq V; 0 \leq \rho(\boldsymbol{x}) \leq 1, \qquad x \in \Omega \tag{3.8}$$

Where $\rho(\mathbf{x})$ ist the design function and E^0_{ijk} are the material properties of a given isotropic material. The $\rho(\mathbf{x})$ is referred to as density, as the volume is evaluated as its integral over the domain. The density interpolates between 0 and E^0_{ijk}.

Specifying p>1 makes intermediate densities uneconomical in the design, as they contribute less to stiffness than elements with density $\rho(\mathbf{x})$=1, but they weigh the same as solid elements. Typically in order to obtain true 0-1 designs, p>3 is required. The effect of the penalization is illustrated in Figure 9.

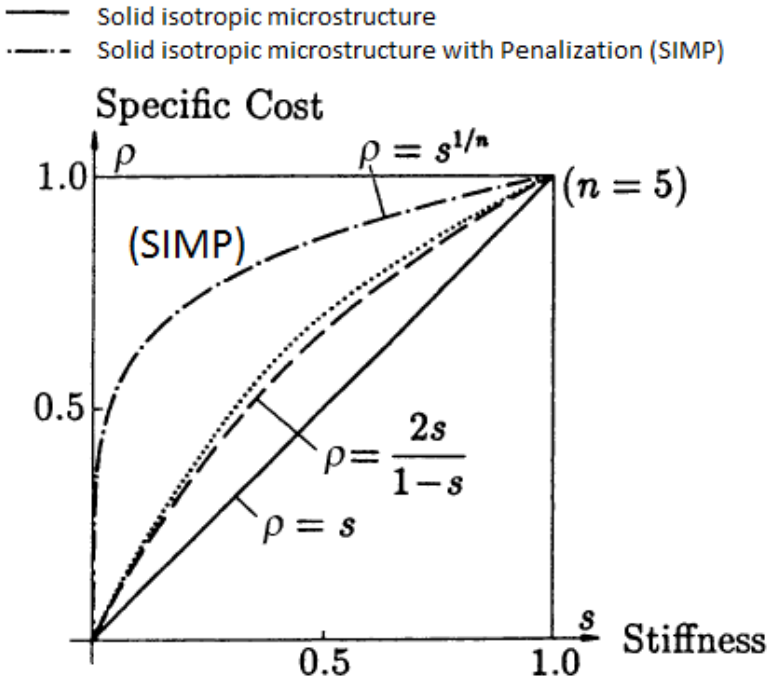

Figure 9. Stiffness vs. relative density (cost) for various types of penalization scheme. [Modified from Rozvany (2001)]

3.1.1 SIMP in OptiStruct

In OptiStruct the penalization factor p is always greater than 1, by default the value is p=2 for shell elements and p=3 for solid elements. When manufacturing constraints are used the value of p starts from 2 and is increased to 3 or 4 along with the iterations. [Altair HyperWorks Help]

Figure 10 and the list below were constructed according to [Bendsøe p. 21] to illustrate the procedure of FEA based topology optimization. Let us assume the compliance is minimized at a given volume fraction constraint.

a) Initially a homogeneous density distribution is applied in the design space elements.
b) Volume constraint is applied from the initial guess onwards.
   - ✓ Alternatively at this point, the density variables are updated according to a previous iteration. (ρ at elements with high/low energy density is scaled up/down)
c) For this distribution of the density variable, a FEA is conducted resulting nodal displacements.
d) The compliance and the associated sensitivity of the design variable are calculated, and the change of compliance with respect to the objective function is examined.
e) If less decrease is obtained than in the convergence criterion, iteration is stopped. Otherwise the iteration is repeated.
f) The final solution is used in post processing with a given threshold value of the density variable.

Once the optimization has converged OptiStruct suggests a solution, that consists of all the elements in the initial design space, but with scaled densities varying in the range of $0 < \rho < 1$. No elements are removed during the optimization. User decides at which relative density the structure is printed out. OptiStruct offers smoothing algorithms to produce a structure with smoothed boundaries.

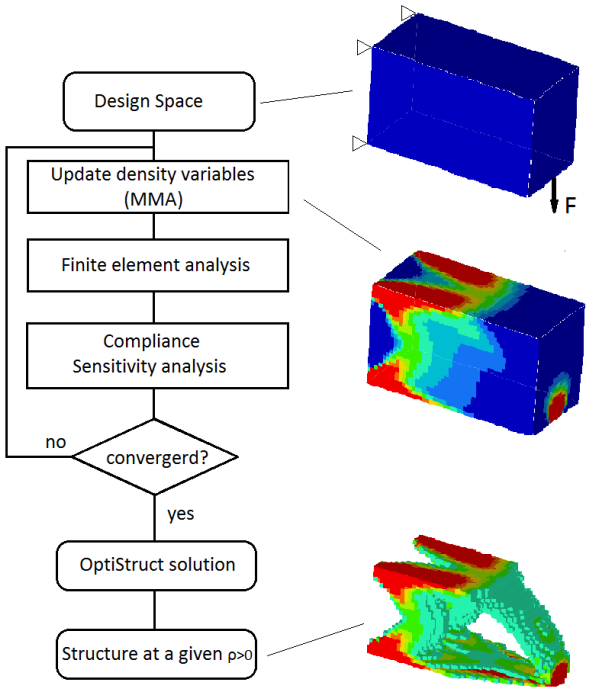

Figure 10.OptiStruct iteration scheme.

3.2 Complications in Numerical Topology Optimization

Two important issues are related to topology optimization as complications, namely dependence of solution on mesh-refinement and appearance of checkerboard pattern.

3.2.1 Mesh-dependency of the Solutions

The SIMP method suffers from the nonexistence of analytical, accurate and discrete solutions. The phenomenon is called mesh-dependency. In SIMP different optimal structure is found just by refining the mesh, i.e. without changing the optimization problem. This is not common in optimization.

In SIMP finer mesh leads to structures of different microstructure and different topology, rather than better description of boundaries. In general the introduction of new smaller holes will increase the efficiency of the structure and the optimal solution is a microstructure instead of a macro structure. However, in applied topology optimization problems, macro structures are typically more interesting. [Bendsøe (2003) p.28-32]

In Figure 11 it is seen that the microstructure of the finest mesh c) is more detailed and much different from the a) and b). The remedies to get clearly defined structures are to reduce the space of admissible designs by a global or local constraint on the variation of the density variable. This will rule out the possibility for finer scale microstructures. This is achieved by adding constraints to the optimization problem, reducing directly the parameter space for the designs, or applying filters in the optimization implementation. [Bendsøe (2003) p.28-32]

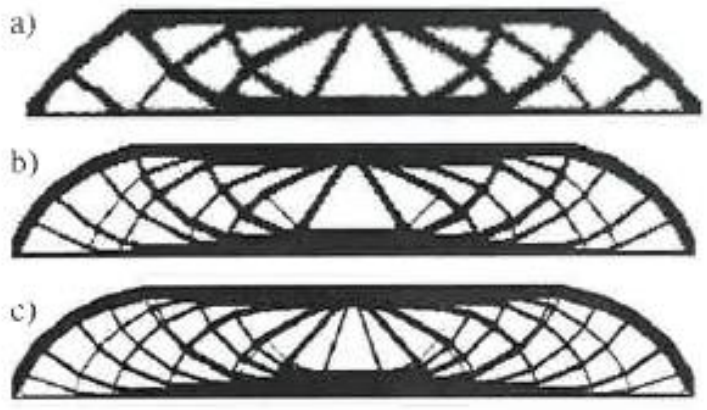

Figure 11. Mesh-dependency phenomenon of SIMP. Discretizations with a)2700, b)4800 and c) 17200 elements. [Bendsøe (2003) p.30]

3.2.2 The Checkerboard Problem

In the checkerboard pattern problem, regions of alternating solid or void elements are formed in the solution. The elements are connected only in their corners and the stiffness of the structure is virtually high. The problem is illustrated in Figure 12. The computational stiffness of the solutions b) and c) are similar in, but only the solutions c) represents a solution that would perform well also in reality.

The checkerboard problem is related to features of finite element approximation and is due to numerical modelling, that overestimates the stiffness in such a structure. A viable solution is to use higher order elements with nodes along the edges. This solution requires more CPU time and also alternative methods have been developed. [Bendsøe (2003) p.39->]

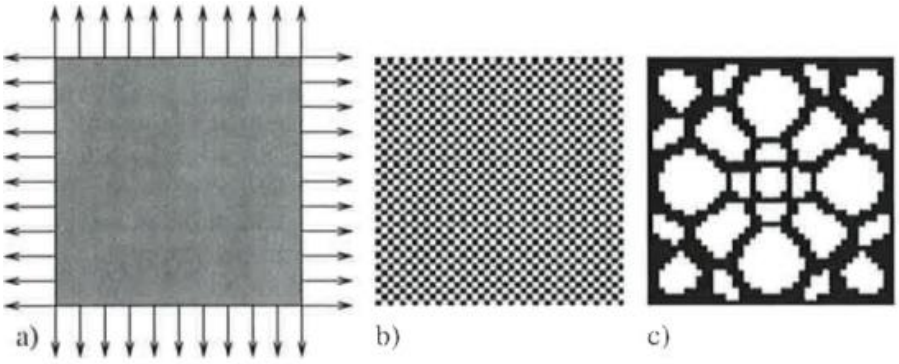

Figure 12. Checkerboard problem of a square structure. a.) Desing problem, b.) solution without checkerboard control, c.) solution with filtering conrols. [Bendsøe (2003) p.41]

4 Validation of the Topology Optimization Software

In this chapter OptiStruct is tested and validated using three known optimal structures. Validation of the used topology optimization software is important to determine whether the software is able to deliver optimal or near optimal results, with the implemented SIMP algorithm. Research [Rozvany, Zhou, Barker (1992)] shows, that the interpolation scheme SIMP alone delivers good results to known analytical optimal topologies.

In the field of nonlinear optimization it is tedious to find an optimal solution. Analytical solutions can only be found for academic topology optimization problems, such solutions are only available for truss and grillage-like structures. The grillage solutions are more realistic than truss like solutions, as no buckling effect is considered in the truss solutions. [Rozvany (2011)] For general solid solutions and higher volume fractions no analytical solutions exist and therefore, global optimality cannot be guaranteed. [Appendix A, Ole Sigmund 5.9.2012] In non-linear, real-life problems the objective function will have some constraints, other than zero or unity. Thus the solution methods are always numerical and based on iteration techniques. Furthermore no general method exists to prove the local or global optimality of a topology optimization result. [Appendix A, Parviainen 6.9.] As a result the neighbourhood of every topology optimization result has to be examined. The way to do this is to carefully alter the boundary conditions, loads or convergence criterion, to see if the solution represents a stable optimum. In an ideal situation the solution represents a stable global or local optimum that is not sensitive to alterations of the boundary conditions or loading. Otherwise small changes in dimensions e.g. caused by manufacturing tolerance of the actual part might lead to an unstable structure in reality. In the following benchmarking, however, this is not done, as the benchmark solutions represent an optimum accepted by the academic community. These solutions are used as a reference.

4.1 Benchmark Cases

OptiStruct is validated using three known benchmark cases presented in the topology optimization literature; the 2D plate benchmark [Lewinski, Rozvany et al. (2008)] and 3D torsion cylinder [Taggart, Dewhurst (2010)] have an analytical formulation. A 3D solution for a cantilever beam is also considered [De Rose, Diaz (2000)]. The material parameters of steel of Table 3 were used for all cases apart from the 3D cantilever model. The models are calculated in units mm, kg, N and MPa. The topology optimizations were run with OptiStruct default setttings so no checkerboard control or manufacturing constraints were used. Penalty factors 2 and 3 were used for shell and solid elements respectively. For further information on OptiStruct specific manufacturing constraints in topology optimization refer to [Zhou, M. Fleury, R. et al. (2011)].

4.2 Exact Analytical Solution for a 2D Truss Structure

In the first test an analytical truss solution is compared to a shell element solution of OptiStruct. The analytical problem is presented in Figure 13. The plate is rigidly mounted from the AB-side and a force is acting downwards in point P. According to the paper the minimal weight structure is sought.

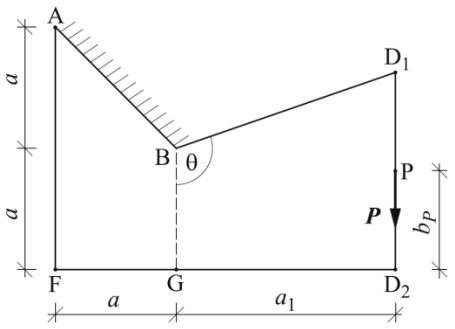

Dimensions and parameters used in OptiStruct model
a=50mm a_1=80mm b_p=40mm
Θ= π/2+tan^{-1}(3/8)= 110,556mm
D_1D_2=80mm
P=10N
ρ=7800*10^{-9} kg/m^3
E=207*10^3 MPa

Figure 13. 2D topology optimization problem. [Lewinski, Rozvany et al. (2008), p.2]

The optimal analytical solution is shown in Figure 14, where a.) illustrates the optimal truss structure and b.) classifies the optimal truss layout and loading condition. In the Figure 14a the rigid support on line AB is converted into pinned support in points A and B. Material is removed from the edges F, D_1, D_2 and region AG_2B is empty. Inside the regions BG_1G_2 and BPG_1 tension truss members carry load. A compression truss spans from $AG_2G_1E_2P$.

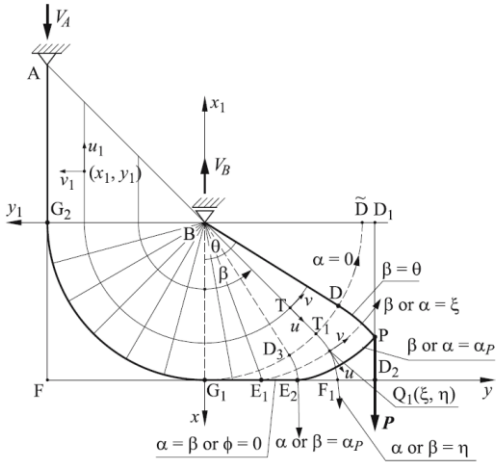

b.)

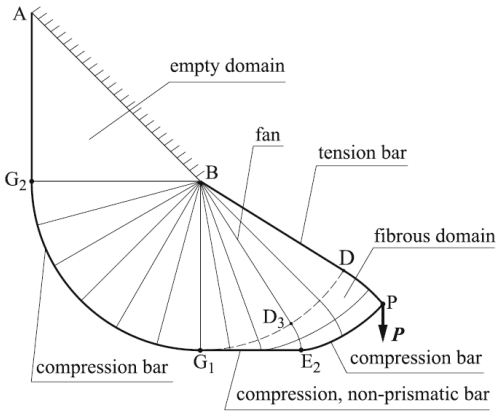

a.)

Figure 14. a.) Optimal truss layout for the inclined support. B.) Illustration of the solution. [Lewinski, Rozvany et al. (2008), p.2]

The above example was modelled in OptiStruct with a shell finite element model. Figure 15 represents the results of a topology optimization with linear and parabolic elements. Dimensions, material parameters and loading are presented in Figure 13. The red areas represent fully dense elements while the blue areas consist of elements with densities close to zero. The areas ranging from light blue to orange represent elements with intermediate density.

The structures are similar to the analytical truss solution in both cases. Material is removed from the same areas and the structure consists of truss-like members. The initial boundary condition at the line support is separated clearly into two areas, but the support in point B is distributed over a larger area than in Figure 16, most likely because the singular support cannot be represented in a FE solution with shell elements. The structure is no longer attached all the way along the side AB. The author finds no explanation why the supporting member near point A is not vertical.

While in the analytical truss solution no bending moments occur, they are present in the FEM solution. Thus in the computational solution all support member connections contain multiple members to distribute both bending moment and tensile/compressive loads. Checkerboard patterns can be recognized in the linear solution, but they were avoided using parabolic elements. Mesh dependence of the optimization is clearly visible in the two solutions. The parabolic model has roughly three times the mesh density of the linear model and thus there are differences in the connectivity of the truss members.

Element type:
Linear CTRIA3
Elements: 29,746.0 DOF: 90,462.0

Element type:
Parabolic CTRIA6 & CTETRA10
Elements: 89,238.0 DOF: 1,254,228.0

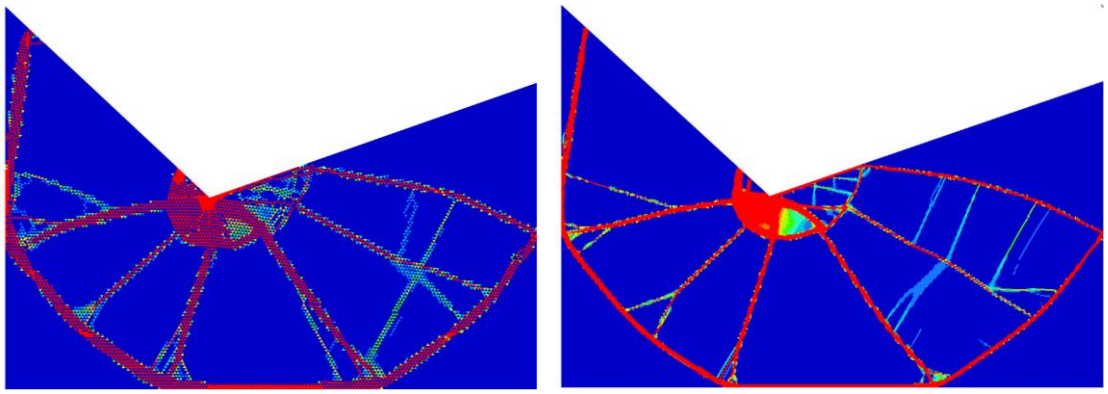

Figure 15. 2D benchmark solutions.

A static stress analysis was conducted on the final topology. The topology of the parabolic solution in Figure 15 was remeshed with 13560 parabolic triangle elements for this analysis. The model is presented in Figure 16. This structure consists of elements where the density was above 0.1 in the final optimization result. In this model, however, all elements have the density of steel. The same boundary conditions and load was applied to this FE-model as in the optimization.

The stress result is illustrated in Figure 17 where the stresses are illustrated as so-called signed von Mises stress. In the FE solver RADIOSS the sign of the signed von Mises stress is taken from the sign of the absolute maximal principal stress; blue members are in compression and red in tension. The loading condition of the trusses is similar to the analytical in solution Figure 14b. A compression member spans from P to near the region point A. Members inside APBA are mainly tension members. Thin compression members near the loading point, inside the domain APBA are unexpected. They were included in this analysis because the structure was exported from OptiStruct with a low threshold of relative density. These members would have been removed if the structure had been exported with the relative density above 0.4.

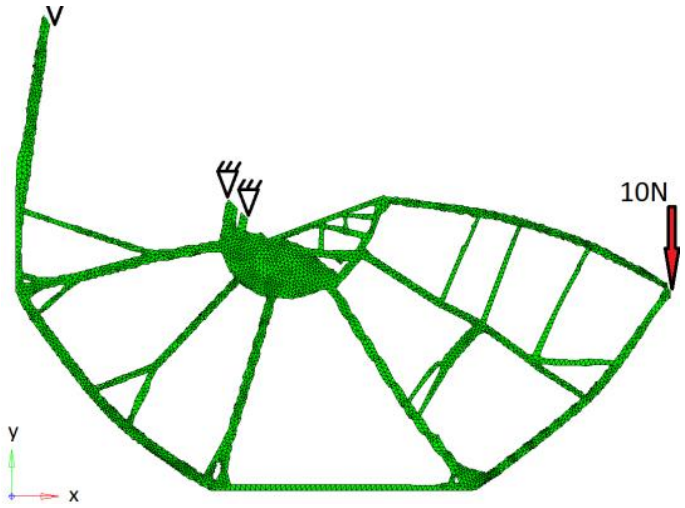

Figure 16. Topology optimization result remeshed for static FEA.

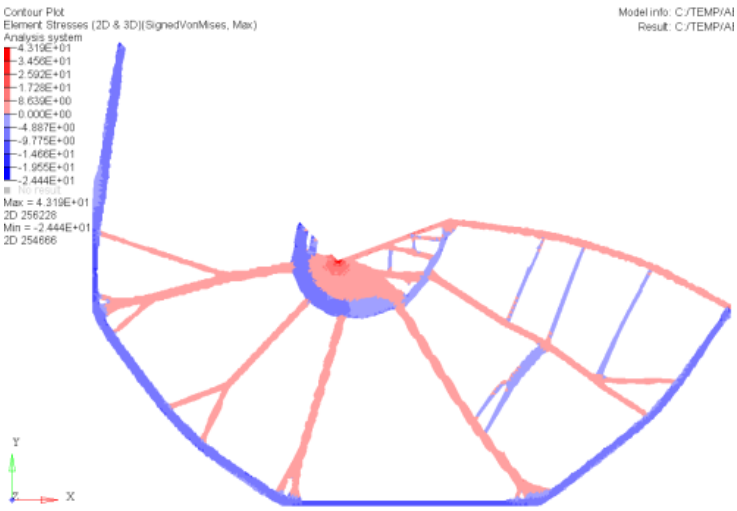

Figure 17. Stress state and displacement field of the 2D benchmark solution.

4.3 Analytical and Numerical Solution for a 3D Torsion Cylinder

In the second validation case a 3D thick walled cylinder with minimum weight is studied. The cylinder is rigidly supported from three points at its bottom and load is applied through three points on the top end of the cylinder. [Taggart, Dewhurst (2010)] The attachment and loading points are cyclically symmetric about the longitudinal axis of the cylinder with a period of $2/3\pi$. The dimensions of the cylinder and optimization problem formulation were not specified in the article. It is assumed to have been to maximize the stiffness with a volume fraction constraint. The constraining volume fraction was probably less than 20%.

Figure 18 presents numerical solutions for the optimal topology of the cylinder for combinations of axial and pure torsion load. The structure on the left is exposed to pure axial tension and the rightmost structure experiences pure torsion. These structures consist of orthogonal families of helices intersecting at angles γ.

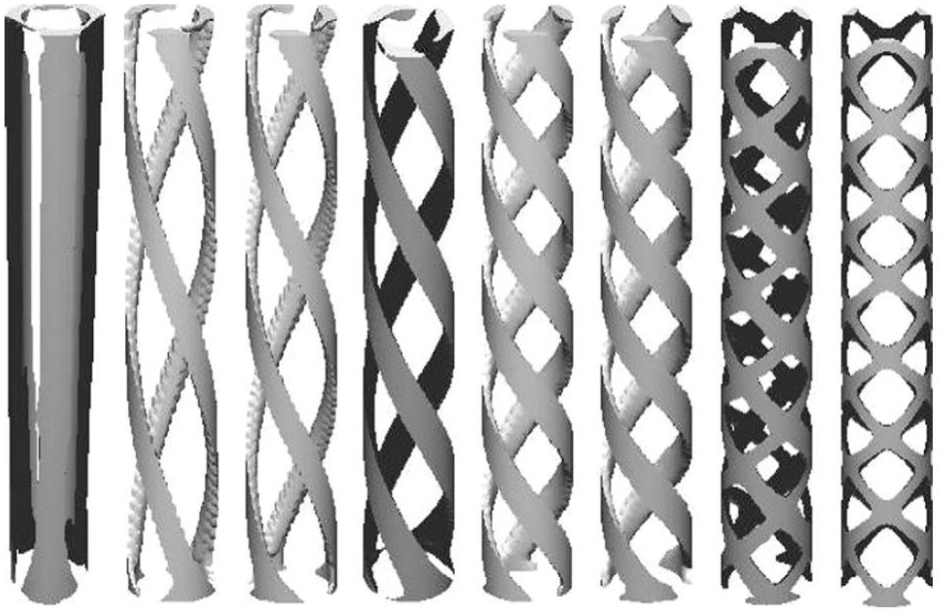

Figure 18. Numerical solution for the optimal topology of a pure torsion cylinder. [Taggart, Dewhurst (2010)]

The paper also represents an analytical solution for this angle:

$$\gamma = \cot^{-1}\left(\frac{Fr}{4T}\right) \qquad (4.1)$$

Where Fr is the longitudinal force and T is the torque applied to the end of the cylinder. [Taggart, Dewhurst (2010)] For pure torsion γ_T (Fr=0, T=1) and for pure tension γ_{Fr} (Fr=1, T=0) becomes:

$$\gamma_T = \cot^{-1}\left(\frac{0}{4T}\right) = \ 90° \qquad (4.2)$$

$$\gamma_{Fr} = (\cot^{-1}(\frac{1}{0})) \qquad (4.3)$$

(4.3) is not defined so the solution is found by examining the graph of cotangent function in Figure 19. When the angle approaches zero, the value of the function approaches infinity, thus it follows:

$$\gamma_{Fr} = lim_{x\to 0}(\cot^{-1}(\frac{1}{x})) = 0°, \qquad [0 < x < \frac{\pi}{2}] \qquad (4.4)$$

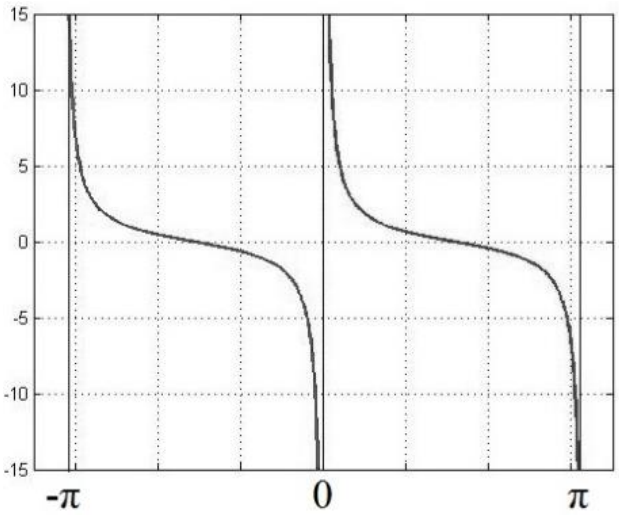

Figure 19. Graph of the cotangent function.

The FEM test model was constructed according to the articles illustrations and the model is presented in Figure 20. The length was 250mm and the outer and inner radii were 60mm and 40mm respectively. 83700 brick elements with six elements across the cylinder wall are used. A rigid interpolation element (RBE3*) was used to distribute the torsion to the cylinder and the cylinder was attached at its bottom in three areas, each consisting of 5x6 nodes. The case was calculated with linear and parabolic elements with a penalty factor *p*=2.5 and the results are shown in in Figure 21.

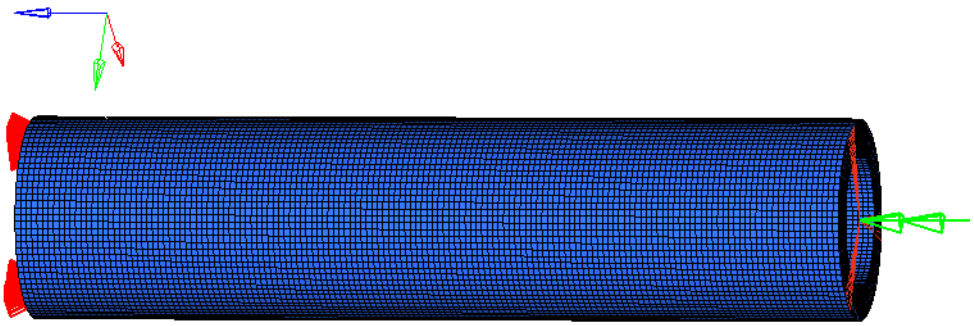

Figure 20. FE-model of the 3D cylinder benchmark case.

**RBE3 elements average the motion of dependent node on the independent nodes. The displacement of the dependent node is a weighted average of the motions at the independent nodes. Forced displacements will be applied to the dependent node in the optimization model.[HW help]*

The result with linear elements converges to a helix-like structure near the boundary condition and loading areas, see Figure 21 a.). The helices intersect the longitudinal axis in approximately 45° as expected, but the model has severe checkerboarding. This leads to a very low compliance as seen in Table 1.

In the parabolic element model, Figure 21 b.), the checkerboard problem is not prevalent in the solution, but OptiStruct failed to converge to a well-defined structure in the centre of the cylinder where also areas with checkerboards are evident. In Figure 21 c.) the parabolic element solutions are illustrated with no density filtering. The structure is similar to the structure in Figure 18, but the helices are more connected internally and noticeably thinner. The helices intersect at approximately 90° angle but not near the boundary conditions. Calculation with parabolic elements required 5-10 times the CPU time of the linear element model solution.

Table 1. End compliance comparison of the torsion cylinder topology optimizations.

Model	Initial state	Linear element solution	Parabolic element solution
Compliance	58 750.59	0.2431214	391.4889

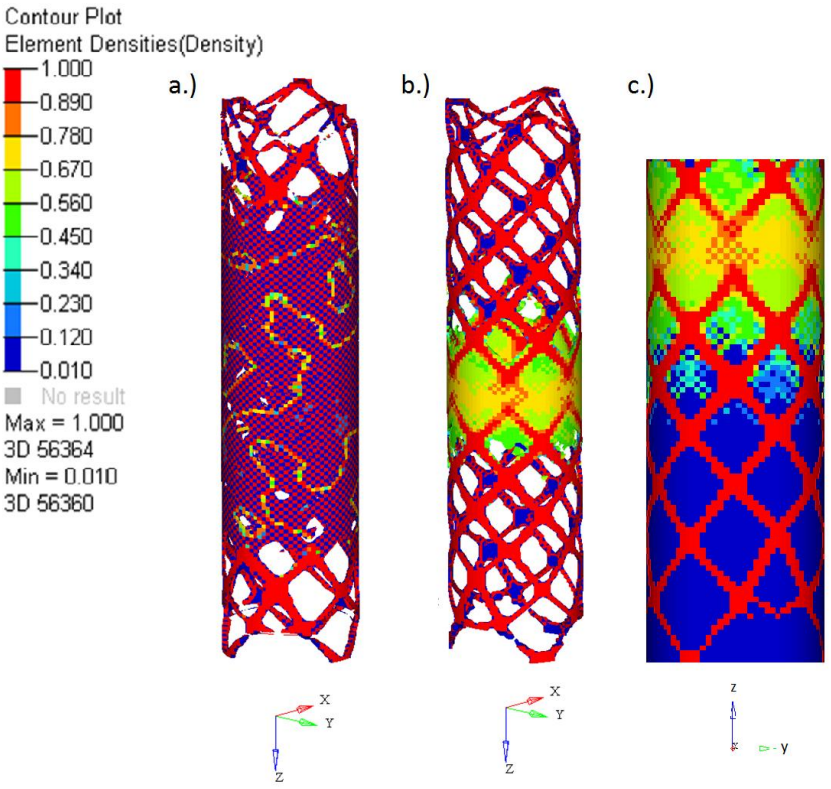

Figure 21. Solution structures for the 3D torsion cylinder benchmark.

In separate analysis the penalty factor was increased to 3.5 and the convergence criterion was tighter. In this analysis OptiStruct had also problems in converging to a well-defined structure in the middle, the helices did not always intersect at 90° and there was checkerboarding in the middle of the cylinder. The method is also very sensitive to boundary conditions; a test case of a cylinder with uniformly distributed torsion loading and boundary conditions at both ends converged to a thin walled pure cylinder with no helix structure. The software developers were able to produce a solution with smooth boundaries, thicker helices and no checkerboarding [Discussion 1.5, Appendix A]. This solution, however, required the use of OptiStructs filtering like minimum member size and checkerboard control.

4.4 Numerical Solution for a 3D Cantilever Beam in Bending

The third test case is a 3D structure that was obtained by a mesh-less wavelet-based solutions scheme for topology optimization. The method utilized is not based on finite element theory; instead the material distribution and displacement field are discretized over the domain using fixed-scale, shift variant wavelet expansions. The elasticity problem is solved using a wavelet-Galerkin technique during each iteration of SIMP. [DeRose, Díaz (2000)] This case serves as a good benchmark for the FE-based OptiStruct.

Figure 22 illustrates the design domain of the test case; a pin-supported cantilever beam is loaded at the centre of an edge with a unidirectional load *P*. The objective function was not specified directly but the optimization problem is assumed to maximize stiffness with a volume constraint. A volume fraction constraint of 25% and a penalty factor 2.5 was given. The model uses a simplified material model with E=1.0, ν=0.3. This optimization setup was used with OptiStruct with force the value P=3N.

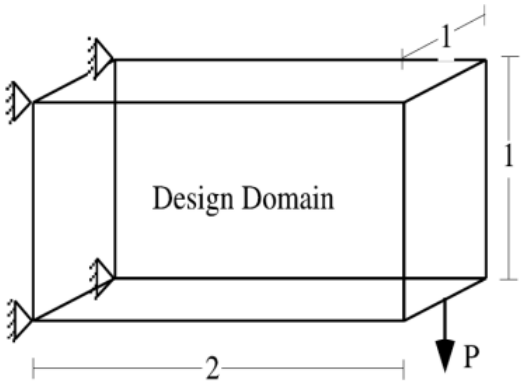

Figure 22. Test case problem statement [DeRose, Diaz (2000), p.280]

A comparison of the resulting topologies from the paper and OptiStruct with the same discretion is illustrated in Figure 23.The OptiStruct solution on the right is illustrated with elements ρ>0.5. Material is removed from unloaded corners and the shape is hollow, the solution is a 3D continuum structure with various thickness structural members, i.e. combined beam-plate structure. This solution is compared to the one on the left hand side and they appear almost identical.

Meshless solution
Discretization: 64x64x64=262144 voxels

Element type: CHEXA , 8 node parabolic
Discretization: 64x64x64=262144 elements
Dimensions: 48 x 48 x 96mm

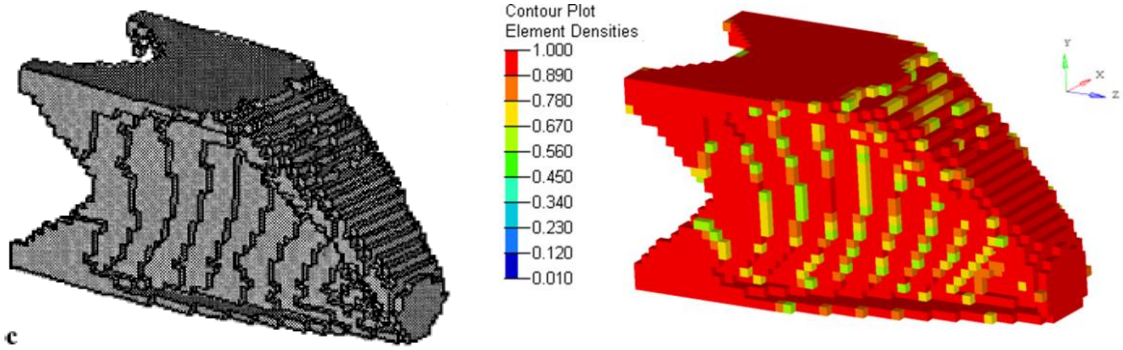

Source: Diaz (2000), p.280.

Figure 23. Comparison of the 3D cantilever beam solutions.

4.5 Concluding Remarks on Benchmark Problems

OptiStruct performs well and converges to near optimal topologies if parabolic element formulation is used. Checkerboard problems were visible in all solutions with linear elements and to some extent also with parabolic element models. The calculation effort is far greater when parabolic elements are used, thus the use of linear elements is sensible for approximate solutions. These can be used for example to get an idea of the resulting structure and to make changes to decisive features of the model like loading direction etc. However, due to virtually high stiffnesses and unrealistic topologies these solutions are of little use.

The topology optimization method is very sensitive to boundary conditions and the initial state of the optimization problem strongly affects the result. The final solutions of OptiStruct can hardly be named optimal as there is no guarantee of the optimality of the solutions in non-linear optimization and as the solutions of the software were only similar to the known optimal ones. Only in one test case the structure appears to be identical to the example optimal topology. The author suggests the solutions to be called “near optimal” or “optimized” to be used in this context. In most cases the final topology is also dependent of and sensitive to the used relative density threshold. High values of relative density should be used in post processing in order to obtain structures that are well defined and have clear load paths. By high values the author means $\rho>0.5$.

The final conclusion is that the software can be used in the substructure topology optimization of this thesis without major restrictions. The software will be capable of producing near optimal topologies with parabolic element models. The use of the software’s built in filters and constraints results in better defined boundaries and load paths of the structure. Thus some symmetry and minimum member size constraints are used in the actual topology optimization.

5 Fatigue Strength Estimation of Welded joints

In this chapter the fatigue strength of a welded joint is estimated in constant amplitude cyclic loading. The estimation of the fatigue strength is performed with the fatigue class (FAT) values according to the IIW recommendation. The intention is to provide means to classify, how big an effect on fatigue strength it has, if no welds exists in the generator attachment area. The new topology will probably be a cast steel component and it consists of basematerial with no welds. The basematerial is regarded concurrent to structural steel in this context. More detailed fatigue calculations and fatigue designs are not in the scope of this thesis, and thus assumptions like constant amplitude loading are made in order to make the comparison straightforward. More accurate fatigue strength assessment methods of cast components are presented e.g. in [FKM].

5.1 IIW Fatigue Class Estimation

In the following, the presented stress range values are valid for structural steels up to 960MPa ultimate strength [IIW p.6]. The fatigue class assessment of welded joints is based on the nominal stress approach. In this study constant amplitude loading is considered and the knee point of the SN-curves corresponds to $N=10^7$ cycles. Welded steel joints of the original structure are considered to have FAT 36 to 90. These regions are to be replaced with a cast component, for which the value FAT160 is used as reference for fatigue strength.

Table 2 presents stress ranges at the knee point for different FAT values. Plate thicknesses up to t=25mm are covered. Table 3 presents material properties of cast steel that is used as reference for the material of the optimized attachment area. The fatigue stress range of non-welded base material corresponds to FAT160. For a welded T-joint FAT90 corresponds to a maximum quality joint with no imperfections. FAT71 corresponds to a welded T-Joint with full penetration and good quality and FAT36 represents a T-joint or a filled joint with partial penetration [IIW p.46-61]. Typical welded T-joints correspond to FAT71 to FAT36.

Table 2. FAT data, stress at knee point of S-N curve. [IIW (2008) p. 114]

Fatigue class	Stress ranges at knee point N=1x10^7 cycles, [MPa]	FAT 160 / FAT XX
FAT 160	116	1
FAT 90	52.7	2.20
FAT 71	41.5	2.80
FAT 36	21.1	5.50

Table 3. GS20Mn5 mechanical properties [MET, ASM]

Young's Modulus	Poisson ratio	Density	Yield Strength	Ult. Strength
207 GPa	0,3	7800-7830 kg/m^3	260-300 MPa	500-650 MPa

The fatigue strength of the cast component is considered to be FAT160. The fatigue strength of the FAT 160 is approximately 2.8 or 5.5 times higher at 1x10^7 cycles than it is for a other considered FAT71 or FAT36 welded joint.

The conclusion is, that by removing welded joints in the attachment area the fatigue strength of the component is at least doubled, see Table 2. Additional increase in fatigue strength can be expected if the optimized is designed to have smooth internal connections and material if material is added to highly stressed areas.

6 Substructure Optimization

In this chapter the stiffness of the attachment area was maximized using topology optimization. The structure was optimized within a fixed design space according to loadings, boundary conditions, objectives and constraints. The loadings of the structure are taken from an earlier computational simulation of the electric device in its operating environment. Static forced displacement load cases with a volume fraction, symmetry and minimum member size constraints are used for the optimization. Maximization of stiffness equals maximization of compliance when forced displacements are used as loadings. For the pre-processing, load extraction and meshing Abaqus 6.12., MATLAB and NX Ideas were utilized. The topology optimization was performed using Altair OptiStruct version 12.0.

6.1 Generator Set W18V46

A diesel generator set, genset, consists of a diesel engine connected to a generator via a flexible coupling. The engine and generator are mounted on a common base frame, which is dynamically isolated from the concrete foundation by steel springs. Generator sets produce electricity for various purposes, e.g. on off-shore facilities, for ship propulsion or as power plants [Wärsilä Powerplants homepage]. Technical specifications of the Wärtsilä 18V46 genset are listed in the table 4.

Table 4. Technical data of the 18V46GD Genset. [Wärtsilä Dual-Fuel Engines homepage]

Technical data 50 Hz/ 500 rpm	**Model: 18V48GD**
Electrical output (MW))	17,076
Electrical efficiency (%)	45.3
Dimensions and dry weight of generating sets	
Length (m)	18,260
Width (m)	5,090
Height (m)	5,890
Weight (t)	358
Engine layout	V18
Turbolader	2

A genset Wärtsilä W18V50 with a generator is illustrated in Figure 1. The scale of the 18V50 and 18V46 are very similar, so the figure serves well for illustrative purposes. An example of a frame construction similar to the studied generator is illustrated in the Figure 24. The considered attachment area of this thesis is marked in the figure. The attachment area transfers all the loads that the generator is exposed to, in its operating environment. Rotor, ventilation unit and bearings are excluded from the figure and stator windings are shown in red. In its present configuration the attachment area is composed of steel plates welded together. As a part of a generating set the generator is exposed to cyclic loadings caused by vibration caused by the diesel engine. Engineering and constructional information was used to define a suitable size for the substructure considered in this thesis.

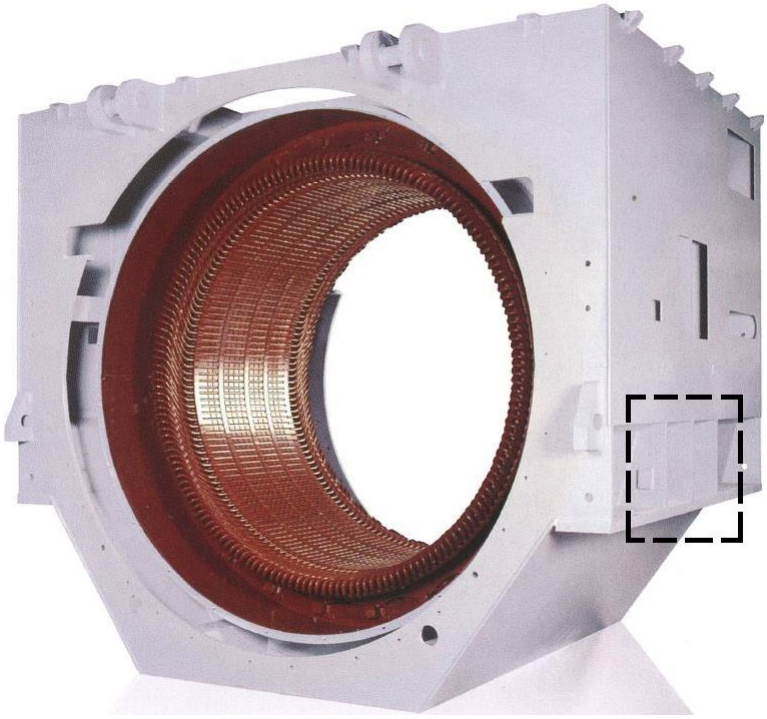

Figure 24. ABB Electric Motor frame with the optimization area illustrated in the boxed area. [ABB Brochure with modifications.]

6.2 Optimization Area

A CAD-model to be meshed with finite elements for the optimization is shown in Figure 26 and multiple geometrical constraints are imposed on the optimization area. A blower unit is mounted on top of the frame for ventilation so the attachment area needs to have sufficient air flow conditions. A trapezoidal shape was selected for the ventilation duct, so that the optimization will be able to converge to a thick beam or plate-like structure near the stator fixing areas. Adequate space for tooling is to be reserved for fastening and tightening of the generator to the base frame. A lead-through has to be kept clear of material at the back. Entry to the stator should be possible from the tooling area, but this condition is dealt with later on as it would have restricted the design space for the optimization too much.

A single coordinate system is used throughout the thesis and applies to all presented models. The origin lies on the rotating axis of the rotor, positive x-axis points towards the back of the generator and x=0 at the centre of the generator, see Figure 25. In the figure the all sides of the generator are named according to coordinate values. A and B-bank have different y-coordinates, A-bank having negative coordinate values. D- and N-end have different x-coordinate values, D-end having negative sign. The abbreviation D stands for the "engine driven end" and N for the "neutral end". In this thesis the generator frame considered symmetric about the zx-plane, x-axis is longitudinal and z-axis horizontal. The yz-plane of the attachment area models lies between the middle frame plate extensions see Figure 26b.

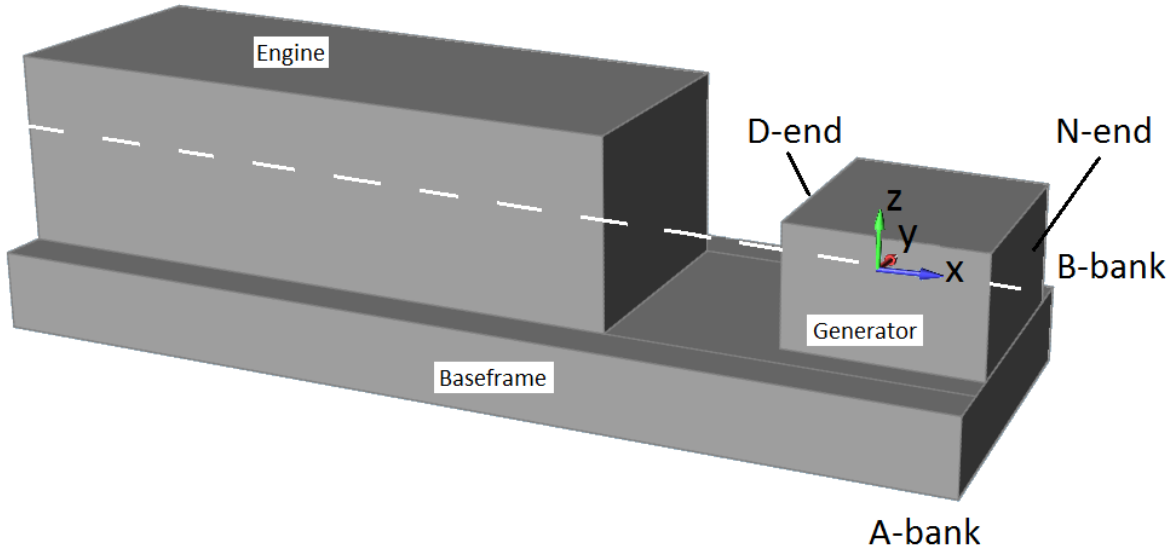

Figure 25. Coordinate system, abbreviations and orientations used in the analyses.

In Figure 26 the dimensions of the topology optimization model are presented. The measures are dimensionless, longest side having the value 1.The substructure is a 45° sector from the shaft line downwards; this area encloses three lines of stator fixing points. These are illustrated Figure 26a alongside with longitudinal beams which, however, are excluded from the optimization models. The length of the model is approximately 0.6 times the total length of the generator. A part of the original cover plates were included in the model. These are 4.8×10^{-3} thick, 0.13 long in D-end and 0.19 long at N-end. The tooling spaces are 0.27 x 0.12 x 0.07 and have a 0.12 rounding. The Attachment flange is 0.03 thick and bolt holes are 0.03 in diameter. The scale of the generator frame is listed in the Table 5 using the corresponding unit less system.

Table 5 ABB Generator steel frame main dimensions.

Main dimensions of the generator	Relative dimensions (unitless)
Height	1.91
Length	1.69
Width	2.12

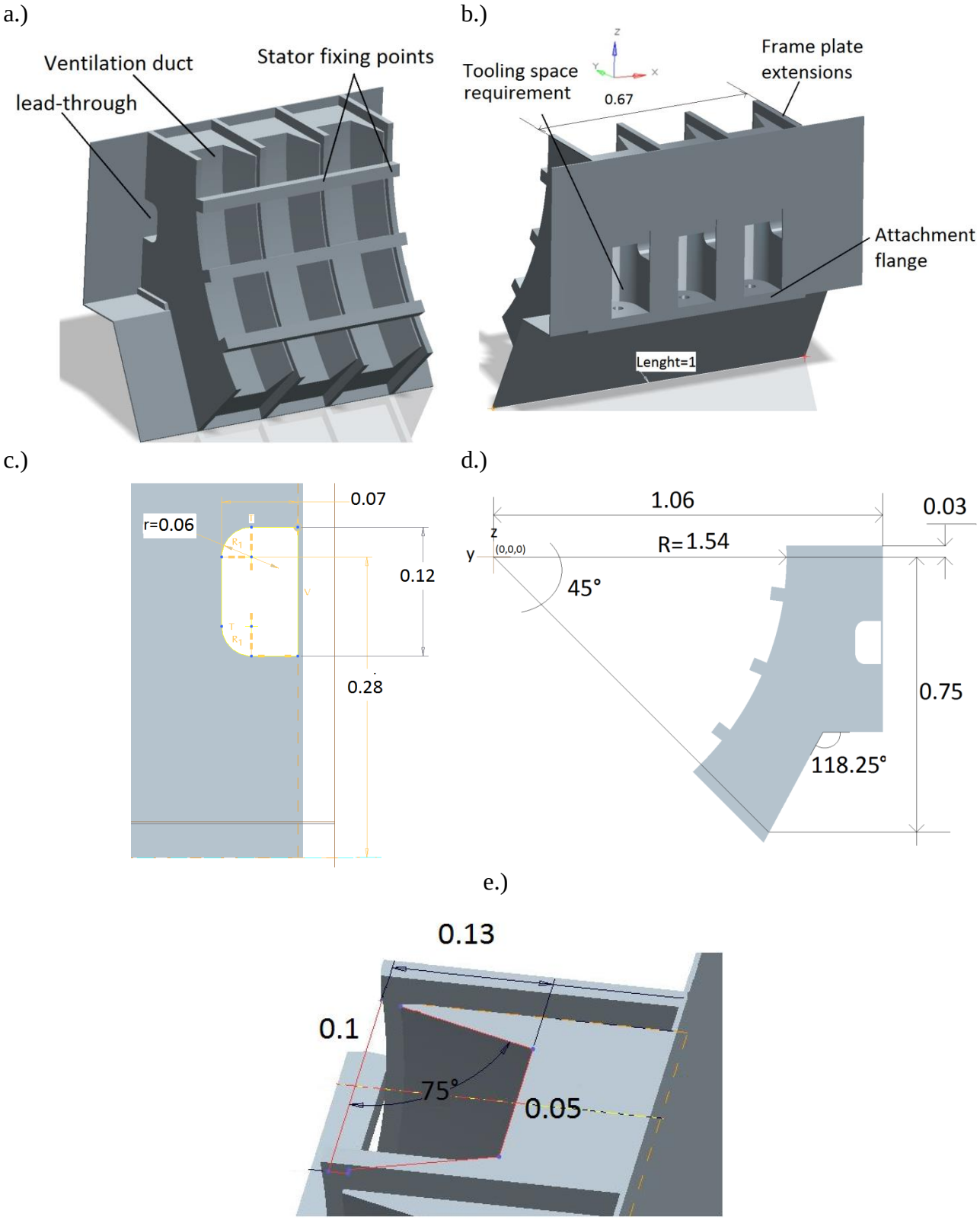

Figure 26. Attachment area, A-bank CAD model dimensions.

6.3 Finite Element Models

A finite element model was created using the CAD geometry of the attachment region, see Figure 27. The FE-model comprises 45 3781 parabolic 10 node tetrahedral elements, and has 1,976,754 degrees of freedom (dof). All solid elements share the same material but colour coding was used to divide the model in two: non-design space, in elements purple and to design space elements in blue. The genset coordinate system is used, i.e. x-axis is the generator rotating axis, where z=0 and y=0. Nodes with positive y-coordinates belong to the so called B-side of the genset and A-side nodes have negative y-coordinate values respectively. ZY-plane lies between the two middle frame plates.

Topology optimization is performed inside the designs space and all optimization constraints only affect this area. The value of the objective function, however, is calculated for the whole model. Boundary conditions are applied only on the non-design space. The purpose of this area is to eliminate convergence problems near boundary conditions and to smooth loading in highly stressed areas, giving more realistic and feasible topologies inside the design space. Element densities will not be scaled inside the non-design space during optimization. Green elements are so called RBE3 rigid elements with one dependent node and multiple independent nodes. With these the boundary condition areas will not deform as rigid planes which avoids stress concentration in these areas. This is important, as the topology optimization method was found to be sensitive to boundary conditions in chapter 4.5. RBE3 elements of the stator attachments are not visible in Figure 27

Material properties for cast steel presented in Table 3 may vary according to the composition of the steel [ASM], so fixed values were chose for the optimization. Following material properties ρ=7800kg/m^3, E=207GPa, ν=0.3 were used in all models of the thesis.

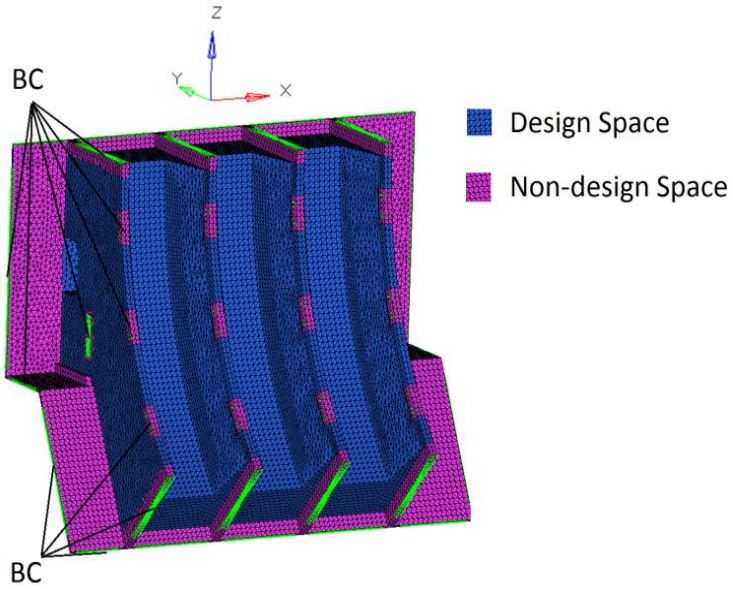

Figure 27. FE-model of the B-bank attachment area.

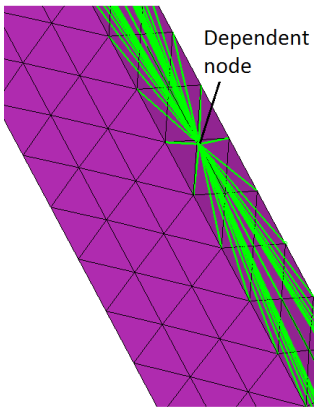

Figure 28. RBE3 element attached to non-design space.

6.4 Extraction of Boundary Conditions from Response Analysis

The complex loading and boundary conditions of the generators attachment area were simplified for topology optimization as forced static displacements.

Initially a dynamic harmonic response analysis was performed with the FE-method for the whole generating set assembly. In the analysis the internal excitations of the diesel engine, due to rotating masses, combustion cycles etc., were used in the response analysis and no excitation of the concrete fundament of the genset was present. Excitation order refers to the frequency of the vibration, excitation order 1 being the crank shaft rotating frequency of the diesel engine. This facilitates illustration of data when internal combustion engines are considered.

The response analysis resulted in complex valued harmonic response data, i.e. frequency dependent displacements of the generating set during operation. This complex valued data included the rotatory movement of the nodes of the FE-model and the phase of the responses varied between the different locations of the structure.

The displacements of the attachment area were printed out in the areas of the cut boundaries of the optimization design space. The cut boundaries are named in Figure 32. The displacements of the boundary nodes at a specific frequency are illustrated in Figure 29. From this data the forces acting on the attachment area during operation were obtained and these are presented in Figure 30. The force level has been scaled, so that the highest resultant force equals unity. Each column represents the sum of nodal forces at a given order of excitation. Significant excitation orders (1, 2, 4.5 and 6) were selected according to the presented force levels.

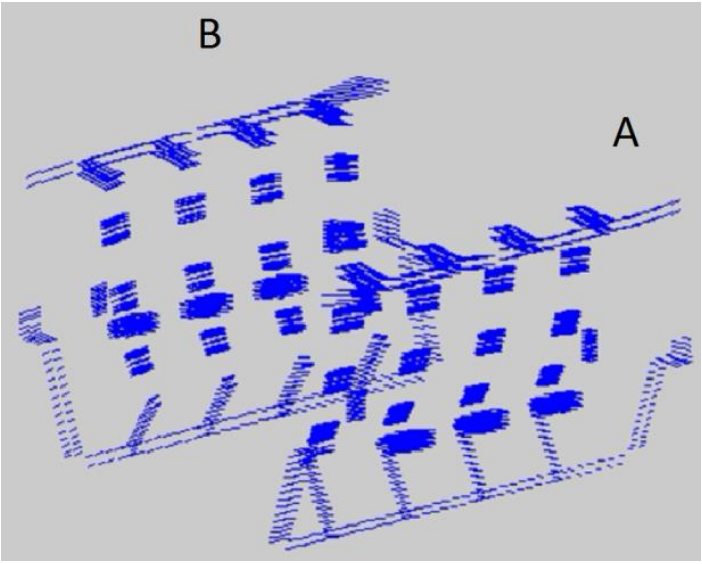

Figure 29. Nodal displacements of the cut boundries from an response analysis.

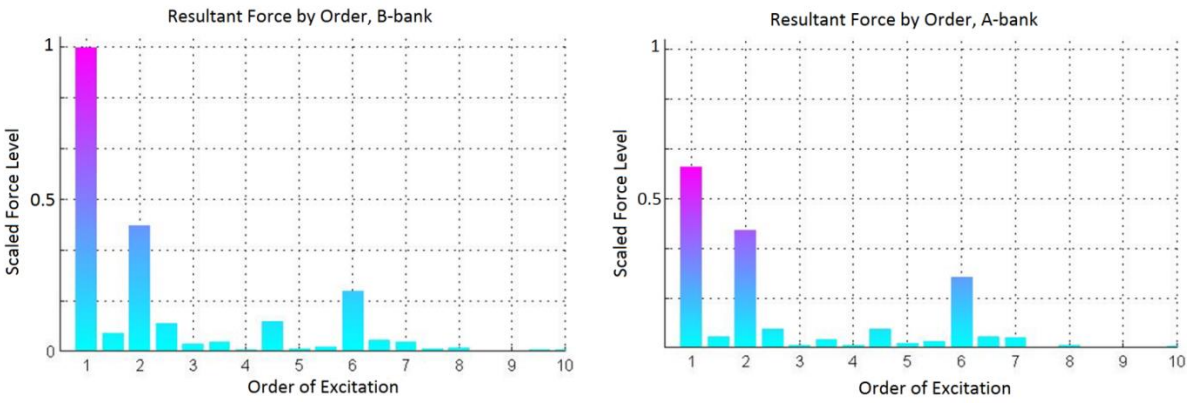

Figure 30. Reaction forces on the boundaries of the excitation model.

The maximum deformation of the attachment area at a critical excitation order was extracted in MATLAB from the complex valued data according to the following procedure;

- in Figure 31 a node is circulating on the unit circle.
- The phase angle ϕ where the peak amplitude of the nodal displacement was found, was used to idealize the data to form real valued, quasi-static boundary conditions for the topology optimization.

In other words, the components cos ϕ of the complex valued data are only used, see Figure 31.

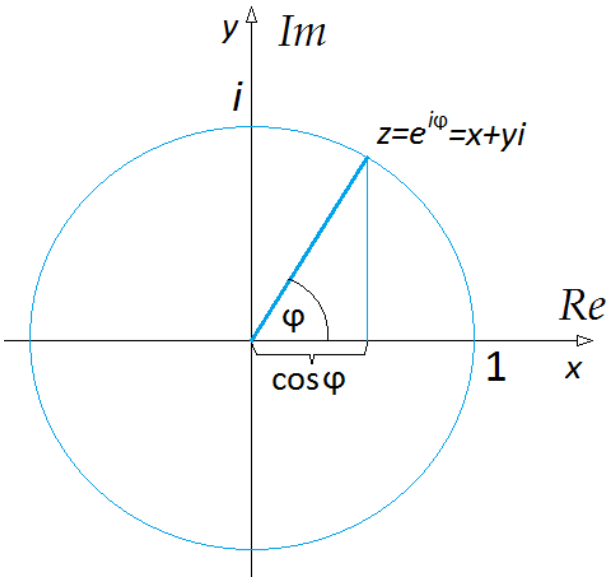

Figure 31. A node at z, circulating a unit circle.

As the meshes of the excitation analysis model and topology optimization model were not identical, the static nodal displacements from the excitation analysis were mapped over to the optimization model in the following manner:

a) Node sets were defined, according to Figure 32, both for the excitation analysis model and topology optimization model.
b) In the excitation analysis model, every node set was assigned a reference node. The coordinates of this node were calculated as the mean values of all node coordinates in the specific node set.
c) The displacements of all nodes in a node set were averaged to give the displacement of the reference node.
d) In the topology optimization model, RBE3 elements were created. The dependent nodes of these elements were created at exactly the same locations as the reference nodes of the excitation model. An RBE3 element and the dependent node are illustrated in Figure 28.
e) The displacements of all reference nodes of the excitation model were brought to the topology optimization model. These displacements were assigned to the dependent nodes of the RBE3 elements.
f) The RBE3 element averaged the displacement of the dependent node to the nodes of the node set.

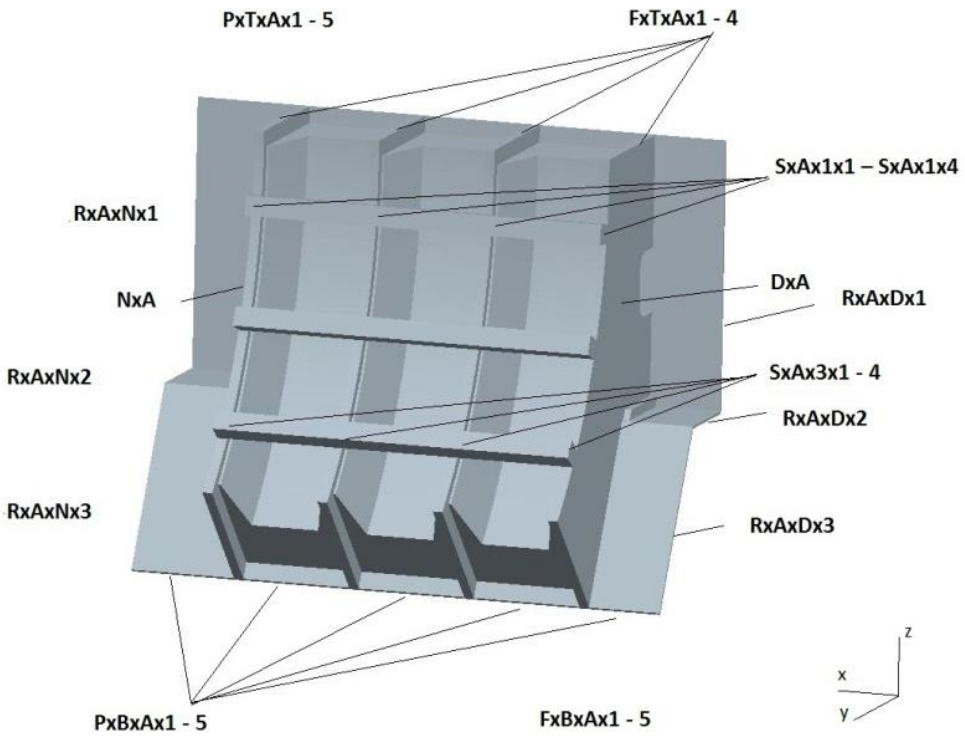

Figure 32. Node sets used in the FE-models, A-Bank.

An illustration of the displacement field mapping procedure is presented in Figure 33. In the figure on the right, the displacements of both attachment areas, A- and B-bank, of the excitation analysis model are illustrated. On the left the displacements of the B-side displacement field is mapped over to the optimization model using RBE3 elements. The procedure of extracting boundary conditions explained above is outlined in Appendix B.

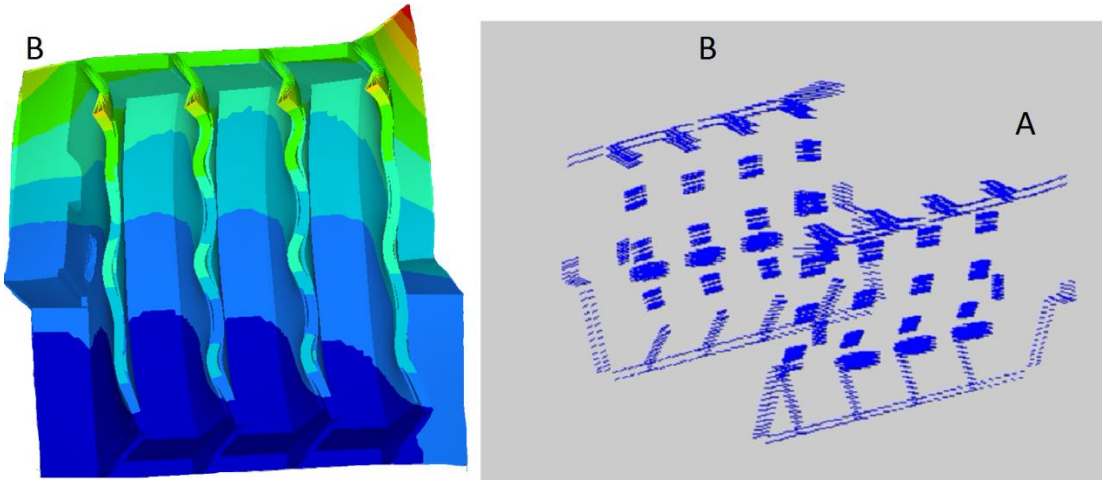

Figure 33. Displacement field mapping of the complex data (right) to static displacements of the optimization model (left).

After the topology optimization analysis the material distribution of the design domain changes and the stiffness, stress levels and displacements change accordingly. Thus the initial boundary conditions cannot be used to test the performance of the optimized structure. A proper test is to insert the new topology back in to the frequency response analysis and analyse it. However this process takes some time and the new topology is tested with more simple boundary conditions later on in a finite element analysis.

6.5 Load Cases

To get an idea of the severity of different excitation orders, nodal forces from the cut boundaries of the excitation analysis model in Abaqus were gathered in Figure 30. The conclusion from this figure is that the absolute force levels are somewhat higher on the B-bank nodes. Thus topology optimization was performed with static displacements from the B-side where the loading is more critical.

Excitation orders 1, 2, 4.5, and 6 were selected as critical frequencies for the attachment area. These orders, or frequencies of vibration, stand out from others orders in force level, see Figure 30. Appendix C illustrates the global movement of the cut-boundary nodes of the excitation analysis model at a given excitation order. The magnification of the amplitude of motion is the same in all figures.

Four load cases were formed according to the orders 1, 2, 4.5 and 6. To form a load case, the static displacement field of the attachment area at an order of excitation, was extracted and mapped on the topology optimization model, according to chapter 6.4. The load cases were given names LC1 (order 1), LC2 (order 2), LC3 (order 4.5) and LC4 (order 6). Topology optimization was performed for each load case individually and by combining them as is presented in the following. The general displacements and deformations of the generator are illustrated in a very simplified manner in Figure 34.

The force levels of orders 1 and 2 are high due to large inertia forces of the generator. At these orders the attachment area has little deformation in relation to the deformation of the generator frame and baseframe. The attachment area is said to move “rigidly” along with the generator.

At order 1 nodes of the attachment area translate mostly in Z-direction. The nodes of the generator FE-model would form a skewed ellipse trajectory, like in Figure 34.

At order 2 the nodes oscillate mainly in XZ-plane. The A and B bank oscillate with an opposite phase angle, so the generator frame has significant elastic deformation.

At order 4.5 the movement of the attachment area at this order is mainly translation of the nodes in Y-direction in opposite phases. Order 4.5 is of additional interest due to it being the ignition order of the diesel engine. In general the torsional excitations from the diesel engine are significant at this.

At order 6 the elastic deformation is mainly shear in XZ-plane. This order has a relatively high reaction force level and the displacement field in is assumed to be critical fatigue wise. For more figures of the displacement field see Appendix C, Figure 4

Scaled static displacement data used as BC’s in the optimization models are gathered in Appendix D and the named node sets in this data are illustrated in Figure 32.

Load case 1, order 1

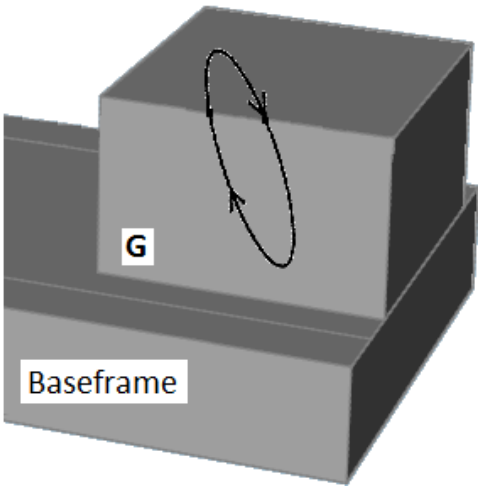

Load case 2, order 2

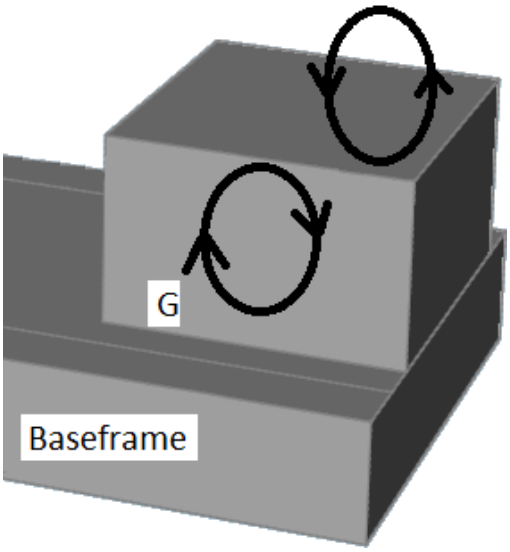

Load case 3, order 4.5

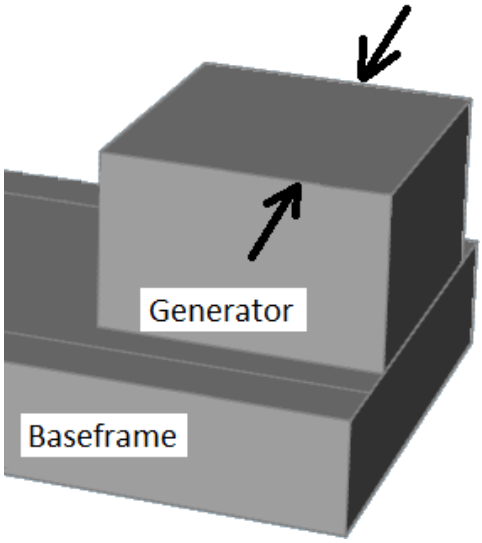

Load case 4, order 6

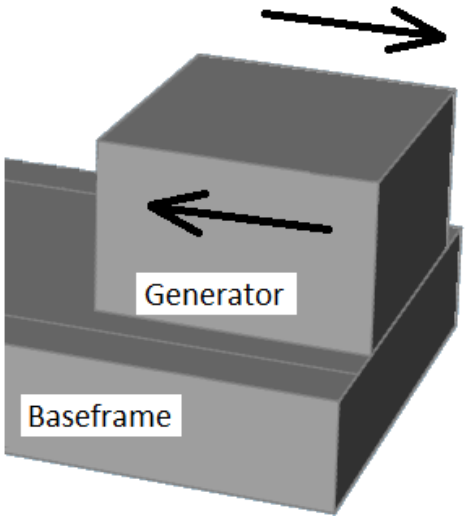

Figure 34. Simplified illustration of the generator frame deformations and displacements in the load cases 1 to 4.

6.6 Optimization Problems

In this work the optimal material layout for stiffness was sought with a given amount of material. The amount of material was limited to the same as in the original design. This facilitated the before-and-after type comparison of the structures and answers the question: "How much was the stiffness increased with approximately the same amount of material at hand."

6.6.1 Single Load Case Topology Optimization

As discovered in chapter 4, the computational effort is multiplied when parabolic elements are used. Thus linear element models are used initially to run topology optimization individually in all load cases, LC1 to LC4, with no additional constraints on e.g. symmetry. The results from these analyses give insight to the optimized material distribution and main load paths in each load case. This is vital information when features of the combined topology optimization are examined.

The optimization problem statement for these analyses was:

$$\text{maximize: } C = C_i = \frac{1}{2}\boldsymbol{u}(\boldsymbol{x})_i^T \boldsymbol{f_i} \qquad (6.1)$$

$$\text{subject to: } V(\rho) = \sum_{1}^{\mathrm{N}} v_e \rho_e \leq \bar{V} = 0.3 \qquad (6.2)$$

$$0 < \rho_{min} < \rho_e < 1, \qquad e = 1, \dots, \mathrm{N} \qquad (6.3)$$

$$\text{Where: } \quad C_i = \tfrac{1}{2}\boldsymbol{u}^t \boldsymbol{f_i}, \text{ with } \boldsymbol{K u_i} = \boldsymbol{f_i} \text{ or } \tfrac{1}{2}\int_V \boldsymbol{\varepsilon}^t \boldsymbol{\sigma} dV \qquad (6.4)$$

C_i is the compliance in a load case, f_i are reaction forces of load case i, $u(x)$ is the displacement field, N is the number of elements, V is the total volume of the model, $\bar{V}$ is the volume constraint value, v_e elemental volume, ρ is the relative density of the whole model, ρ_e relative element density and ρ_{min} is a minimum treshold for "void" elements.

As the displacement field stays constant, the internal forces of the optimized structure are increased with increasing compliance.

6.6.2 Combined Load Case Topology Optimization

In the combined load case topology optimization the structure is optimized with respect to all four load cases LC1 to LC4. Parabolic element models are used to obtain well defined structures.

The optimization problem statement used for these analyses was:

$$\text{maximize: } C_w = \sum w_{ij} C_i = \frac{1}{2} \sum w_{ij} \boldsymbol{u}(\boldsymbol{x})_i^T \boldsymbol{f_i} \qquad (6.5)$$

$$\text{subject to: } V(\rho) = \sum_{1}^{\mathrm{N}} v_e \rho_e \leq \bar{V} = 0.3 \qquad (6.6)$$

$$0 < \rho_{min} < \rho_e < 1, \qquad e = 1, \dots, \mathrm{N} \qquad (6.7)$$

Where C_w is the weighted compliance, w_{ij} are the weighting factor of analysis i and load case j, C_i Compliance of a load case, f_i are reaction forces of load case i, $u(x)$ is the displacement field, V is the total volume of the model, $\bar{V}$ is the volume constraint value, v_e elemental volume, ρ is the relative density of the whole model, ρ_e relative element density and ρ_{min} is a minimum treshold for "void" elements.

The above statement says that topology optimization of the structure with multiple load cases is a minimization problem of the weighted average of the compliances of each load cases. The load cases are weighted by factors, which are selected manually. The weighting of the load cases has a profound effect on the final solutions, so care must be taken when weighting factors are selected. The *weighted compliance topology optimization* is also referred to as *combined load case topology optimization* in the following text.

Four analyses were conducted. Each analysis consists of a *combined load case topology optimization* with specific weighting factors on the LC1 to LC4. This is illustrated in Table 6.

Table 6. Combined load case topology optimization: Weighting factors and compliances of different analysis.

Load case	Analysis 1		Analysis 2		Analysis 3		Analysis 4	
	W_1	Init. Comp.	W_2	W. Comp.	w_3	W. Comp.	w_4	W. Comp.
LC1	W_{11}=1	413.65	W_{21}=0.1	41.37	W_{31}=0.05	20.68	W_{41}=0.10	39.61
LC2	W_{12}=1	589.96	W_{22}=0.1	59.00	W_{32}=0.05	29.49	W_{42}=0.07	39.61
LC3	W_{13}=1	9.14	W_{23}=1	9.14	W_{33}=1	9.14	W_{43}=4.33	39.61
LC4	W_{14}=1	39.61	W_{24}=1	39.61	W_{34}=1	39.61	W_{44}=1.00	39.61

Descriptions of the analyses:

- Analysis 1 was conducted without any weighting of the load cases, i.e. w_{11} to w_{14} =1, or additional constraints on the optimization.
- Analyses 2 and 3 the highest compliances of LC1 and LC2 were brought to the lower magnitudes similar to LC3 and LC4.
  - Additional constraints were applied: symmetry in YZ-plane and a minimum member size of 0.036 units.
- Analysis 4 has same compliances in all load cases, compliance of LC4 serving as reference. Compliances, weighting factors and weighted compliances of the runs are presented in the Table 6.

The weight of the final optimization result will differ from the value given by "volume fraction constraint * density of the material"; this is because a varying density threshold is used to print out the optimization result. According to chapter 4.5, high density threshold values should be used. In the following optimization, the value ρ=0.8 was selected according preliminary tests, on which density threshold is suitable. Thus the weight of a topology optimization result may have about 10-20% less weight than given by the volume constraint. This variation in turn is affected by other optimization parameters that affect the amount of intermediate density elements.

7 Results

The resulting topologies of the linear and parabolic element model analysis at ρ>0.8 are presented in this chapter.

7.1 Single Load Case Topology Optimization, Linear Elements

Figure 35 illustrates the solutions of the linear element model runs. For more detailed figures refer to Appendix E.

In the result of load case 1 the material was mainly concentrated to the N-end, for reference see Figure 25, of the attachment area. Two thick plate-like areas were formed and they followed the stator circumference. These were connected in the area between stator fixing points, in x-direction, for reference see Figure 26. In y-direction supporting members stretched out to the attachment flange beyond the bolt line towards the exterior of the generator. Some material was also distributed in the area of the service hatch, behind the former frame plates. At the D-end some irregular material distribution was present. This is due to linear element formulation and checkerboarding.

Material distribution of the load case 2 was concentrated at the D-end and two plate-like structures were formed. These were connected in the area between stator fixing points, in x-direction. No supporting members were formed to the bolt flange area like in order 1. The result had some irregular material at the N-end of the model and a badly defined support for one lower stator attachment at the SxAx3x3 fixing point, for reference see Figure 32.

Solution of the load case 3 had mainly material above the attachment flange. Thick supporting members were formed to the attachment flange in y-direction. In this area the general material orientation seemed to be in (-1,0,1) in the global coordinate system, for reference see Figure 25. Only minimal material was distributed below the attachment flange, where also some irregular material distribution was present. N- and D-end attachments had reinforcements and were highly connected to surrounding material.

The results for the load case 3 and 4 shared many features. In load case 3 the material was concentrated above the bolt flange with no material below this level. The solution had very little irregular material distribution. All stator attachments above the attachment flanges and N- and D-end attachments were connected to surrounding material. Connectivity to the attachment flange is not as strong as in load case 4. Exceptional to other solutions was the hollow cavities that formed inside the domain.

An additional analysis was conducted in which the sign of the displacements was changed. This had no effect on the material distribution of the solutions.

Load case 1 - Order 1

Load case 2 - Order 2

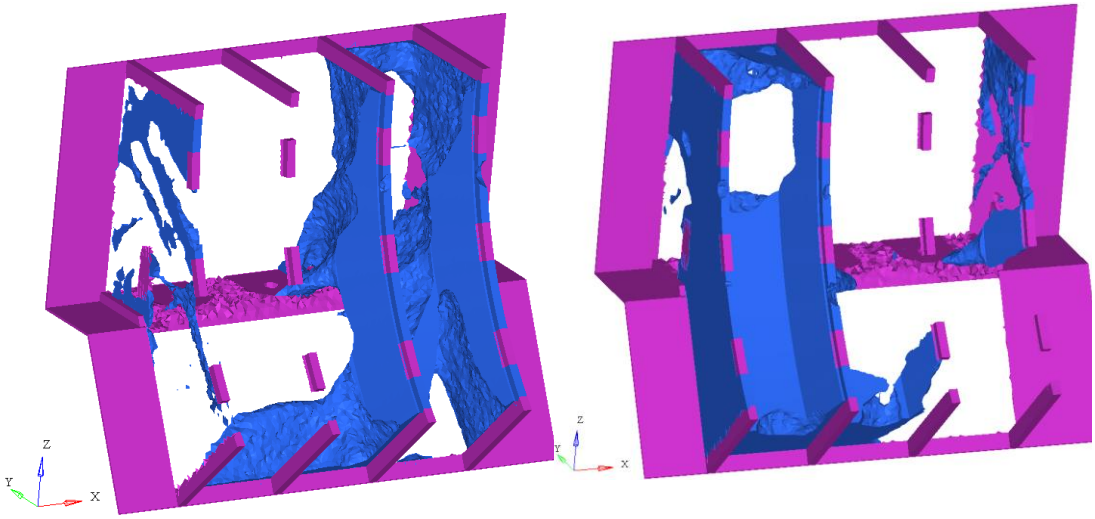

Load case 3- Order 4.5

Load case 4 - Order 6

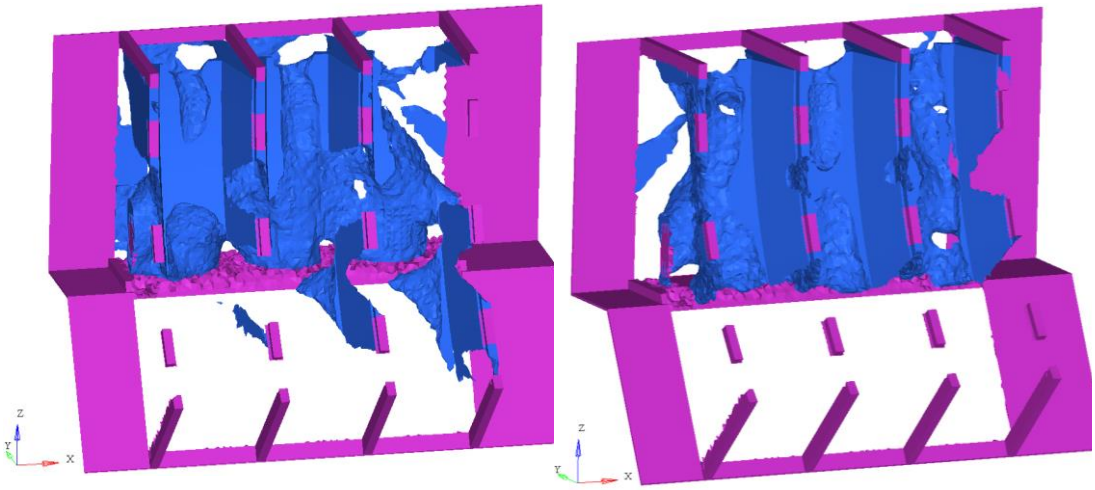

Figure 35. Single load case linear element model solutions, ρ>0.8.

7.2 Combined Load Case Topology Optimization, Parabolic Elements

As presented in Table 6 four analyses with different weighting factors were performed. The results of the parabolic element model analysis at ρ>0.8 were illustrated in the Figure 36 and Figure 37. The results are compared to the linear element model analysis results. For more detailed figures of the topologies refer to Appendix F.

Resulting topology of the analysis 1, without weighting factors, was somewhat irregular. The unconnectivity of the material in the Figure 36 is due to the high selected relative density threshold. The solution of load case 2 is dominant in the structure, i.e. at D-end of the design space. The influence of other load cases was hard to distinguish.

In the result of the analysis 2, in Figure 36, material was distributed mainly below the attachment flange, symmetrically about the ZY-plane. Higher compliances of load cases 1 and 2, see Table 6, most probably cause this emphasis in the material distribution. Upper middle stator attachments SxAx1x2 to SxAx1x3, see Figure 32, were connected to the frame plate non-design space probably due to the influence of load cases 3 and 4.

In the result of the analysis 3, in Figure 37, material was distributed above the bolt attachment flange and practically no material was placed below this level. The structure was connected to the attachment flange before or at the bolt line, which seemed to be characteristic for the load case 4. No support members extended beyond this line as in the linear element solution of the load case 3. The structure has internal cavities and the dominance of the load case 4 is evident in the solution. The compliance of this load case was the highest in the analysis.

The solution of the analysis 4, in Figure 37, shared many features with the solution of the analysis 3, but at N- and D-end material was also extended up to the lower stator attachments and frame plate non-design space. This seemed to be characteristic of the load cases 1 and 2. Elsewhere material was mainly distributed above the attachment flange. The compliance of all load cases had been scaled to the same value, but load case 3 and 4 seemed to define the structure above the attachment flange. Unlike in the analysis 3 supporting members extended further into the attachment flange from the middle area of the design space, which was characteristic of the load case 3. In general the solution consisted of thinner and individual support members than in the solution of analysis 3.

Analysis 1:
Combined compliance, non-weighted.

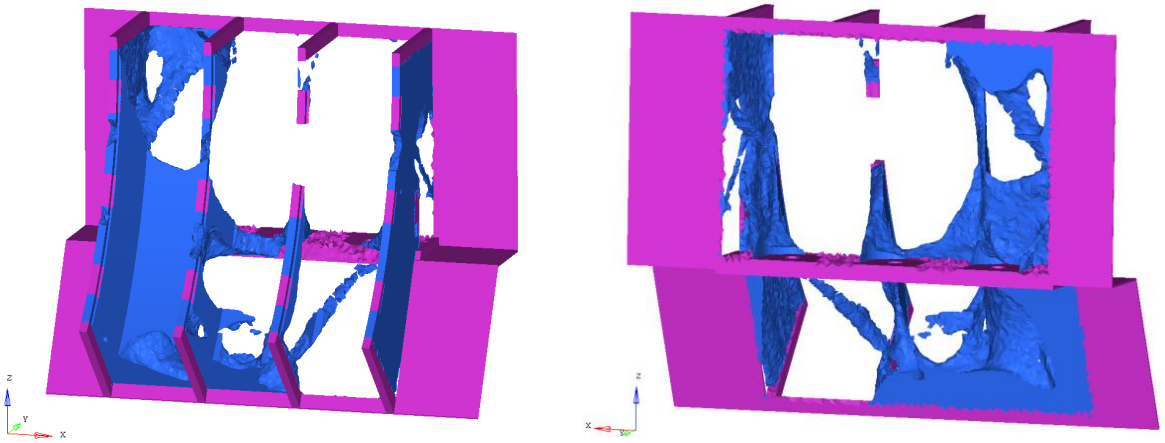

Analysis 2:
Combined compliance, w_1, zy-sym.

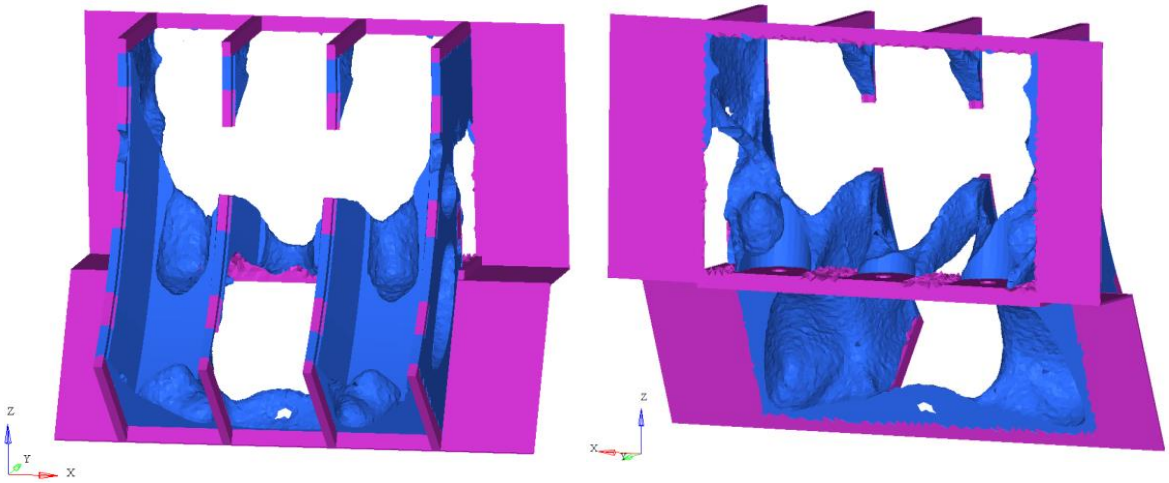

Figure 36. Parabolic element model solutions for combined load case analyses 1 to 2, ρ>0.8

Analysis 3:
Combined compliance, w_2, zy-sym.

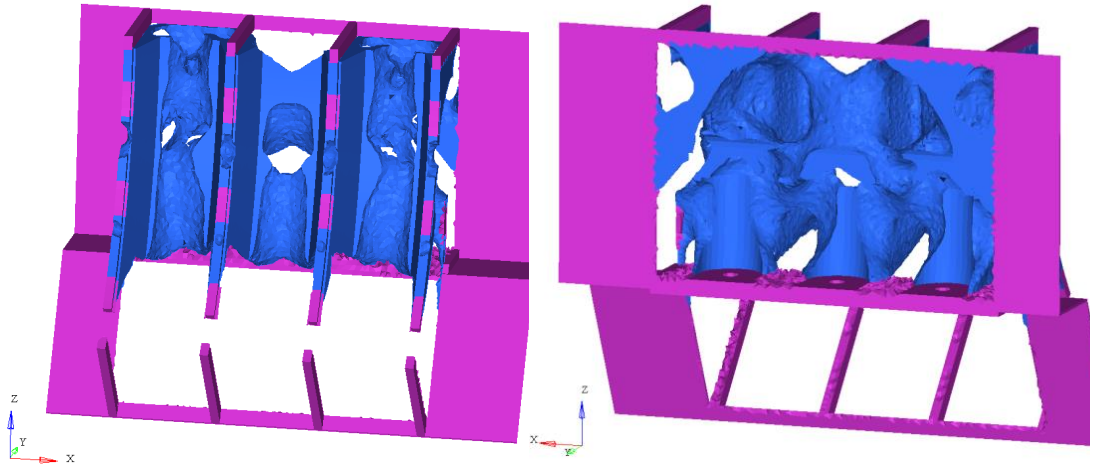

Analysis 4:
Combined compliance, w_3, zy-sym.

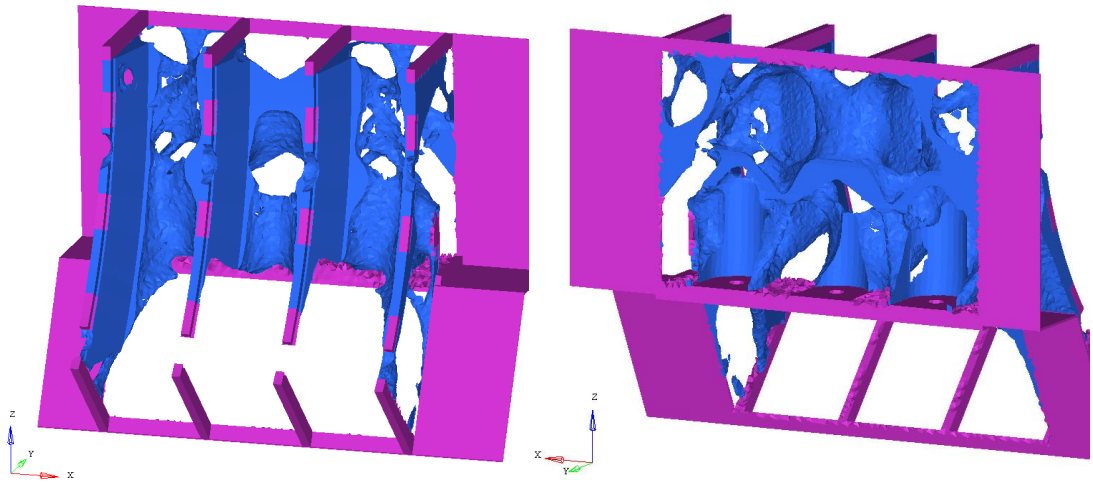

Figure 37. Parabolic element model solutions for combined load case analyses 3 to 4, ρ>0.8

7.3 Concluding Remarks on the Topology Optimization

The linear element models served as good references for the combined compliance analysis. With the results of the linear element models it was possible to detect presence of the load cases 1 to 4 in the solutions of the combined compliance analysis with parabolic elements.

Combined compliance analysis 1 and 2 were highly dominated by load cases 1 and 2. Should these topologies be suggested as the feasible design for the generators attachment area would the result probably have been very unoptimal in loading conditions similar load case 3 or 4. Also the linear element solutions for load cases 1 and 2, and the combined compliance analysis 1 and 2 indicated that near optimal topologies for these loading conditions would comprise of plate-like structures. Dominant features in the mentioned cases were plate structures that expanded over the design domain, along the stators circumference. This configuration was similar to the original design of the original construction, i.e. welded steel plate generator frame. This indicates that a plate-like design would perform well in loading conditions LC1 and LC2.

Results of the combined compliance analysis 3 and 4, with more weighted compliances, were similar in many features. In general the load case 4, i.e. order 6, seems to dominate the final topology in both cases. The solution of the analysis 3 was more robust in design and comprised of thicker members everywhere in the design space. This is because in this analysis the weighting of the LC4, had the highest effect on the topology, see Table 7. This resulted in a stable and robust topology. When analysis 4, where all load cases have the same effect on the final topology, is compared to the solution of the analysis 3, this topology is a compromise between all load cases. The structure appears to be less robust and comprises of more detailed and slender supporting members. Noticeable difference is the longer extending supports at the bolt flange, at the back of the attachment area.

As a conclusion it proved to be tedious to find a topology optimization solution, comprising all load cases in the final optimization result. The variation of the weighting parameters would have required an optimization of its own to examine more combinations of load cases. The solution of the analysis 3 is selected as feasible solution for the reality however. It represents most of the load cases and especially the fatigue critical LC4, order 6, is dominant. Based on previous experiences from the generators operating environment and cyclic loading this is beneficial. The solution from this analysis needs some modifications, however to fit in the generator frame; the frame plates have to be extended to the bolt flange level. As mentioned above in this paragraph, plate-like structures in these areas seem to be beneficial in load cases 1 and 2.

8 Analysis of the Suggested New Topology

Figure 38 presents the result of the thesis. It is a manually modified and near optimal topology for the considered four load cases. The performance of the structure is analysed in this chapter and its features are discussed.

The structure is based on the solution from the analysis 3, but with plate-like extensions from the attachment flange downwards. Ideally and according to the solution of analysis 4, the topology would also have more reinforcements at the attachment flange in the y-direction, Figure 38, on the right. However at the time the model was created, the author did not have the results from analysis 4. As mentioned in chapter 6.6 due to the density threshold value ρ=0.8, the analysis 3 solution has less weight than in the original structure. After adding the frame plate extensions to the structure in Figure 38, the weight of the structure is 108.5% of that of the original structure.

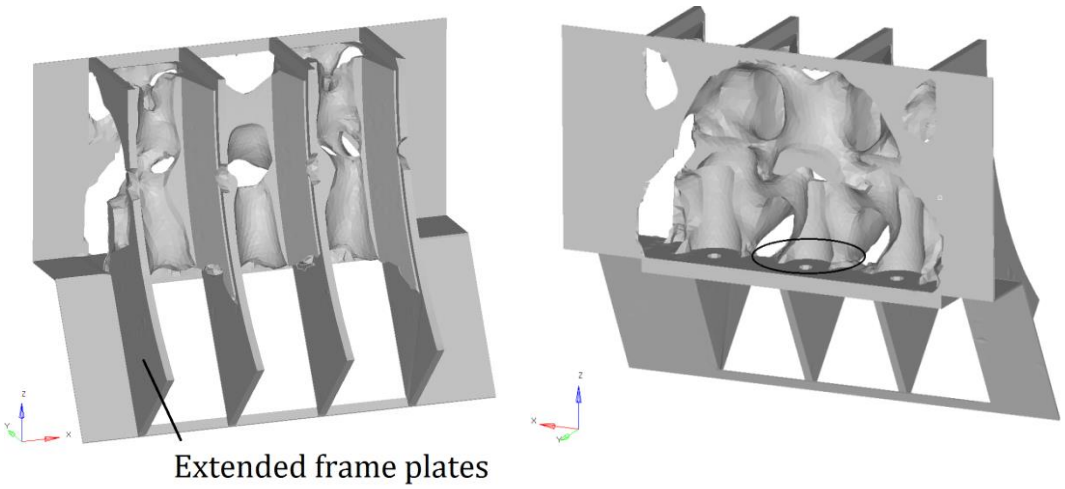

Figure 38. Suggested new topology for the generator attachment area.

8.1 Finite Element Analysis of the New Topology

The finite element model comprised of 148803 parabolic tetrahedral solid elements and had 770388 DOF. The model was attached rigidly from the bottom of the attachment flange at all nodes.

Four static load cases were defined to compare stiffness changes of the optimized structure to the original one. The load cases are illustrated in Figure 39. Simple unidirectional displacements were used in the load cases to facilitate the extraction of reaction forces, their components and the comparison of stiffnesses between the original and the new topology.

In load case 1 all nodes on the xy-plane of the upper frame plate extensions are forced to displace $6x10^{-4}$ units in the positive x-axis. The purpose of this load case is to demonstrate the distribution of shear stiffness in x-direction. Probably the stiffness increase in load case 2 is higher than in load case 1.

In load case 2 stator fixing points in the lines SxBx1 and SxBx2, see Figure 32, are forced to displace $6x10^{-4}$ units to the positive x-axis. This load case corresponds well with the loading condition of the order 6 in chapter 6.5.

In load case 3 all stator fixing points are forced to displace $3x10^{-5}$ in the positive y-axis. This load case demonstrates the performance of the structure in a loading condition similar to order 4.5 in chapter 6.5.

In load case 4 all stator attachments the top frame plate ends are displaced $3x10^{-5}$ in the negative z-direction. This load case demonstrates the performance of the structure in a loading condition similar to order 1 and 2 in chapter 6.5.

Both the original and the optimized structure were analysed in the aforementioned load cases. The reaction forces from the support nodes were printed out and equivalent stiffness of the structure were calculated in all directions. In addition stress data was extracted from the analysis.

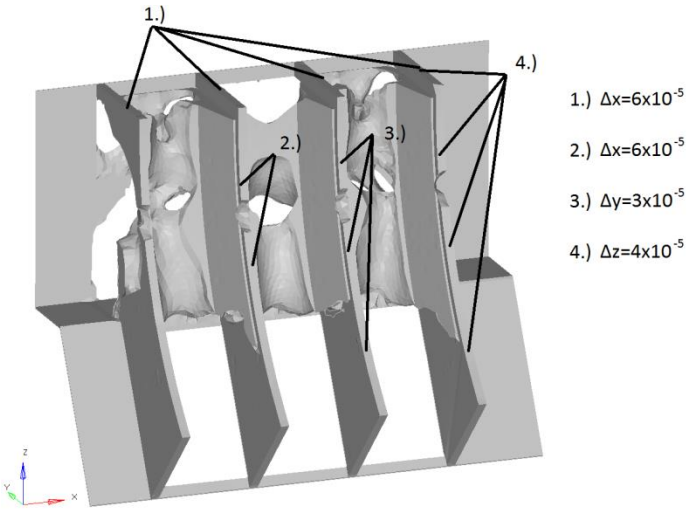

Figure 39. Forced displacements in the analysis of the new topology.

8.2 Static Analysis Results

Table 8 presents a comparison of the stiffness in various directions. Low stiffnesses with values lower than 10^{-2} were ignored in the comparison in order to obtain reasonable results. Results of the stress analysis of load cases 1-4 and more detailed stiffness calculation data is presented in Appendix G. Lower index 1 refers to a stiffness value of the new topology, Kx_1 being the stiffness in x-direction for example. The results of Table 8summarised:

a) In load case 1 the optimized structure had 3.8 times the stiffness of the original structure in x-direction.
b) In load case 2 the optimized structure had 6.5 times the stiffness of the original structure in the x-direction.
c) In load case 3 the optimized structure had 1.6 times the stiffness of the original structure in the y-direction.
d) In load case 4 the optimized structure had 0.7 times the stiffness of the original structure in the z-direction.

Table 8. Stiffness Comparison, Optimized vs. Current Structure.

Directional stiffnesses	Load Case1	Load Case 2	Load Case 3	Load Case 4
Kx_1/Kx_2	3.78	6.50	0.00	0.00
Ky_1/Ky_2	0.00	0.00	1.55	0.00
Kz_1/Kz_2	0.00	0.00	0.00	0.73

The FE-mesh of the new topology was rough from the topology optimization, and had high stress regions. The general stress state and regions of high stress in the component are examined rather than singular element stresses, thus averaging of the von Mises stress was used. Stress analysis figures are presented more detailed in the Appendix G.

In load case 1 the shear loading is distributed quite evenly to the support members and onwards to the attachment flange. Concentrated stress regions are found between the middle frame plates near the loading points and also at the junction of the attachment flange and side plates.

The stress analysis results of load cases 2 and 3 indicate that connection to the attachment flange will have concentrated stress regions. Reinforcements like in the solution of the combined compliance analysis 4, of chapter 7.2, would have facilitated this situation. The reinforcements would have distributed stresses further into the attachment flange.

In load case 4 stresses are distributed in wide areas, but clear concentration of stress is seen near the upper frame plates and at the junction of the support members to the attachment flange. This indicates that uniform plate-like structures along the stator circumference indeed would be good load carrying structures in this case. Also the reinforcements that were discussed above would distribute stresses into the attachment flange more evenly.

Load case 1, Δx=6e-4

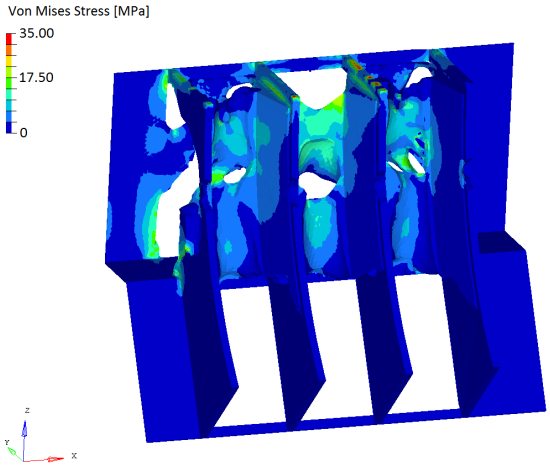

Load case 2, Δx=6e-4

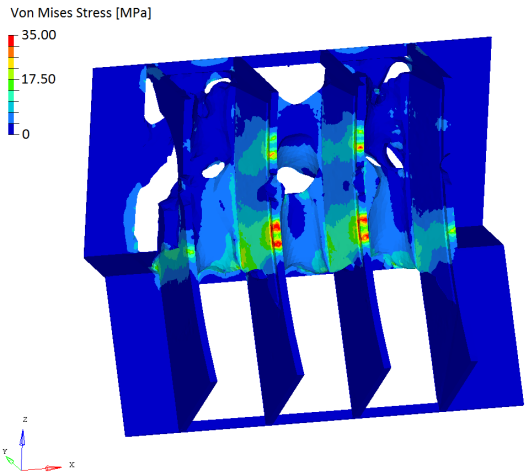

Load case 3, Δx=3e-5

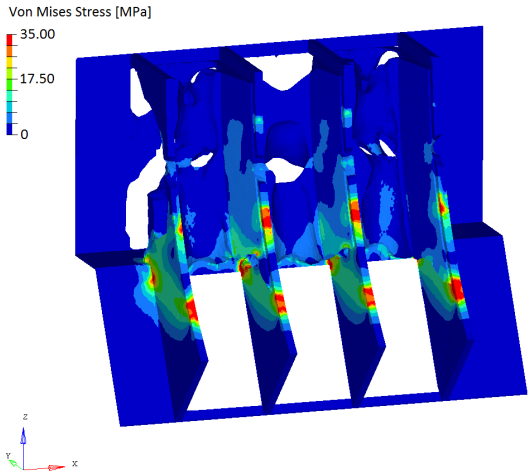

Load case 4, Δz=3e-5

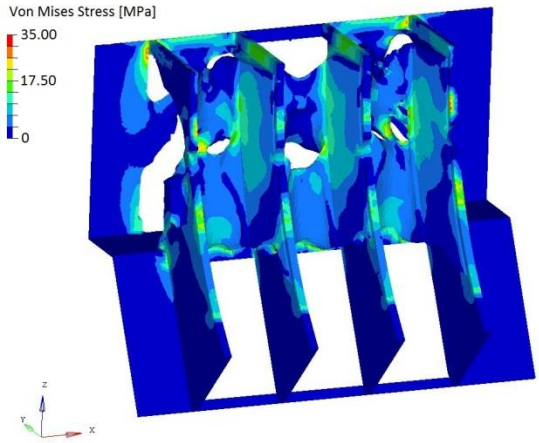

Figure 40. Von Mises Stress analysis results of the new topology.

9 Discussion

In this chapter the scope and results of the thesis are analysed according to the demands of the generators operating environment. Other possible approaches or interesting analyses are presented and compared to the ones used in the thesis.

This discussion is followed with an introduction to ways of working with the topology optimization method and outlines some suggestions for future research. An example workflow for a product development procedure utilizing topology optimization as an integral part is presented. The procedure starts with a concept and results with a near optimal component for engineering applications. The chapter also presents an example CAD geometry made from a topology optimization result of the thesis.

9.1 Outcome of the Optimization

The stiffness of the optimized attachment was increased in load cases 1 to 3 in chapter 8.2, especially in load case 3 a 6.5 time stiffness increase is considered significant. This result demonstrates the potential of the topology optimization method. The fatigue strength and allowable stress amplitudes of the new topology will be at least double as presented in Chapter 5. On behalf of these load cases and the fatigue strength study the objectives of the thesis was obtained.

The result of load case 4, however, revealed a 27% decrease in stiffness in a loading condition mimicking excitation orders 1 and 2. Earlier topology optimization in Chapters 7.1 and 7.2 indicated that the best structure for the orders 1 and 2 would be plate-like or beam structures along the stators circumference. As these structures are not dominant in the tested topology, its performance was lower in the load case 4, than in the case of the original attachment area. This fact and the stress concentration regions at the attachment flange, mentioned in Chapter 8.2, indicate that the proposed new topology should undergo some modifications, if stiffness in this load case should be increased and stress concentrations lowered. These modifications include extensions of support members longer onto the attachment flange, like in the solution of analysis 4 of Chapter 7.2, and smoother junction of the lower frame plates into the attachment flange, see Figure 41.

The changed stiffness characteristics of the model will affect its dynamic behaviour as a part of the genset. The frequency response analysis of the genset with the new topology is outside the scope of this thesis, but it would reveal important information on how the attachment area performs in its operating environment.

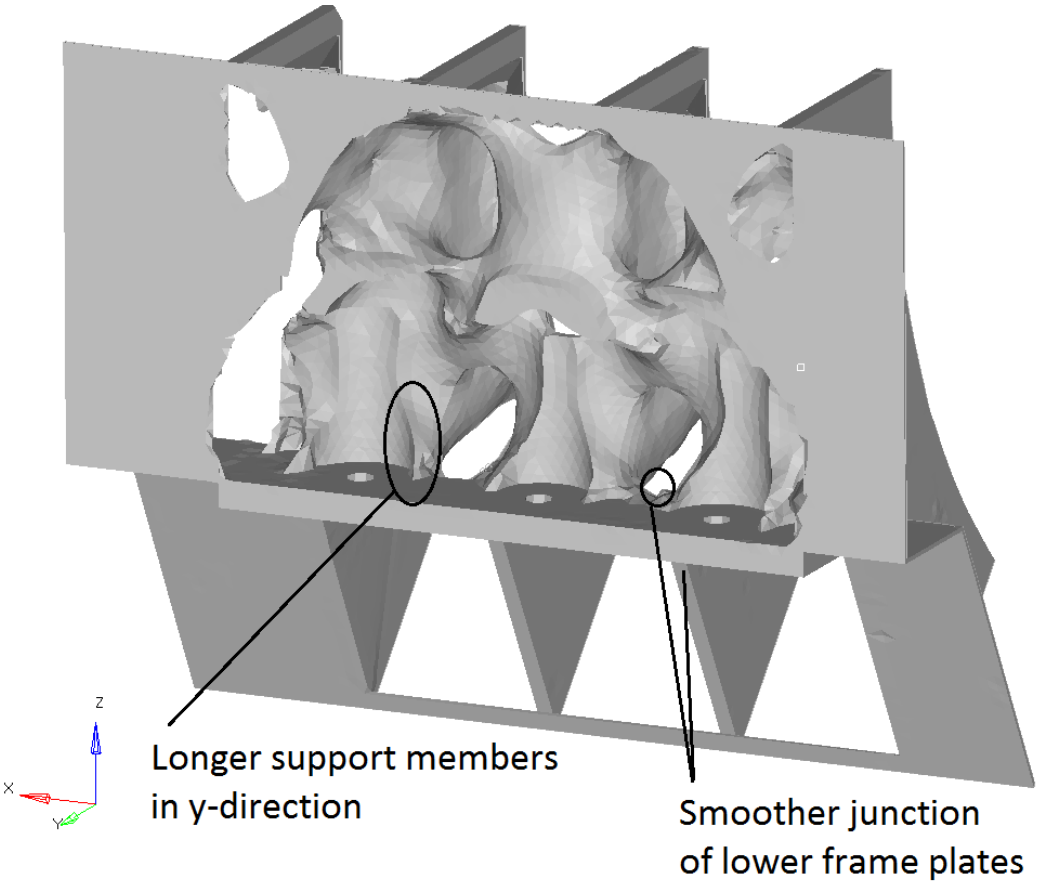

Figure 41. Possible modifications of the new topology.

9.2 Alternative Approach

In the presented optimization setup much effort was put into extracting static displacements from complex valued frequency response data. Due to the idealization of using the real part of the complex displacement data some information was lost during this extraction. The used load cases, in Chapter 6.5, represent the approximate deformation of the generator attachment area during operation at different frequencies.

Changing sign of the static displacements was attempted in order to get topologies representing an optimized structure from loadings with a 180 degree phase angle difference. This however had no effect on the optimization which is not surprising; the topology optimization method relies on linear elastic material behaviour and changing the sign does not affect the response of the structure. Instead the used static displacements should have been extracted with 180 degree phase difference from the excitation analysis model.

An alternative, simpler approach might have been just to study differences of the deformations of the frequency response model at different orders of excitation. According to this information, simplified unidirectional or varying direction load cases might have been formulated, similar to ones that were made in Chapter 8. This approach would have saved enough time to run both the topology optimization and the frequency response analysis of the genset with the modified attachment area.

9.3 Ways of Working With the Method

Topology optimization is a conception approach which, in an ideal situation, is a part of a product development procedure. The method is readily applicable to situations where very little a priori knowledge of the structure is at hand. If main dimensions, loading and boundary conditions are known, the method offers an appealing way to search feasible structures. Figure 42 presents how an initial guess with a simple design domain leads to a topology optimization result and to a 3D printed part. Figure 42a shows the boundary conditions, loading and symmetry planes in red. Figure 42b is the result of a static maximum stiffness topology optimization with 20% volume constraint and Figure 42c is a 3D printed part from the result.

a.) b.) c.)

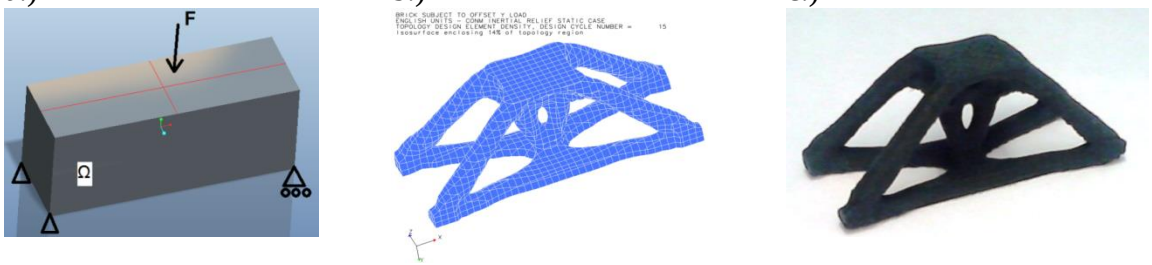

Figure 42. Steps from model to 3D printed part. a.) Design space, BC's and loading, d.) topology optimization result 20% volume fraction, c.) Plastic 3D printed part.

On the other hand the method may be applied to structures that are very well defined and critical loading conditions can be stated. In this case the result might be an updated structure, with less material and superior performance with regard to the optimized condition. However, it requires a systematic approach and simultaneous the use of multiple software to re-engineer a component.

Once the structure has been modelled and a suitable optimization set-up is ready, multiple optimization runs have to be conducted in order to be able to find feasible structures. These results of are often complicated and branched, which is many times the case in near optimal structures as they consist of regions with various purpose supporting members; compression-tension members or meshed structures, for reference see for ex. Figure 14. The actual topology optimization result is not likely feasible to be used as such in real life. This is due to the limitations of many manufacturing methods. Additive manufacturing for example provides an interesting alternative in many cases, like in Figure 42 where the topology optimization result was manufactured directly without any postprocessing of the model.

When conventional manufacturing methods, such as casting, machining of forging are regarded, the use of manufacturing constraints of the software facilitates the reproduction of real life geometries in most cases. Typically also these solutions require further modifications before the structure is manufacturable. The constraints might also suppress some interesting topologies. Thus initial optimization runs with minimal manufacturing constraints are recommended.

OptiStruct lacks proper tools for geometry synthesis from topology optimization results. The current approach requires simultaneous usage of different software. At the moment a CAD-file exported from OptiStruct consist of thousands of faces and manipulation of the geometry with common CAD tools is troublesome. One solution to select only a few faces from critical support members or conjunctions of the topology optimization result to be exported into STEP or IGES file. These faces serve as reference for forming the actual CAD-geometry of the final part. This procedure is also recommended by topology optimization professionals at Altair and surprisingly seems to be the most effective one, though still tedious.

The finished CAD model will then be meshed for FE analysis which reveals critical areas of the model are recognized, like hot-spot stress regions. With this information a suitable shape optimization could be constructed; minimizing the maximum Von Mises stress with a volume constraint for example. Shape optimization is ideal for finding right member sizes or roundings to enable good performance in working environment. The optimization result has to be once again reformulated in CAD. At this point shape optimization results, however, are easier to deal with than branched topology optimization results. To bear in mind is that producing a manufacturable part from optimization results contributes to the unoptimality of the final suggested part; manufacturable part is a near optimal structure based on a near optimal solution. The final outcome is a near optimal structure for real-life working environment.

An example CAD-geometry was produced from a topology optimization result to illustrate what the structure might look like in CAD after some modifications. The outcome is presented in Figure 43. The presented CAD part would still require fine tuning of features, FE analysis to determine structural response and possibly shape optimization to reduce stress concentration. These however were left out as the scope of this thesis is the topology optimization of the attachment area and not the post-processing. More figures can be found in Appendix H.

a) Result of analysis 4, Design space elements.

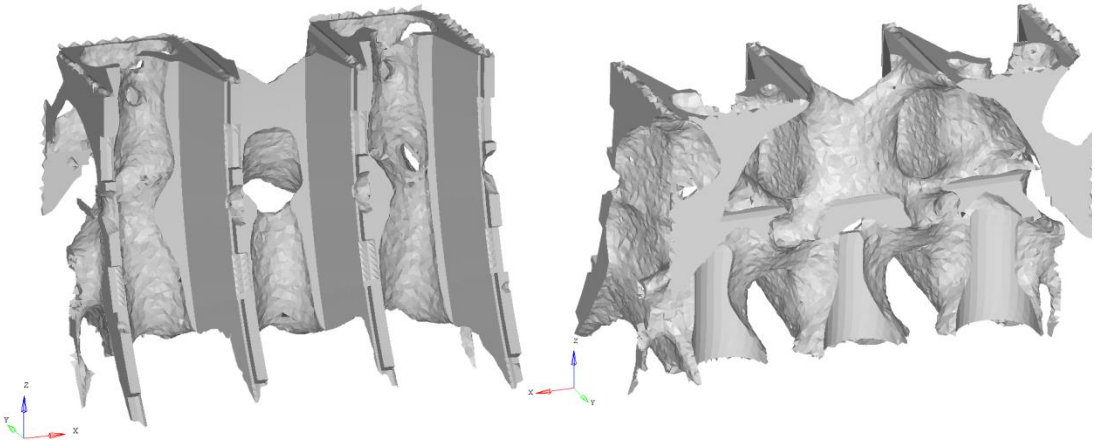

b) Example CAD-model.

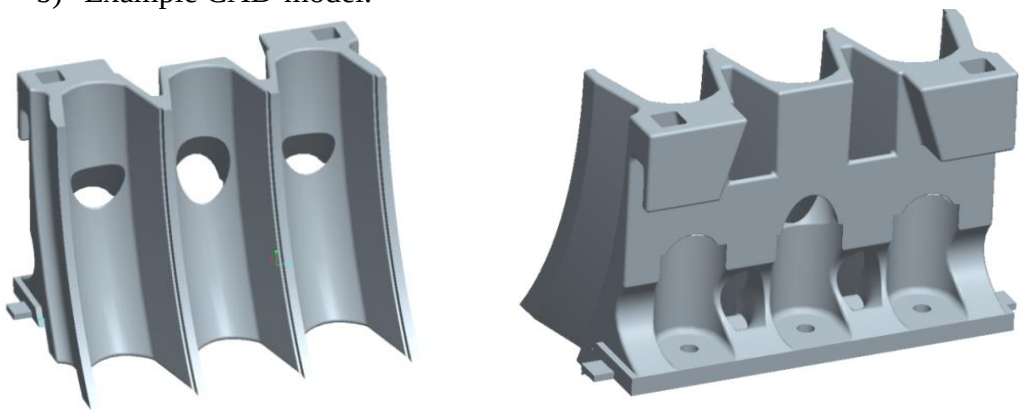

Figure 43. Converting topology optimization solution into a CAD-model.

9.4 Workflow from Concept to Component

The following procedure describes generally the workflow to get from concept to component.

1) Building the design space in CAD or in FE-software
    a. Main dimensions, loading conditions. Design / non-design space definitions.
    b. FE discretization according to the needs of the topology optimization.
2) Topology Optimization
    a. Defining the optimization set-up, what is optimized, what is critical at which cost and constraints?
    b. Use of additional constraints. Are they needed yet?
    c. Running multiple topology optimizations. Screening sensitivity for boundary and loading conditions. Fine-tuning optimization parameters.
    d. Selecting the feasible structure.
3) FE analysis
    a. Examine the topology optimization results in various analyses. Obtain data from the performance of the structure.
    b. Recognise critical load paths and member sizes etc.
4) Building the CAD model
    a. Remove non-manufacturable and noncritical members and branches of the mesh. Remove most of the finite elements that are not needed to describe the structure.
    b. Reserve elements in critical load paths and at conjunctions.
    c. Export in CAD format & read-in CAD software.
    d. Building CAD features with the aid of the remaining element faces.
    e. Remove the original element faces.
    f. Main dimension check: volume, mass, member sizes, angles of load carrying members etc.
5) FE reanalysis
    a. Import the CAD geometry to FE software.
    b. Mesh and run FE-analysis for stresses / displacements according operating environment.
    c. Examination of results, Hot-spot recognition.
6) Shape optimization in optimization software.
    a. Import the FE-model to optimization software.
    b. Building a suitable optimization set-up according to 5c. Example: [objective: Min(Max Von Mises), constraint: $0.9< V_{tot} <1.1$)]
    c. Set appropriate design variables in the elements/nodes in the regions of hot-spots.
    d. Define move-limits, move directions, additional constrains for the optimization.
    e. Optimize for stresses, deflection etc.
    f. Examine results and compare the performances.
    g. Export in a CAD format.
7) Final adjustments in the CAD software.

9.5 Proposals for Future Work

The use of topology optimization as a part of a larger optimization setup for example is attractive, as this enables screening of solutions with different parameters. For example in optimizations like in this thesis finding the right weighting factors might have been done in another optimization loop.

Figure 44 illustrates the implementation of Topology Optimization n in another optimization loop. The topology optimization model would have to be parameterized; i.e. main dimensions or loading directions or discretization of the mesh. The higher optimization loop could then vary loading direction, volume fraction constraint or compliance weighting parameters. Objectives and constraints of this higher optimization setup could be minimizing mass with multiple displacement constraints in various load cases.

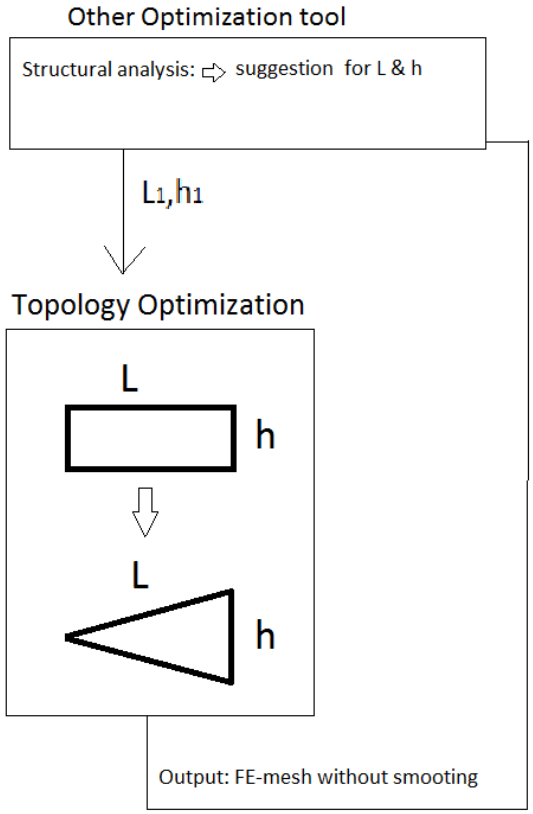

Figure 44. Topology optimization as a part of a higher optimization loop.

To test effects of the initial constraints of the topology optimization of the thesis a short combined compliance test analysis was performed with the load cases of Chapter 6.5 and scaling factors for compliances of the analysis 4 were used. The model presented in Figure 45a. It had no space requirements on the design space, i.e. for e.g. ventilation. The design space is the elements in blue, and non-design space is the elements in purple. A symmetry constraint in YZ-plane and a volume fraction constraint of 40% were applied. The same load cases and scaling factors for compliances were used as in analysis 4.

The result in Figure 45b indicates interesting aspects for future analysis; initial optimizations should be run also with minimal space requirements. In this case the result indicates, that the ventilation duct cross should be closed in the middle area of the stator fixing points to maximize stiffness. Also according to the solution lead-through space requirement would not needed in the optimization.

a.) b.)

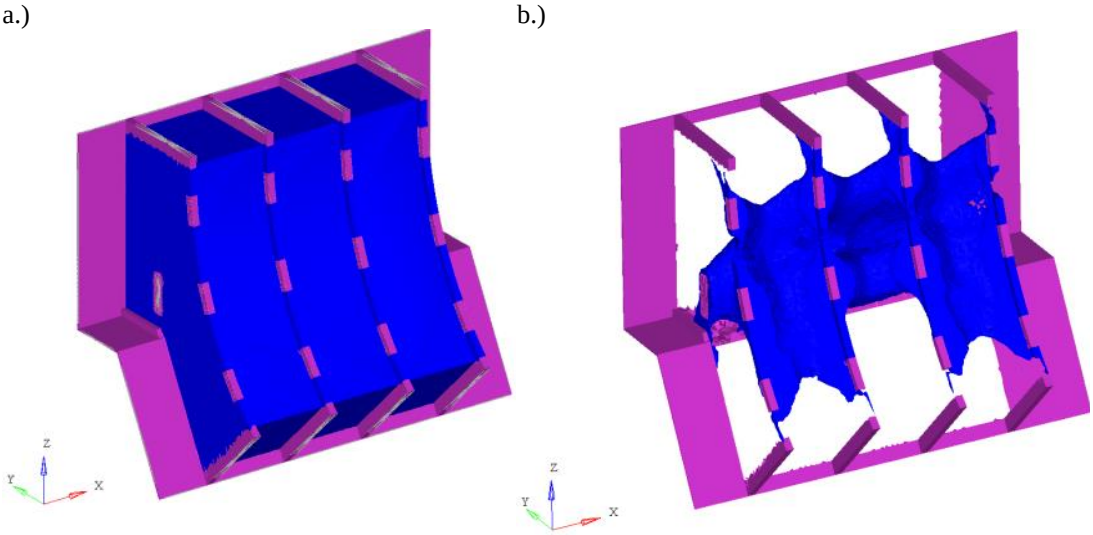

Figure 45. Topology optimization with minimal constraints. a.) Optimization model, b.) Result, ρ>0.8.

10 Conlusions

In the benchmarking optimization analysis OptiStruct performed well and converged to near optimal topologies. Checkerboarding is an issue with linear element models and parabolic elements formulation should be used. Linear element models, however, can be used for initial analysis. For relative density $\rho>0.5$ values should be used in post processing in order to obtain structures that are well defined and have clear load paths.

The solutions of OptiStruct can hardly be named optimal as there is no guarantee of the optimality of the solutions in non-linear optimization, and as the solutions of the software were only similar to the known optimal ones. Topology optimization method is very sensitive to boundary conditions and the initial state of the optimization problem strongly affects the result. The solutions should be called "near optimal" or "optimized" in this context. OptiStruct's additional constraints resulted in better defined solutions. Thus some symmetry and minimum member size constraints were used in the actual topology optimization of the thesis.

In Chapter 7.1 initial analyses with linear element models, without combining compliances in the objective function, gave a good insight to different solutions of the applied load cases. This information facilitated decision making in the combined compliance analysis with parabolic elements in Chapter 7.2.

First combined compliance parabolic element model solutions were dominated by few load cases and the outcome would not have been optimal in the operating environment of the generator. Scaling of the compliances of the load cases was needed to obtain a feasible structure in the generators working environment. Two structures with similar features were found. Based on the result from analysis 3 and experiences from the linear element model analysis a new model was constructed and tested in a FE analysis. The analysis showed significant stiffness increase in critical loading conditions. Although the model has some stress concentration regions, allowable stress range in fatigue calculations can be at least doubled when compared to the original structure. This is because there are no welds in the critically loaded areas. The presented structure is a combination of different features from the optimization analysis. The structure lacks some supporting members in the bolt flange area due to shortage of information at the time the model was constructed, but improvements are presented.

Running topology optimization as a part of a bigger optimization loop with a parameterized topology optimization model is suggested for a future research topic. This approach would provide some interesting benefits for example in finding the optimal weighting factors or volume fraction constraints. Also the examination of the generator attachment area with minimal initial space requirements or manufacturing constraints might give an interesting insight on how to distribute material in coming concepts of the attachment area.

REFERENCES

ABB Finland Homepage. [Referred 8.4.2013] Available: http://www.abb.fi/cawp/fiabb251/49ec18cae8cea8b1c12575bc002a085e.aspx

ABB Brochure: Motors & Generators. Synchronous motors. High Performance in all Applications. 9AKK105576 EN12-2011

Altair HyperWorks Help. [Referred 10.4.2013]. Available: http://www.altairhyperworks.com/hwhelp/Altair/hw12.0/index.aspx

ASM International. (1978). Metals Handbook Volume 1. Properties and Selection: Irons, Steels, and High-Performance Alloys. 9th Edition. Ohio, United States: American society for metals. ISBN: 0-87170-007-7. p. 393

Bendsøe, M.P. Sigmund, O. (2003). Topology Optimization. Theory, Methods and Applications. Berlin Heidelberg, Germany: Springer-Verlag. ISBN 3-540-42992-1.

Christensen, Peter W. Klarbring, A. (2008). An Introduction to Structural Optimization. Berlin Heidelberg, Germany: Springer-Verlag. ISBN-13: 978-1402086656

DeRose, G. C. A. Jr., A. R. Díaz. (2000). Solving three-dimensional layout optimization problems using scale wavelets. Computational Mechanics 25:274 – 285. DOI 10.1007/s004660050476

Dowling, N.E. (1999). Mechanical Behaviour of Materials. 2nd Edition. New Jersey, United States: Pentrice Hall. ISBN 0-13-905720. p. 362.

FKM, Forschungskuratorium Maschinenbau e. V. Festigkeitsnachweis nach der FKM-Richtlinie. Frankfurt am Main. [Referred 10.4.2013]. Available: http://www.fkm-net.de/fkm-richtlinien/index.html.

International Institute of Welding. (2008). Recommendations for Fatigue Design of Welded Joints and components. IIW document IIW-1823-07. p. 41-21, 46-61. [Referred 10.4.2013]. Available: http://www.iiwelding.org/Publications/BestPractice_Statements/Pages/C-XVBestPracticeDocuments.aspx

MET, Metalliteollisuuden keskusliitto. (2001). Raaka-ainekäsikirja. Valuraudat ja valuteräkset. Helsinki, Finland. Metalliteollisuuden kustannus Oy. ISBN 951-817-757-0. p. 165

Griva, I. Nash, S.G. Sofer, A. (2009). Linear and Nonlinear Optimization. 2nd Edition. Society of Industrial and Applied Mathematics (SIAM). Philadelphia, United States. ISBN 978-0-898716-61-0.

Rozvany, George I. N. (2011) A review of new fundamental principles in exact topology optimization. Warsaw, Poland. CMM-2011 – Computer Methods in Mechanics. [Referred 24.5.2013]. Available: http://www.cmm.il.pw.edu.pl/cd/pdf/053_f.pdf

Rozvany, George I. N. (2001). Aims, scope, methods, history and unified terminology of computer-aided topology optimization in structural mechanics. Structural Multidisciplinary Optimization. 21:90–108. DOI 10.1007/s001580050174

Rozvany, George I. N. (2007). A Critical review of established methods of structural topology optimization. Structural Multidisciplinary Optimization. DOI 10.1007/s00158-007-0217-0.

Rozvany, G.I.N. Zhou, M. and Birker, T. (1992) Generalized shape optimization without homogenization. Structural Optimization 4: 250-252. DOI 10.1007/BF01742754

Singiresu, S. Rao (2009). Engineering Optimization Theory and Practice, 4th Edition. New Jersey, United States. John Wiley & Sons, Inc. ISBN978-0-470-18352-6

Svanberg, Krister. (1987). The Method of Moving Asymptotes – A New Method for Structural Optimization. International Journal for Numerical Methods in Engineering. 24: 359-373. [Referred 15.4.2013]. Available: http://www2.math.kth.se/~krille/originalmma.pdf

Springer Images. Image of a long optimal cantilever. [Referred 27.5.2013]. Available: http://www.springerimages.com/Images/RSS/1-10.1007_s00158-010-0557-z-2

T-Lewinski. Rozvany, G. I. N. Sokol, T. Bolbotowski, K. (2008). Exact analytical solutions for some popular benchmark problems in topology optimization |||: L-shaped domains. Structural Multidisciplinary Optimization 3.5:165-174. DOI 10.1007/BF01197436

Taggart, D.G., P. Dewhurst. (2010). Development and validation of a numerical topology optimization scheme for two and three dimensional structures. Advances in Engineering Software 41: 910-915. Elsevier. DOI: 10.1016/j.advengsoft.2010.05.004

Wärtsilä Power Plants. Homepage. [Referred 27.11.2012]. Available: http://www.wartsila.com/en/power-plants/smart-power-generation/gas-power-plants

Wärtsilä Power Plants. Dual-Fuel Engines. [Referred 27.11.2012]. Available: http://www.wartsila.com/en/power-plants/technology/combustion-engines/dual-fuel-engines

Wärtsilä Power Plants. Lokaraari, Tero. Figure of an 18V50 Genset

Zhou, M. Fleury, R. et al. (2011). Topology Optimization. Practical Aspects for Industrial Applications. 9th World Congress on Structural and Multidisciplinary Optimization 2011. Shizuoka, Japan. [Referred 15.4.2013]. Available: http://www.altairuniversity.com/2011/05/25/topology-optimization-practical-aspects-for-industrial-applications/

APPENDICES

APPENDIX A: Email Discussions

Discussion 1

From: *Parviainen Heikki,*
Sent: *6. syyskuuta 2012 15:59*
To: *Hämäläinen Juhani,*
Subject: Topologian optimointisoftien validointi

Tervehdys,

en kovin paljon osaa tähän vastata… Jos halutaan ohjelmistoja validoida, niin kyllä on järkevää käyttää vertailuratkaisuina tunnettuja tarkkoja ratkaisuja. Rozvanyn ratkaisut ovat sopivia, mutta kuten sanoit sauvapohjaisia, ja tarkasti ottaen niitä voi käyttää vain sellaisiin tapauksiin. Mutta kyllä sauvaratkaisuja voi hyvin käyttää eräänlaisena kontinuumiratkaisun raja-arvona ainakin topologisessa mielessä (oikea määrä aukkoja oikeissa kohdissa jne.), ja myös muotomielessä, jos käytetään tiheitä elementtiverkkoja. Epälineaarisessa optimoinnissa on ylipäätään hyvin vaikeata löytää oikeasti ”tarkkoja” ratkaisuja. Analyyttisiä ratkaisuja voi odottaa vain ns. akateemisiin tapauksiin.

Realistisissa ongelmissa on lähes aina aktiiviseksi tulevia (muutakin kuin nollaa tai ääretöntä) rajoituksia suunnittelumuuttujien funktioille (rajoitusfunktioille), ja ratkaisut ovat tällöin lähes aina numeerisia. Jos löydät journaaliartikkeleissa vertailuratkaisuina käytettyjä tai niissä laskettuja numeerisia ratkaisuja, niin kyllähän niitä voi käyttää. Mutta analyyttinen ratkaisu realistiselle pinta-/tilavuusrakenteelle topologian optimoinnissa kuulostaa aika haastavalta, eikä minulle tule mieleen. Yksi ongelmahan on se, että pitäisi paitsi löytää lokaali ratkaisu, niin myös osoittaa että tämä lokaali ratkaisu on myös globaali. Siihen ei yleisesti ole 1-käsitteistä
tapaa, mutta tietenkin jos tiedetään etukäteen jotakin kohdefunktion muodosta suunnittelumuuttujien suhteen (yleistettyjä konveksisuusominaisuuksia tms.), niin silloin ratkaisuun on mahdollisuuksia.

Vastaan kysymyksiisi niin, että kaikki tarkat vertailuratkaisut ovat käyttökelpoisia ja siinä mielessä tämä tapa on järkevä; kuitenkaan ne yksinkertaisuudessaan eivät kerro paljon ohjelman mahdollisuuksista yleisessä tapauksessa; ja topologia-optimoinnin (pinta-/tilavuusrakenteet) analyyttisiä ratkaisuja ei minulla ole tiedossa.

Suosittelen löysentämään kriteereitä niin, ettei pyri vertaamaan ainoastaan tarkkoihin ratkaisuihin (koska niitä ei juuri löydä), vaan eri ohjelmien ratkaisuja samaan tehtävään keskenään, ja ottamaan kirjallisuudesta (artikkeleista) ratkaisuja, vaikka ovat numeerisia, likimääräisiä ja mahdollisesti lokaaleja, ja vertaamaan myös niihin. Koska optimointialgoritmien toiminta on usein aika parametriherkkää (ja mesh-herkkää jne.), saattaa tasapuolinen vertailu olla toisinaan vaikeata.

Terveisin,
Heikki

Discussion 1

From: Hämäläinen Juhani
Sent: 5. syyskuuta 2012 10:53
To: Parviainen Heikki; Kokkonen Petteri
Subject: Topologian optimointisoftien validointi

Hei, diplomityössäni oleellinen osa on käytettyjen FEM-pohjaisten topologian optimointiohjelmien validointi ja tulosten testaus. Ajattelin kysyä kokeneemman mielipidettä tässä asiassa.
Suoritan ohjelmien tulosten arvioinnin kirjallisuudesta löytyvillä benchmark – tapauksilla, joita ovat esim.: Rozvany G.I.N:

- Exact analytical solutions for some popular benchmark problems in topology optimization.
- Exact analytical solutions for some popular benchmark problems in topology optimization 2: three-sided polygonal supports.
- Exact analytical solutions for some popular benchmark problems in topology optimization 3:L-shaped domains.

Nämä kaikki käsittelevät sauvaratkaisuja ja työssäni käsiteltävää rakennetta ei voi toteuttaa sauvoilla. Onko tämä validointitapa mielestäsi järkevä? Osaatko neuvoa, mistä löytäisin esim. analyyttisiä ratkaisuja 3D tapauksille ja paksuille poikkileikkauksille?

Ystävällisin terveisin,
Juhani Hämäläinen

Discussion 2

From: Ole Sigmund [mailto:sigmund@mek.dtu.dk]
Sent: 5. syyskuuta 2012 15:47 To: Hämäläinen Juhani Cc: Kokkonen Petteri
Subject: RE: Validation of Topology Optimization Software

Hi Juhani,

Analytical solutions are only available for grillage and frame-like solutions. Since optimal solutions (at least for one load case problems) always have bars crossing at perpendicular angles and hence introduce no bending moments, Rozvany, Hemp and Mitchell type solutions are valid both for frame and truss like solutions (but assuming low volume fractions). For more solid solutions there don't exist analytical solutions. Here you may use some of my recent papers that contain some benchmark examples for comparisons. Obviously I cannot guaranty them to be globally optimal but they can serve as good goals.

Ole Sigmund
Department of Mechanical Engineering, Section for Solid Mechanics
Technical University of Denmark, Building 404, Room 112, DK-2800 Lyngby, Denmark

Phone: (+45) 4525 4256, Fax: (+45) 4593 1475,
E-mail: sigmund@mek.dtu.dk,
Homepage: http://www.fam.web.mek.dtu.dk/os.html
Group homepage: www.topopt.dtu.dk

From: Hämäläinen Juhani [mailto:Juhani.Hamalainen@vtt.fi]
Sent: 5. September 2012 08:31
To: Ole Sigmund Cc: Kokkonen Petteri
Subject: Validation of Topology Optimization Software

Hello Mr. Sigmund,

I am Juhani Hämäläinen from the Technical Research Centre of Finland and I am working on my Master's Thesis about Topology Optimization of a frame structure. I will use different commercial optimization software in my work. My question is:

What approach would you suggest for the validation and verification of the commercial software?

I have found four articles of analytical benchmark cases from Mr. Rozvany, but these utilize truss solutions. My professor would also like to see some optimal analytical beam solutions. Would you know if there are any?

I really appreciate your opinion and help.
Best regards,
Juhani Hämäläinen

Discussion 3

Sent: 15 April 2013 15:33
To: Fredrik Nordgren; Joakim Truedsson
Subject: OptiStruct Topology Optimization formulation

Hi Juhani,

Yes, and there is also a new method in v12, (-level set method, there is a description in v12 help, did you install v12 yet?). I think it's gradient based.

Best regards
Joakim

Sent: den 15 April 2013 12:39
To: Fredrik Nordgren; Joakim Truedsson
Subject: OptiStruct Topology Optimization formulation

Hi,

I would like to know what methods are applied in the Topology optimization in OptiStruct. Apparently the SIMP material interpolation scheme is used.

How is the optimization problem solved? With gradient based methods (MMA) or optimality condition based methods?

B.r.
Juhani Hämäläinen

Discussion 4

From: Joakim Truedsson
Sent: den 11 Januar 2013 09:00
To: Hämäläinen Juhani
CC: Henrik Molker
Subject: RE: OptiStruct support
Attachments "A animation of the solution of the torsional cylinder validation case.s"

Hi Juhani, No problem :)
I was just about to suggest running with MINDIM or Stress constraint .. but I guess that is not an option then. (I got a discrete structure when trying the run with MINDIM).
When running with MINDIM it takes many iterations before it starts to get discrete structure. Perhaps the tolerances needs to be tightened.
You can try to decrease the tolerance OBJTOL and increase max number of iterations DESMAX.
If I remember correct DISCRETE =3 gives p=4, yes. CHEXA should be good to use.
Unfortunately I can't tell if reducing the volume constraint would help.
I will try some more runs tomorrow,
Best regards
Joakim

From: Hämäläinen Juhani
Sent: den 10 januari 2013 14:38
To: Joakim Truedsson
CC: Henrik Molker
Subject: RE: OptiStruct support

Hello Joakim,
sorry for hammering you with difficult questions all the time:
Here is another figure attached of the convergence problem for a longer cylinder.
The attached picture shows that the helical structure ends after three stages and the middle section is a pure cylinder. (Analytical solutions says that the helices go all the way down)
How can I force the solution to a truss like structure? (DISCRETE, dese mesh?)
My volume constraint is 10%, what if I put it down to 5%?
Is it actually optimal already? DeSaint Venant's principle says that stress state equalises after some distance from the loading/boundary conditions. Has the helical structure made an even shear stress loading to the centre section? Optimal in this area would be a pure cylinder.
I want to use CHEXA because the actual structure to be optimizes is modelled with them.
Is CHEXA worse element for topology optimization than TETRA and why?
MINDIM is definitely an additional filter that should not be used in this validation, says my professor.
DISCRETE=3 would mean that my penalty exponent p=4? Right? I might test this next…
Best regards, Juhani

APPENDIX B: Extraction of BCs from Excitation Analysis

1. Finite element excitation analysis in ABAQUS
    a. Create node sets of the nodes at suitable locations and at suitable division along the planned cut-boundaries of the sub-model region.
    b. Calculate the responses at the cut-boundaries of the sub-model region of the structure by dynamic harmonic response analysis for the genset.
2. Data transfer from ABAQUS to MATLAB
    a. Write the response data, nodal coordinates and node and element set data from the FE-software to output files.
    b. Read the data to MATLAB.
    c. Recollect the response and coordinate data in MATLAB.
3. Animate the responses over the phase angle at all orders of excitation for visual assessment and validation of the data. Select significant orders of excitation.
4. Determine the master node definitions.
    a. Calculate the master node coordinates as mean values of the coordinates of the nodes in the node sets.
    b. Calculate the displacements at the master node locations as mean values of the displacements responses of the nodes in the node sets.
    c. Seek the highest displacement amplitude and the corresponding phase angle.
    d. Transform the phase angle of the complex valued responses to real valued.
5. Write the OptiStruct input –files for RBE3 element:
    a. Dependent node coordinates.
    b. Dependent node node sets.
    c. Dependent node displacements
    d. Independent node sets.
6. Run Topology Optimization model.

APPENDIX C: Displacement Fields of Different Orders

1^{St} order of excitation

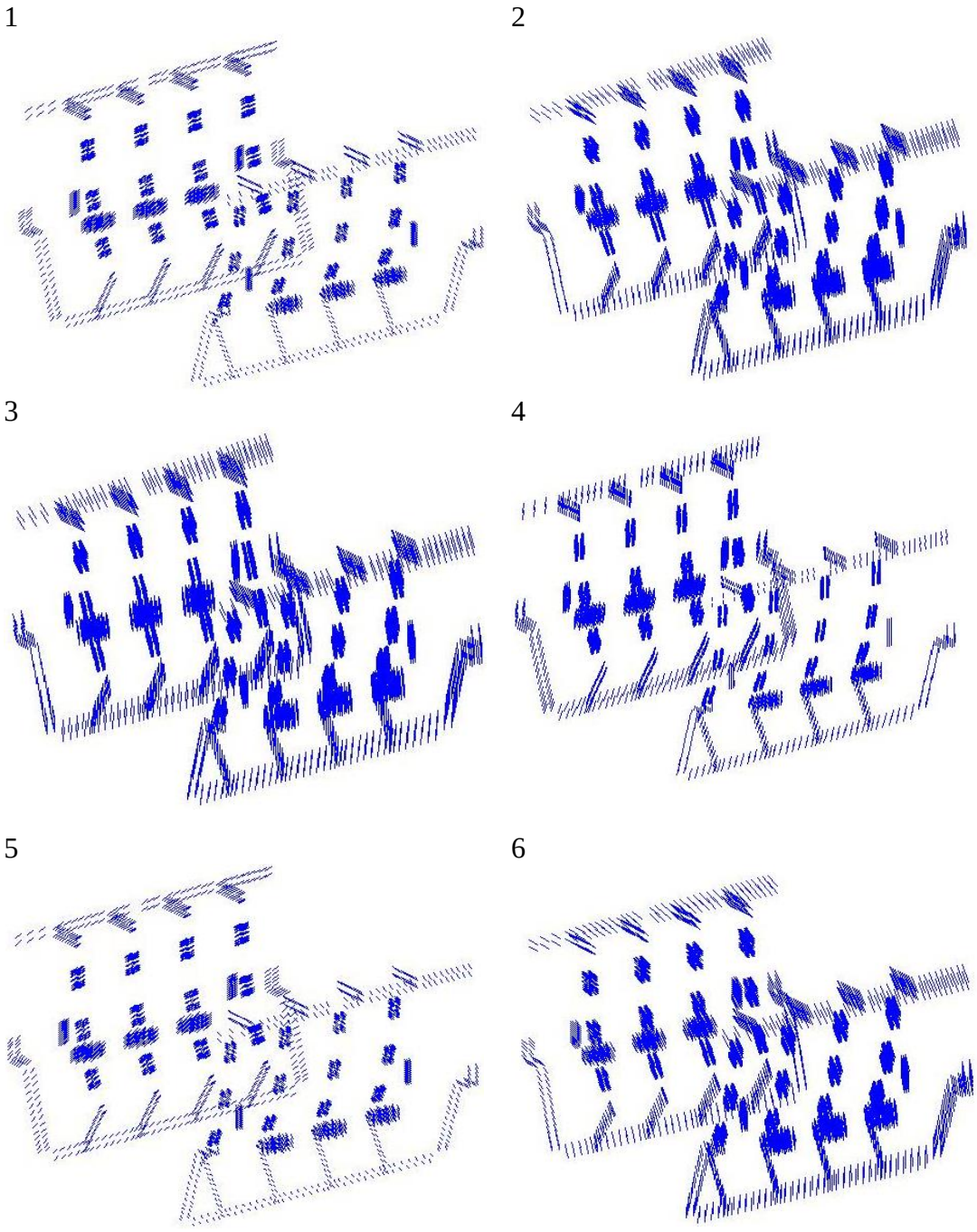

Figure 46. Nodal displacements of the attachment area in frequency response model, 1^{st} order of excitation.

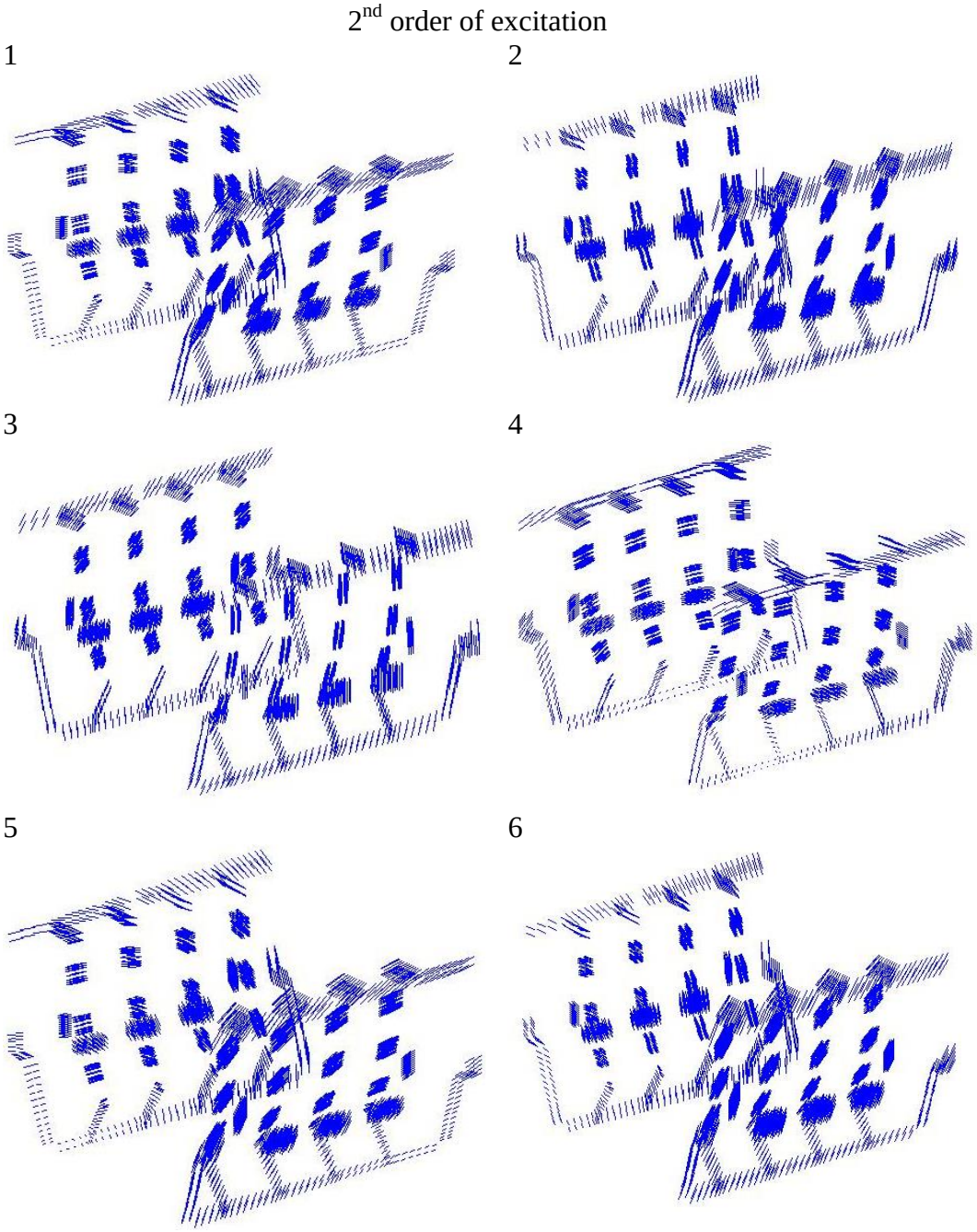

Figure 47. Nodal displacements of the attachment area in frequency response model, 2nd order of excitation.

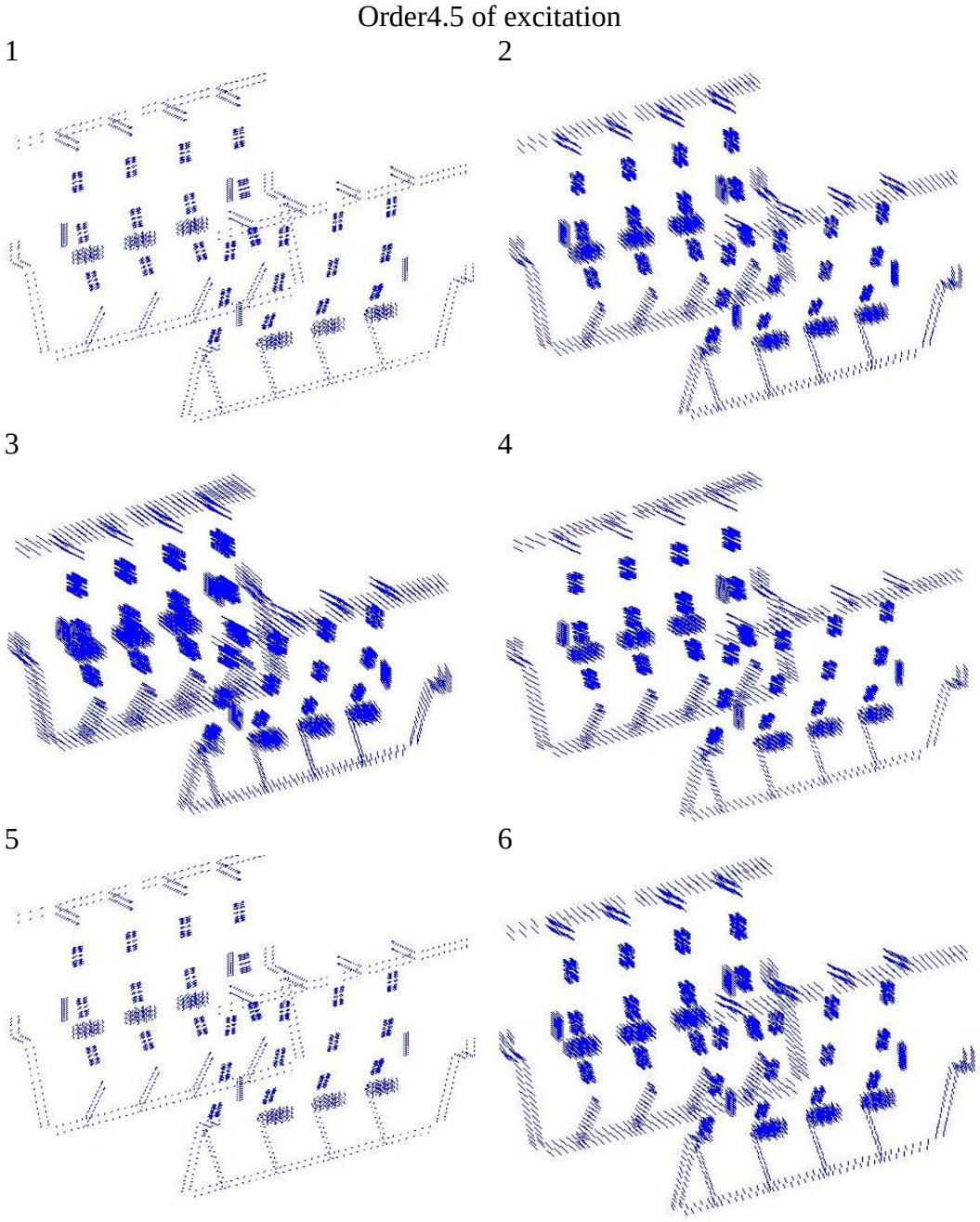

Figure 48. Nodal displacements of the attachment area in frequency response model, 4.5th order of excitation.

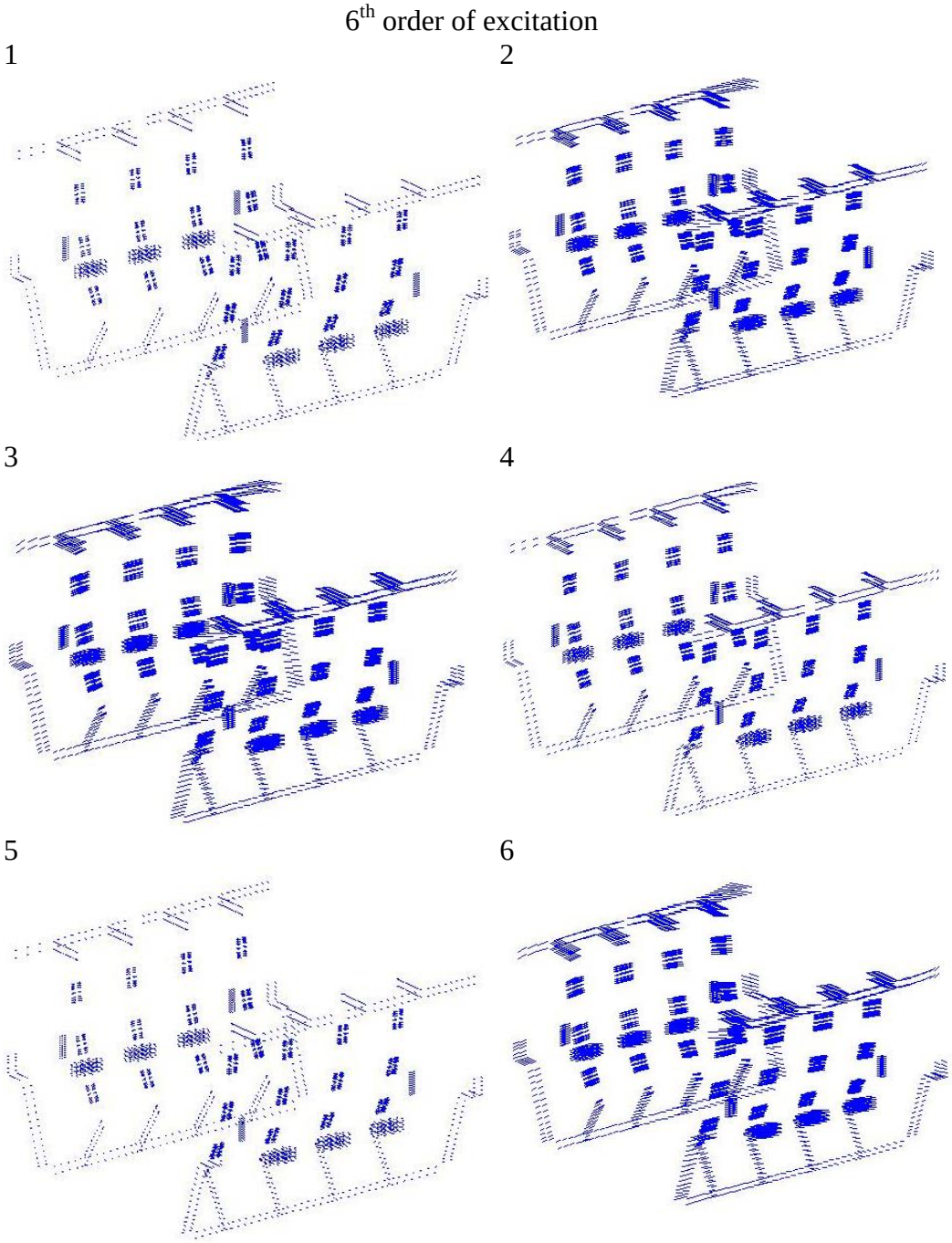

Figure 49. Nodal displacements of the attachment area in frequency response model, 6th order of excitation.

APPENDIX D: Scaled Forced Displacements.

Forced Displacement Fields

Ref.N	Node Set	DOF	Analysis 1 Scaled disp	Analysis 2 Scaled disp	Analysis 3 Scaled disp	Analysis 4 Scaled disp.
39	FxTxBx1	1	0,8309	0,3865	-0,0594	0,1727
39	FxTxBx1	2	0,2440	-0,2693	-0,2476	0,1606
39	FxTxBx1	3	0,4843	0,2391	-0,0210	0,0228
40	FxTxBx2	1	0,8345	0,3865	-0,0597	0,1751
40	FxTxBx2	2	0,2911	-0,3056	-0,1824	0,0791
40	FxTxBx2	3	0,1461	0,0964	-0,0129	0,0034
41	FxTxBx3	1	0,8370	0,3877	-0,0597	0,1751
41	FxTxBx3	2	0,3406	-0,3454	-0,1153	0,0111
41	FxTxBx3	3	-0,2065	-0,0615	-0,0062	-0,0099
42	FxTxBx4	1	0,8357	0,3877	-0,0588	0,1739
42	FxTxBx4	2	0,3901	-0,3829	-0,0517	-0,0924
42	FxTxBx4	3	-0,5447	-0,2041	0,0044	-0,0291
43	PxTxBx1	1	0,7778	0,3575	-0,0816	0,1606
43	PxTxBx1	2	0,2174	-0,2512	-0,2874	0,2476
43	PxTxBx1	3	0,6473	0,2476	0,0258	0,0074
44	PxTxBx2	1	0,7802	0,3563	-0,0803	0,1582
44	PxTxBx2	2	0,2669	-0,2874	-0,2150	0,1203
44	PxTxBx2	3	0,3309	0,1173	0,0349	-0,0111
45	PxTxBx3	1	0,7850	0,3563	-0,0796	0,1570
45	PxTxBx3	2	0,3164	-0,3261	-0,1486	0,0361
45	PxTxBx3	3	-0,0488	0,0622	0,0377	-0,0149
46	PxTxBx4	1	0,7899	0,3563	-0,0801	0,1594
46	PxTxBx4	2	0,3659	-0,3659	-0,0833	-0,0496
46	PxTxBx4	3	-0,3587	-0,1884	0,0409	-0,0185
47	PxTxBx5	1	0,7911	0,3575	-0,0816	0,1643
47	PxTxBx5	2	0,4203	-0,4336	0,0441	-0,3092
47	PxTxBx5	3	-0,6969	-0,3370	0,0510	-0,0354
48	FxBxBx1	1	-0,3128	-0,0737	0,0615	-0,0182
48	FxBxBx1	2	-0,2053	0,2053	-0,0162	0,0616
48	FxBxBx1	3	0,5000	0,3780	-0,1094	0,0486
49	FxBxBx2	1	-0,3104	-0,0743	0,0609	-0,0180
49	FxBxBx2	2	-0,1473	0,1498	0,0400	0,0126
49	FxBxBx2	3	0,2391	-0,2609	-0,1006	0,0279
50	FxBxBx3	1	-0,3092	-0,0742	0,0614	-0,0180
50	FxBxBx3	2	-0,0908	0,0977	0,0937	-0,0412
50	FxBxBx3	3	-0,3188	-0,1812	-0,0897	0,0044
51	FxBxBx4	1	-0,3104	-0,0736	0,0626	-0,0182
51	FxBxBx4	2	-0,0370	0,0454	0,1461	-0,0932
51	FxBxBx4	3	-0,6159	-0,1969	-0,0797	-0,0187
52	PxBxBx2	1	-0,5145	-0,1739	0,0547	-0,0337
52	PxBxBx2	2	-0,2428	0,2428	0,0453	0,0341
52	PxBxBx2	3	0,3273	0,2548	-0,0719	0,0271
53	PxBxBx3	1	-0,5121	-0,1727	0,0550	-0,0316
53	PxBxBx3	2	-0,1824	0,1872	0,1010	-0,0200
53	PxBxBx3	3	0,1558	-0,1437	-0,0645	0,0087
54	PxBxBx4	1	-0,5121	-0,1739	0,0560	-0,0314
54	PxBxBx4	2	-0,1268	0,1377	0,1534	-0,0749
54	PxBxBx4	3	-0,4191	-0,1316	-0,0550	-0,0097
55	PxBxBx5	1	-0,5109	-0,1739	0,0566	-0,0309
55	PxBxBx5	2	-0,0725	0,0789	0,1993	-0,1174
55	PxBxBx5	3	-0,7319	-0,2222	-0,0495	-0,0161

56	SxBx1x1	1	0,6232	0,3031	-0,0306	0,1449
56	SxBx1x1	2	0,1498	-0,1643	-0,1908	0,1244
56	SxBx1x1	3	0,4819	0,2874	-0,0558	0,0411
57	SxBx1x3	1	0,6244	0,3043	-0,0314	0,1473
57	SxBx1x3	2	0,2500	-0,2488	-0,0709	-0,0141
57	SxBx1x3	3	-0,2367	-0,0835	-0,0351	-0,0068
58	SxBx1x4	1	0,6232	0,3043	-0,0306	0,1449
58	SxBx1x4	2	0,3007	-0,2923	-0,0162	-0,0809
58	SxBx1x4	3	-0,5640	-0,1848	-0,0227	-0,0330
59	SxBx2x1	1	0,3007	0,1763	0,0105	0,0987
59	SxBx2x1	2	0,0215	-0,0257	-0,1208	0,0865
59	SxBx2x1	3	0,4855	0,3140	-0,0731	0,0472
60	SxBx2x2	1	0,3031	0,1763	0,0107	0,1007
60	SxBx2x2	2	0,0733	-0,0714	-0,0665	0,0342
60	SxBx2x2	3	0,1824	-0,1860	-0,0620	0,0205
61	SxBx2x4	1	0,3019	0,1763	0,0105	0,0993
61	SxBx2x4	2	0,1824	-0,1739	0,0406	-0,0748
61	SxBx2x4	3	-0,5773	-0,1812	-0,0380	-0,0316
62	SxBx3x1	1	0,0395	0,0762	0,0357	-0,0533
62	SxBx3x1	2	-0,0932	0,0941	-0,0664	0,0700
62	SxBx3x1	3	0,4952	0,3659	-0,1033	0,0525
63	SxBx3x3	1	0,0399	0,0775	0,0367	-0,0529
63	SxBx3x3	2	-0,0219	-0,0141	0,0400	-0,0303
63	SxBx3x3	3	-0,3056	-0,1655	-0,0809	0,0030
64	SxBx3x4	1	0,0402	0,0769	0,0368	-0,0535
64	SxBx3x4	2	0,0774	-0,0671	0,0919	-0,0816
64	SxBx3x4	3	-0,6075	-0,1908	-0,0693	-0,0250
65	NxB	1	0,1872	0,0831	0,0082	0,0066
65	NxB	2	0,0048	-0,0161	-0,1098	0,0791
65	NxB	3	0,5048	0,2391	-0,0199	0,0268
66	DxB	1	0,2017	0,1006	0,0051	0,0128
66	DxB	2	0,1618	-0,1534	0,0510	-0,0737
66	DxB	3	-0,5519	-0,2114	0,0093	-0,0320
67	VxBx1	1	-0,0079	-0,0071	-0,0002	-0,0034
67	VxBx1	2	-0,0545	0,0645	-0,0446	0,0338
67	VxBx1	3	0,3285	0,1365	-0,0110	0,0095
68	VxBx2	1	0,0000	0,0000	0,0000	0,0000
68	VxBx2	2	0,0000	0,0000	0,0000	0,0000
68	VxBx2	3	0,0000	0,0000	0,0000	0,0000
69	VxBx3	1	0,0044	0,0040	0,0001	0,0013
69	VxBx3	2	0,0552	-0,0570	0,0455	-0,0405
69	VxBx3	3	-0,3164	-0,1304	0,0028	-0,0032
70	RXBXDX1	1	0,1316	0,0525	-0,0190	0,0198
70	RXBXDX1	2	-0,0850	0,1208	-0,1256	0,0911
70	RXBXDX1	3	0,7464	0,2995	0,0140	0,0365
71	RXBXDX2	1	0,0554	0,0237	-0,0027	0,0068
71	RXBXDX2	2	-0,1139	0,1522	-0,1126	0,0752
71	RXBXDX2	3	0,7488	0,3200	-0,0022	0,0382
72	RXBXDX3	1	-0,2464	-0,0762	0,0355	-0,0203
72	RXBXDX3	2	-0,2186	0,2500	-0,0580	0,0783
72	RXBXDX3	3	0,7633	0,3865	-0,0531	0,0348
73	RXBXNX1	1	0,1365	0,0595	-0,0216	0,0368
73	RXBXNX1	2	0,1993	-0,2319	0,1156	-0,1329
73	RXBXNX1	3	-0,8478	-0,4155	0,0682	-0,0671
74	RXBXNX2	1	0,0595	0,0327	-0,0038	0,0175
74	RXBXNX2	2	0,1763	-0,2101	0,1094	-0,1144
74	RXBXNX2	3	-0,8442	-0,3865	0,0498	-0,0542
75	RXBXNX3	1	-0,2452	-0,0709	0,0354	-0,0178
75	RXBXNX3	2	0,2174	-0,1292	0,1981	-0,1558

75	RXBXNX3	3	-1,0000	-0,3418	-0,0337	-0,0056
76	PxBxBx1	1	-0,5157	-0,1751	0,0546	-0,0349
76	PxBxBx1	2	-0,2874	0,2911	0,0121	0,0609
76	PxBxBx1	3	0,5918	0,3575	-0,0761	0,0385
80	SxBx1x2	1	0,6244	0,3031	-0,0315	0,1473
80	SxBx1x2	2	0,1981	-0,2041	-0,1316	0,0579
80	SxBx1x2	3	0,1655	-0,1534	-0,0452	0,0147
81	SxBx2x3	1	0,3031	0,1775	0,0107	0,1010
81	SxBx2x3	2	0,1280	-0,1244	-0,0130	-0,0210
81	SxBx2x3	3	-0,2585	-0,1088	-0,0505	-0,0051
82	SxBx3x2	1	0,0395	0,0773	0,0364	-0,0527
82	SxBx3x2	2	-0,0373	0,0403	-0,0128	0,0203
82	SxBx3x2	3	0,2258	-0,2464	-0,0928	0,0278

APPENDIX E: Linear Element Model Solutions

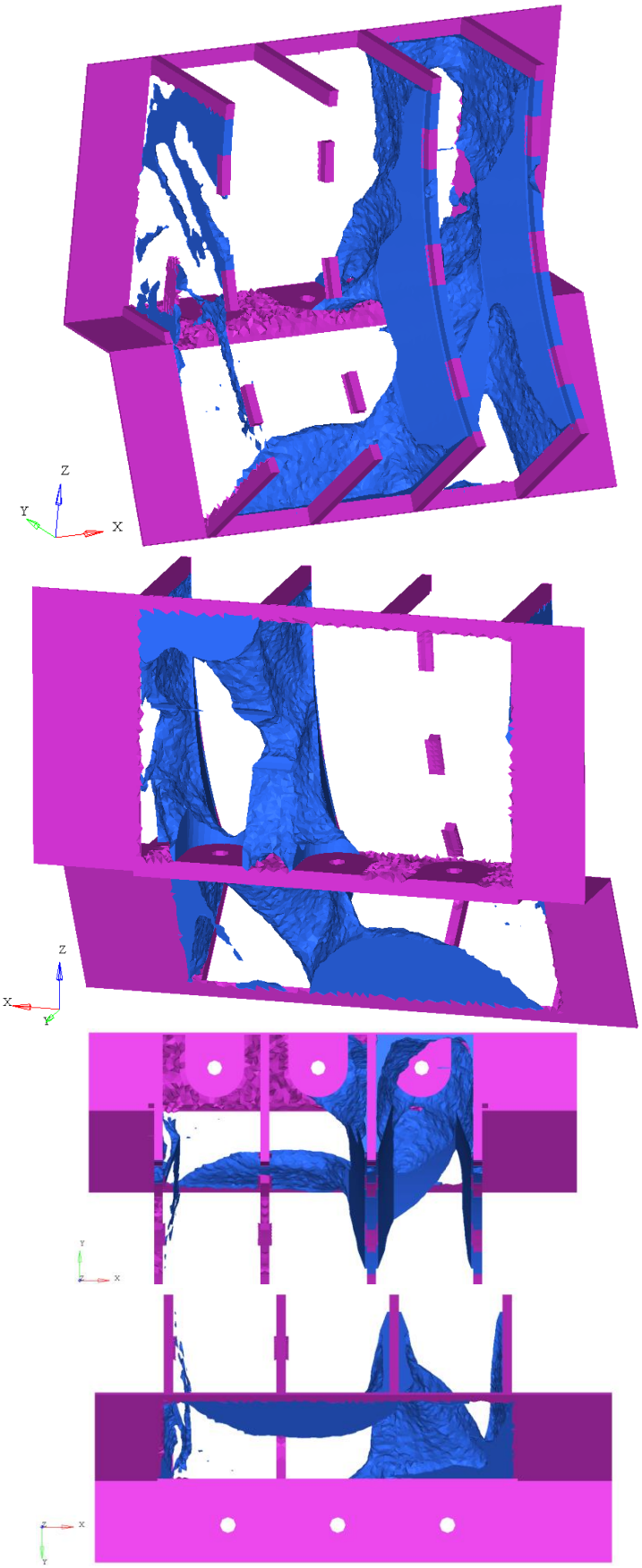

Figure 50. Topology optimization result of linear element model in load case 1, order 1, ρ>0.8.

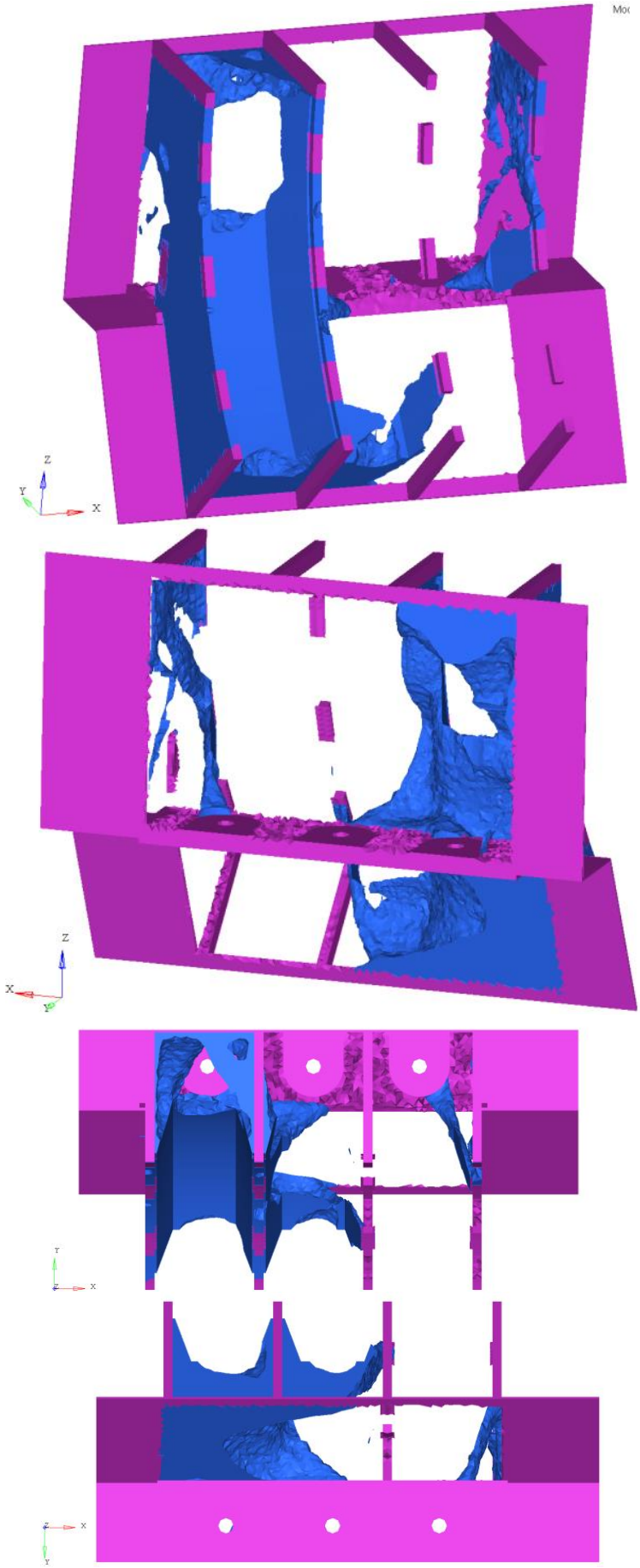

Figure 51. Topology optimization result of linear element model in load case 2, order 2, ρ>0.8.

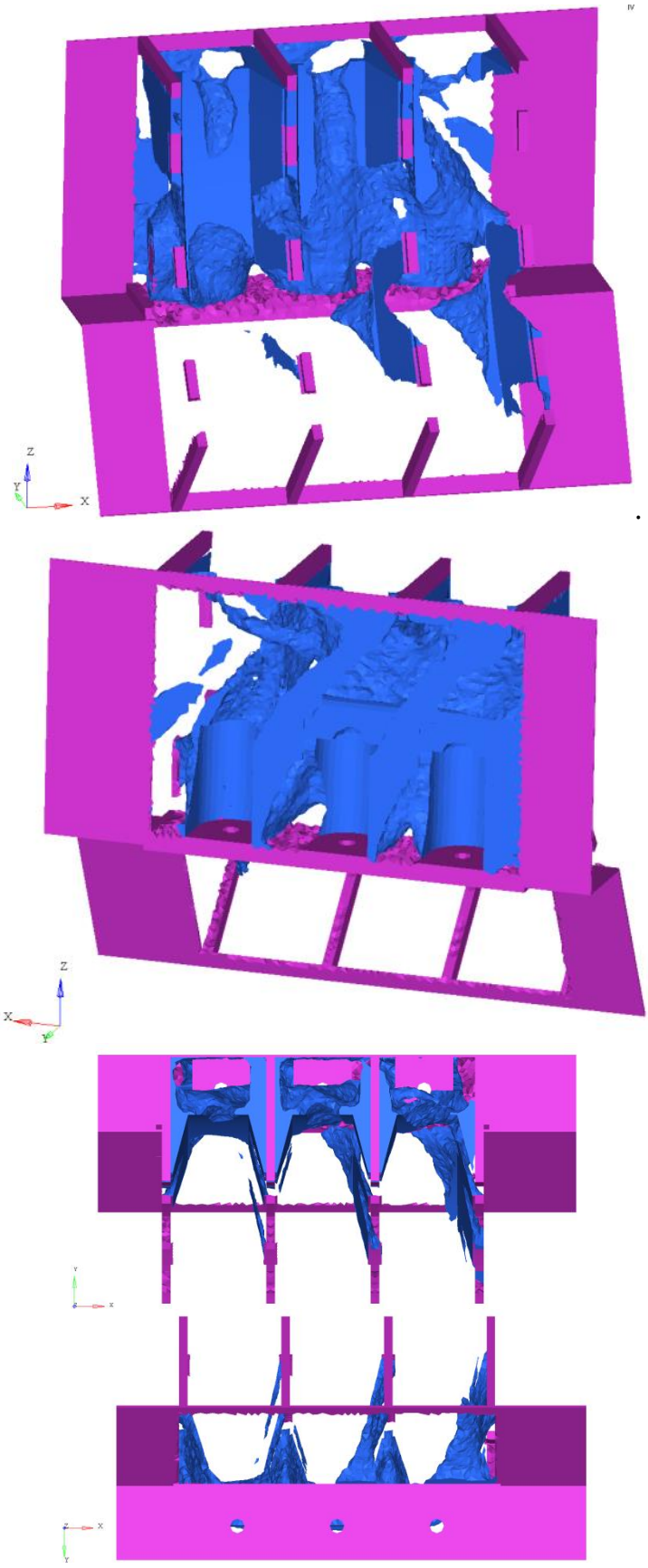

Figure 52. Topology optimization result of linear element model in load case 3, order 4.5, ρ>0.8.

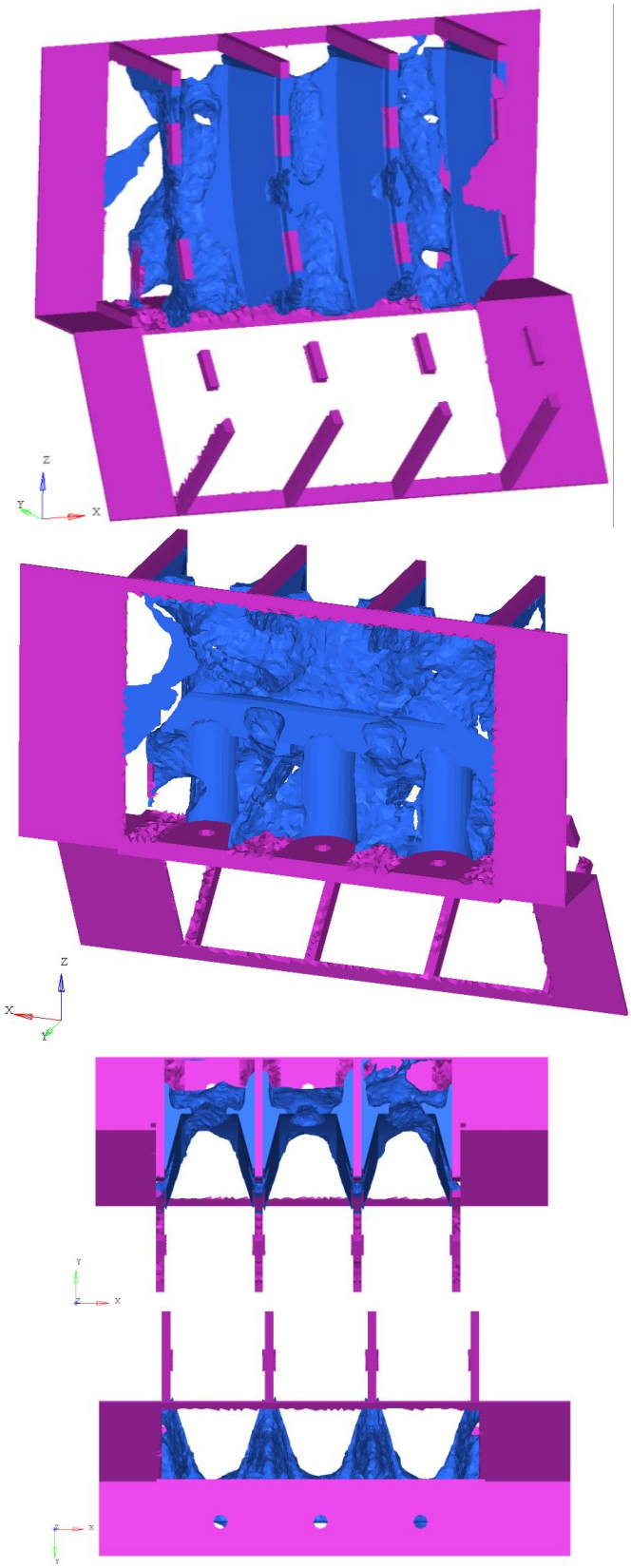

Figure 53. Topology optimization result of linear element model in load case 4, order, ρ>0.8.

APPENDIX F: Parabolic Element Model Solutions

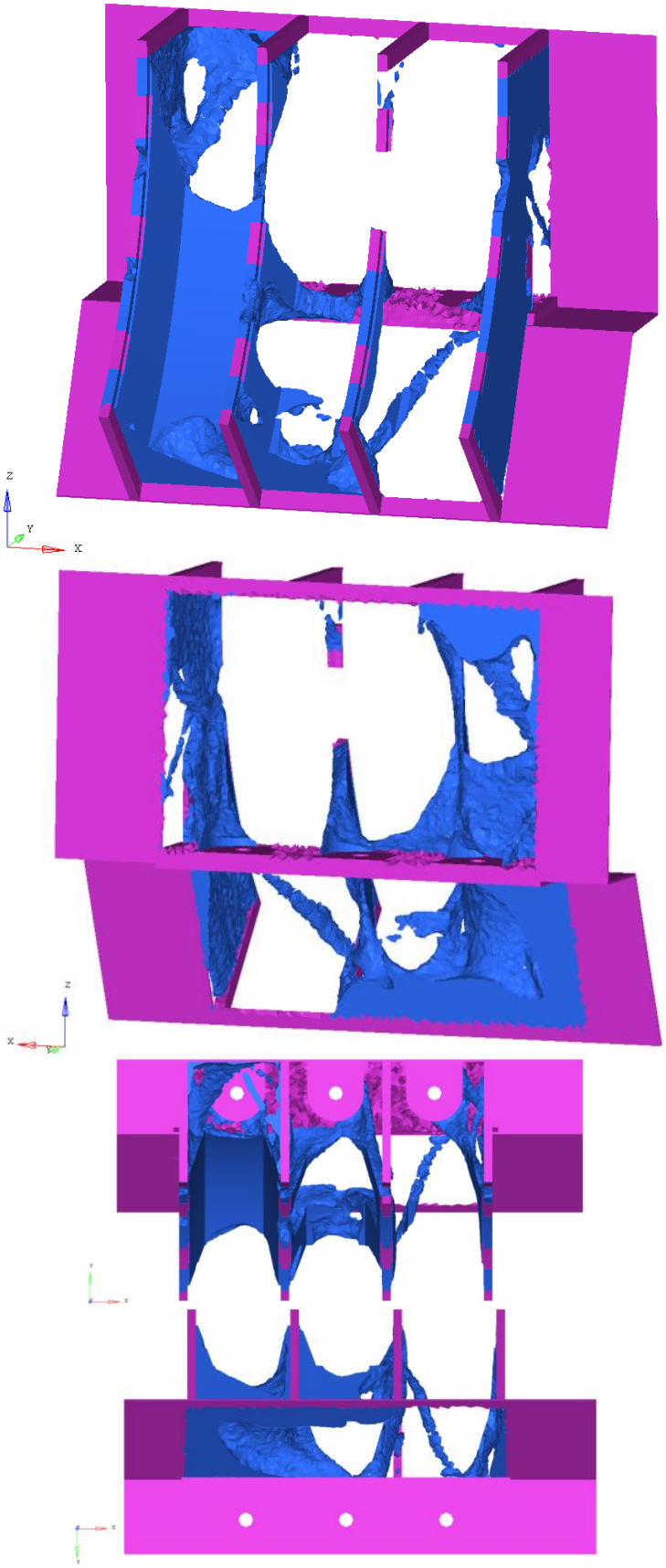

Figure 54. Topology optimization result of combined load cases with parabolic elements, analysis 1, ρ>0.8.

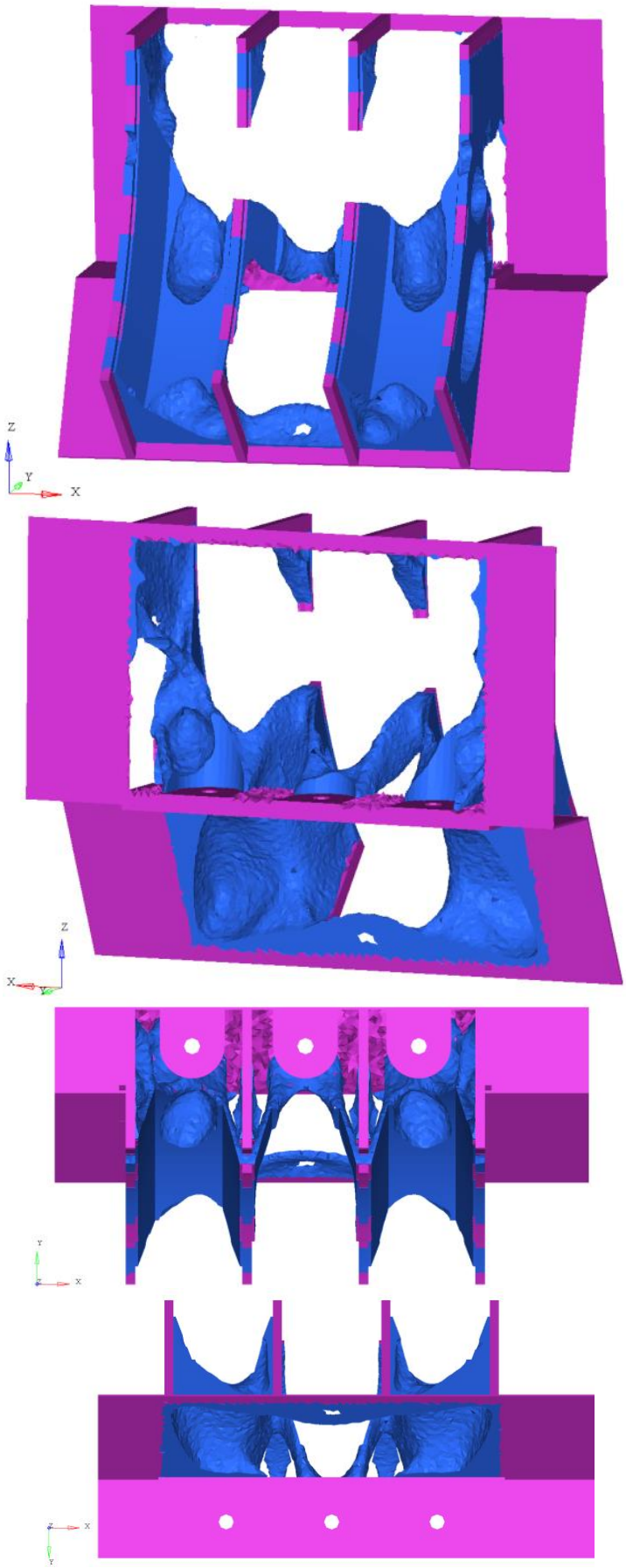

Figure 55. Topology optimization result of combined load cases with parabolic elements, analysis 2, ρ>0.8

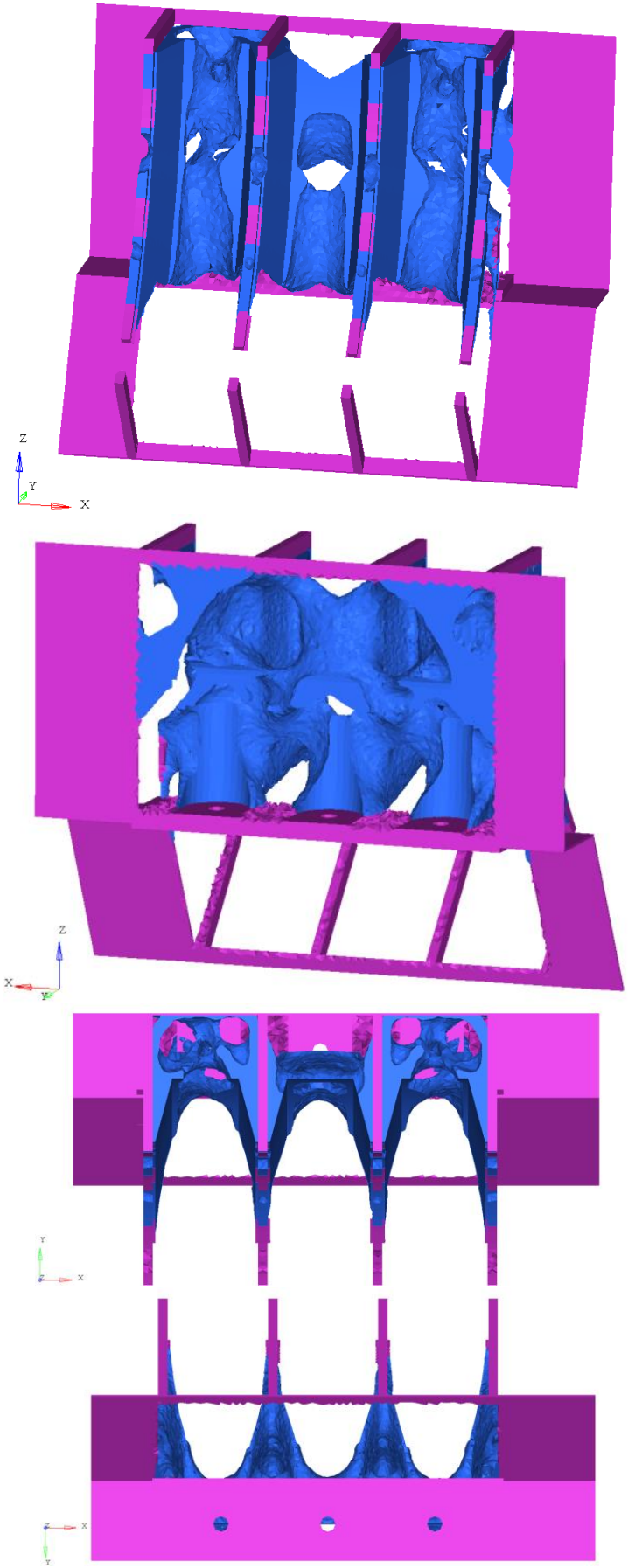

Figure 56. Topology optimization result of combined load cases with parabolic elements, analysis 3, ρ>0.8

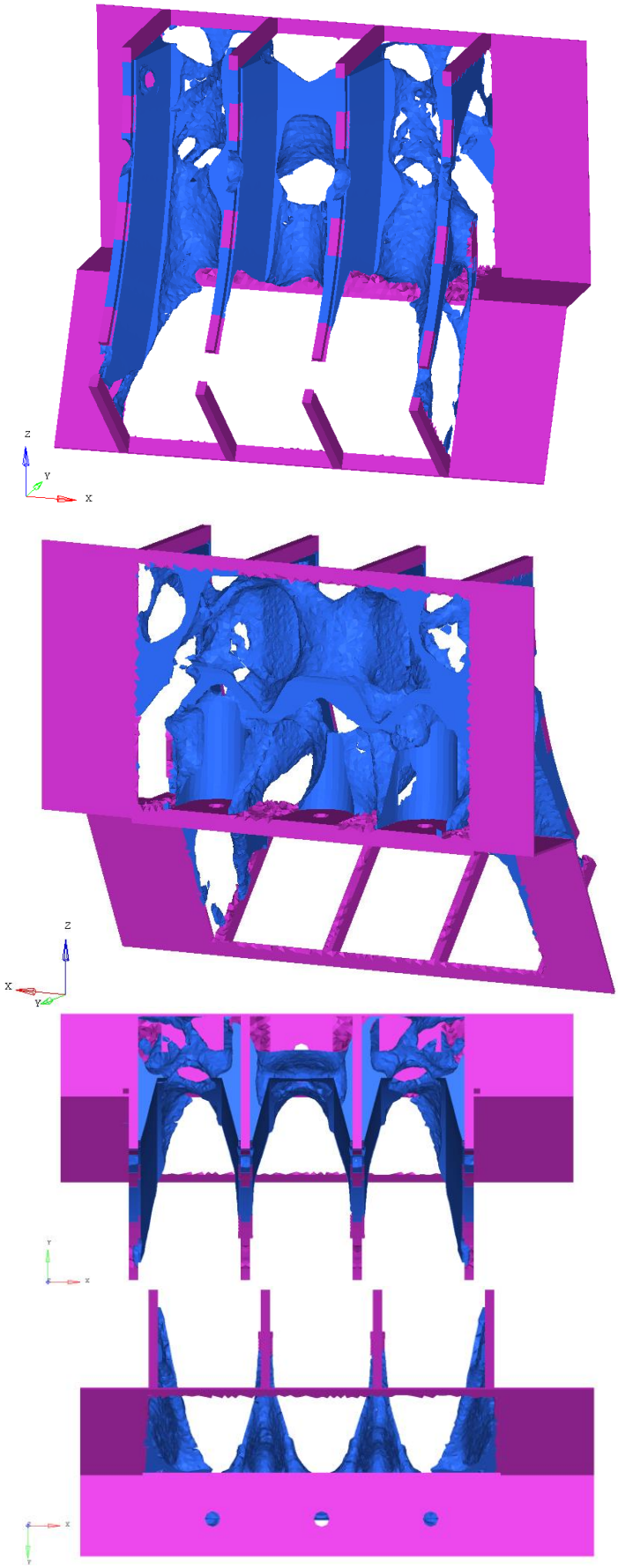

Figure 57. Topology optimization result of combined load cases with parabolic elements, analysis 4, ρ>0.8

APPENDIX G: Static Finite Element Analysis

Load case 1, Δx=6e-4

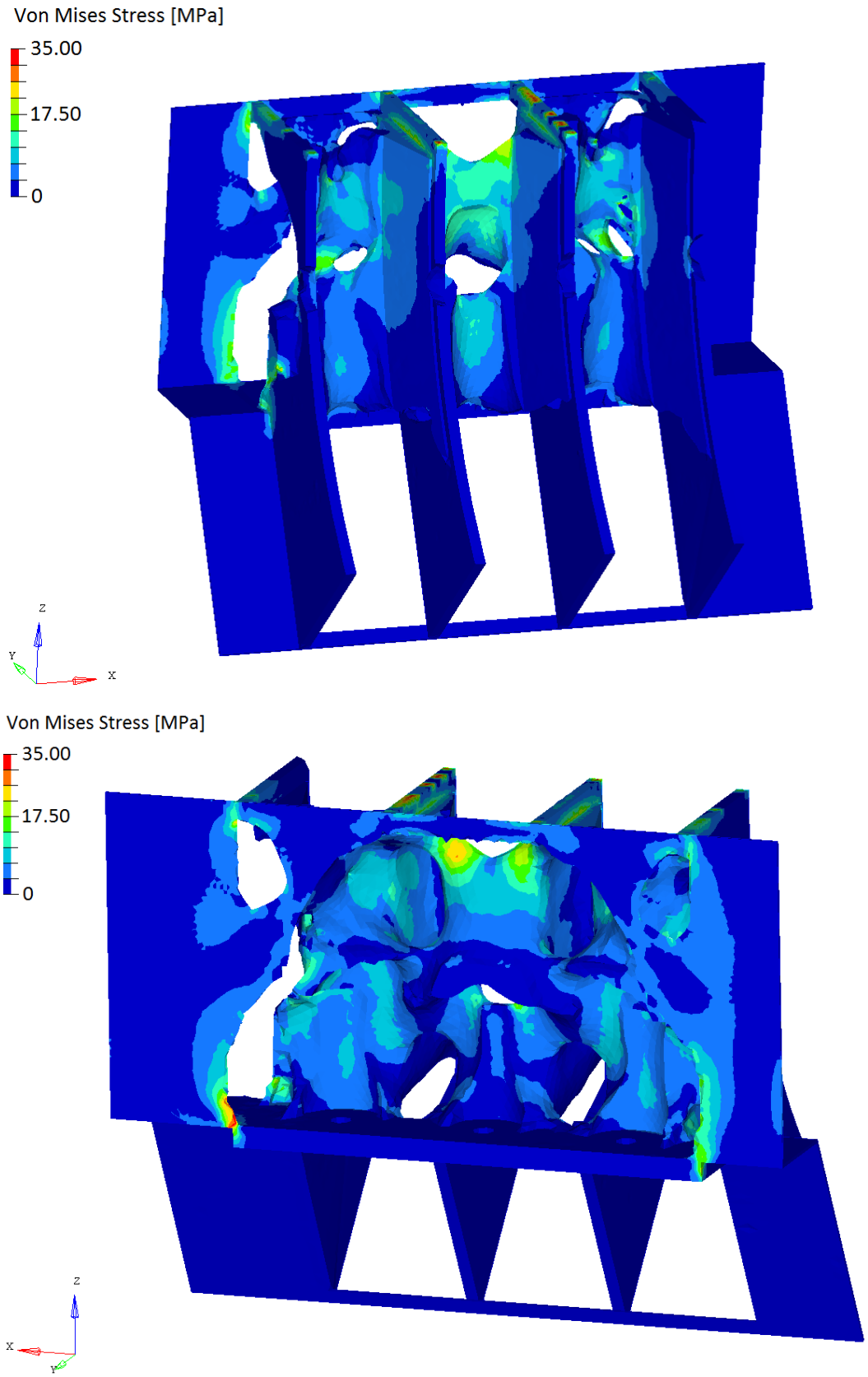

Figure 58. Static stress analysis of the new topology with simplified static displacements, load case 1

Load case 2, Δx=6e-4

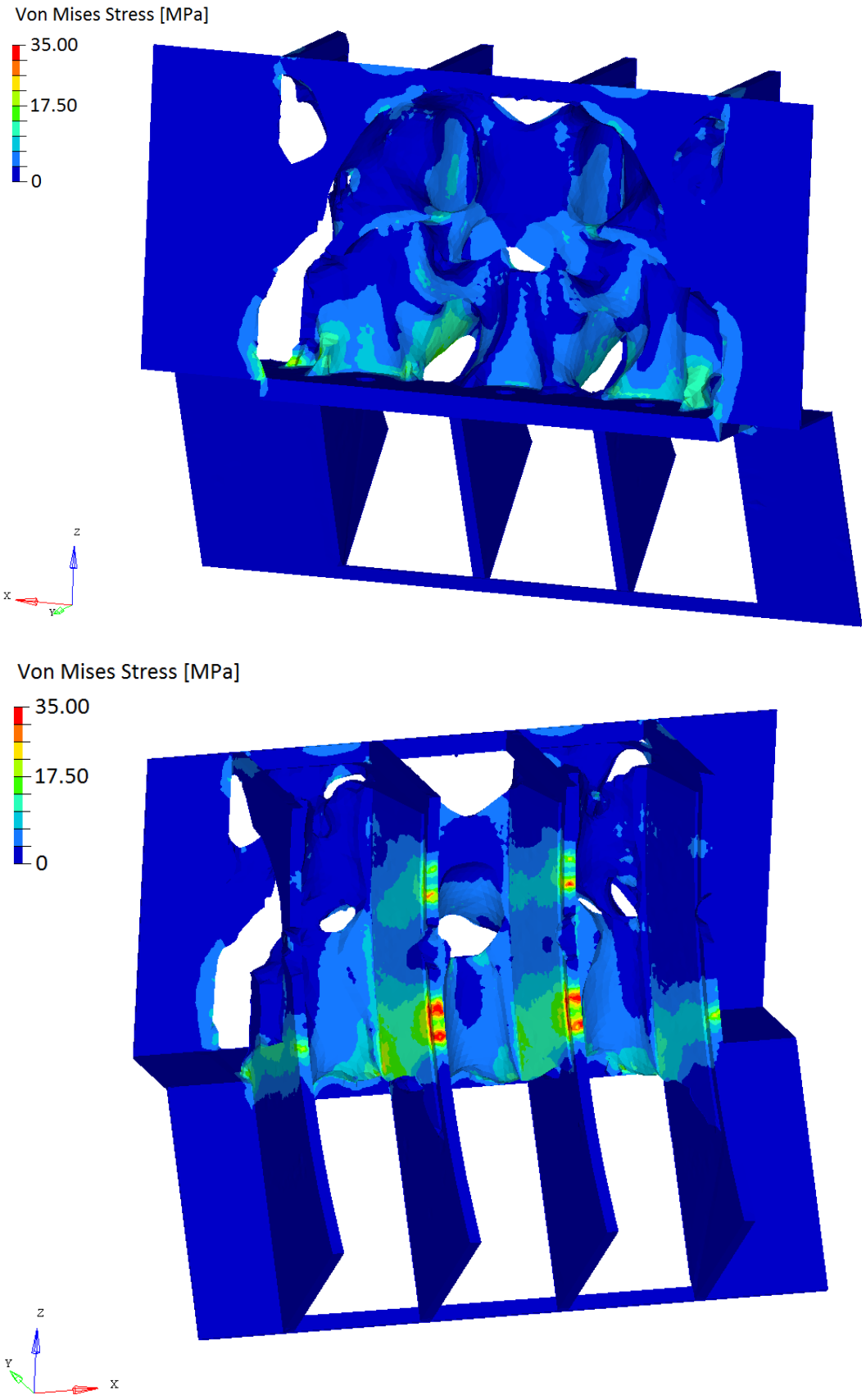

Figure 59. Static stress analysis of the new topology with simplified static displacements, load case 2

Load case 3, Δx=3e-5

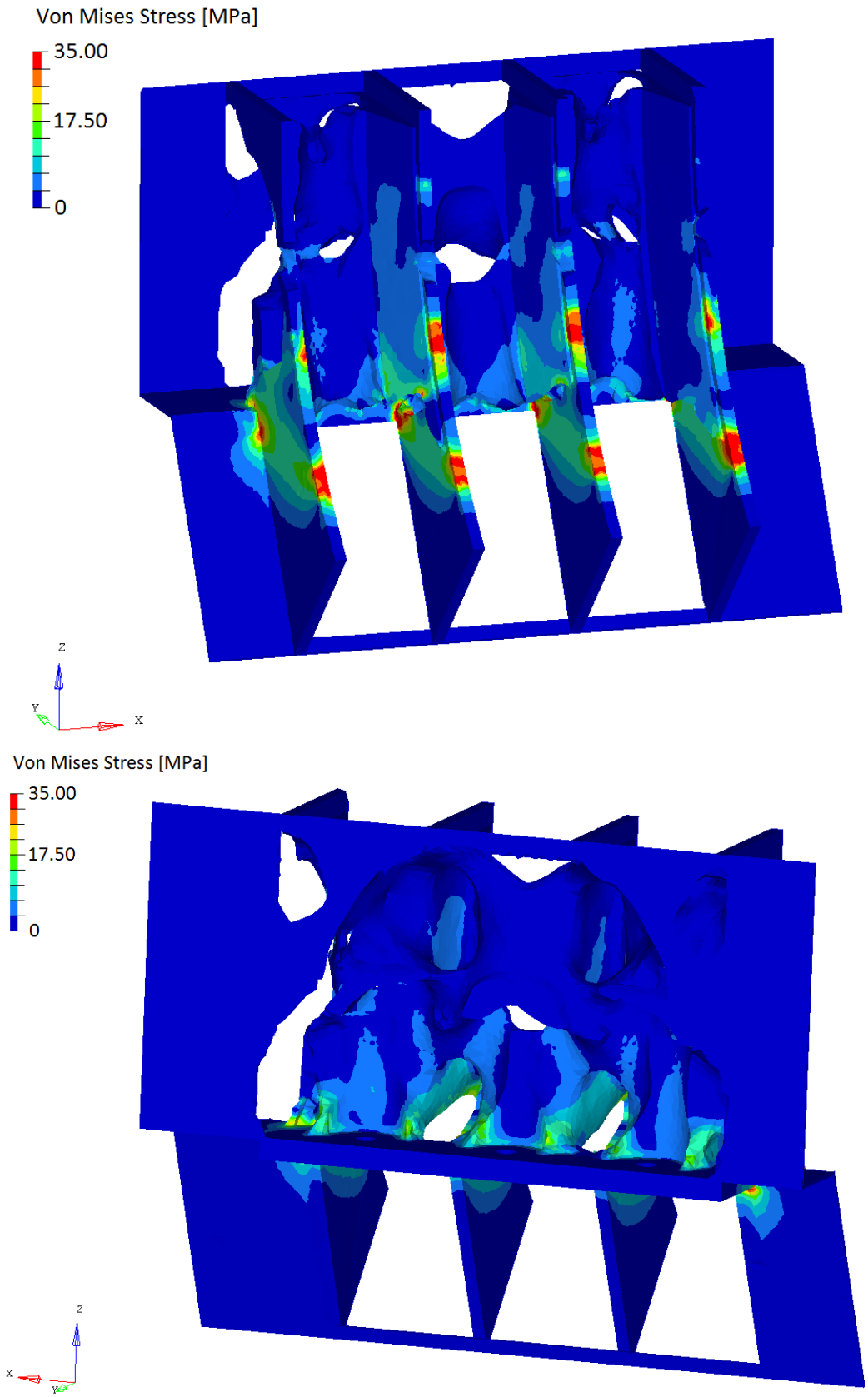

Figure 60. Static stress analysis of the new topology with simplified displacements, load case 3

Load case 4, Δz=3e-5

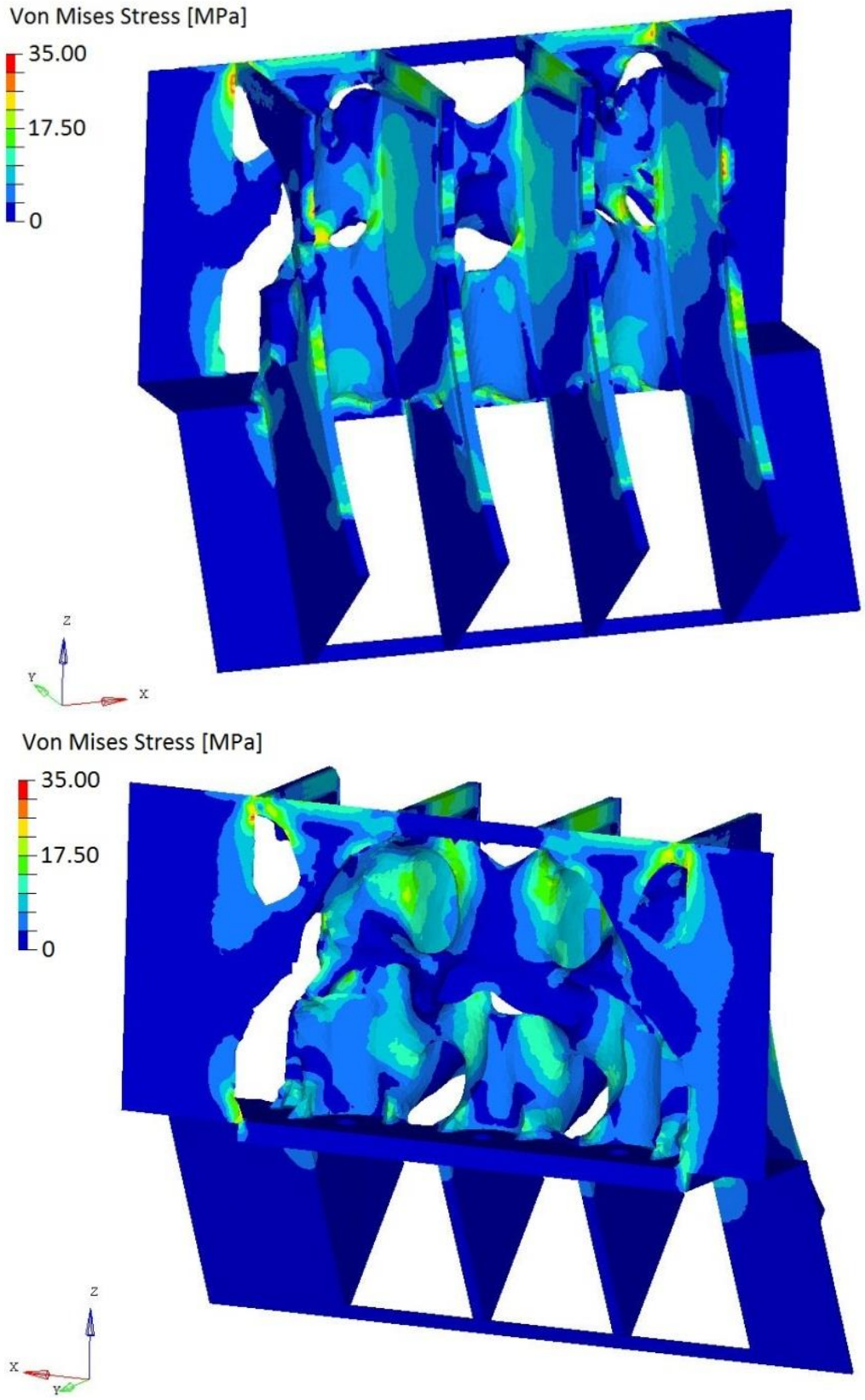

Figure 61. Static stress analysis of the new topology with simplified displacements, load case 4

Table 1. Stiffness Comparison. Optimized vs. Original Structure

	Optimized Structure				Spring rates	LC1	LC2	LC3	LC4
	LC1	LC2	LC3	LC4					
	x	x	y	z					
Disp. [Dim.less]	6,00E-04	6,00E-04	3,00E-05	3,00E-05					
Fx [KN/mm]	-7,58E+01	-9,47E+01	1,21E-10	-2,06E-10	Kx [KN/mm]	-1,26E+05	-1,58E+05	4,03E-06	-6,85E-06
Fy [KN/mm]	7,14E-12	2,31E-10	-3,45E+02	-7,35E-10	Ky [KN/mm]	1,19E-08	3,85E-07	-1,15E+07	-2,45E-05
Fz [KN/mm]	1,13E-10	-1,75E-10	4,75E-09	2,84E+02	Kz [KN/mm]	1,88E-07	-2,92E-07	1,58E-04	9,46E+06
Fmag [KN/mm]	7,58E+01	9,47E+01	3,45E+02	2,84E+02	Kekv [KN/mm]	1,26E+05	1,58E+05	1,15E+07	9,46E+06

	Original Structure				Spring rates	LC1	LC2	LC3	LC4
	LC1	LC2	LC3	LC4					
	x	x	y	z					
Disp. [Dim.less]	6,00E-04	6,00E-04	3,00E-05	3,00E-05					
Fx [KN/mm]	-2,00E+01	-1,46E+01	-1,42E-12	3,29E-12	Kx [KN/mm]	-3,34E+04	-2,43E+04	-4,72E-08	1,10E-07
Fy [KN/mm]	1,70E-03	1,09E-11	-2,23E+02	-9,88E-10	Ky [KN/mm]	2,84E+00	1,81E-08	-7,44E+06	-3,29E-05
Fz [KN/mm]	1,61E-01	-2,19E-14	4,20E-10	3,88E+02	Kz [KN/mm]	2,69E+02	-3,65E-11	1,40E-05	1,29E+07
Fmag [KN/mm]	2,00E+01	1,46E+01	2,23E+02	3,88E+02	Kekv [KN/mm]	3,34E+04	2,43E+04	7,44E+06	1,29E+07

Stiffness comparison				
	LC1	LC2	LC3	LC4
Kx	3,78	6,50	-85,44	-62,44
Ky	0,00	21,28	1,55	0,74
Kz	0,00	7987,82	11,29	0,73
Kekv	3,78	6,50	1,55	0,73
	Change in %			
Kx	278,40 %	550,02 %	-8643,90 %	-6344,48 %
Ky	0,00 %	2028,28 %	54,56 %	-25,63 %
Kz	0,00 %	798682,18 %	1029,31 %	-26,85 %
Kekv	278,40 %	550,02 %	54,56 %	-26,85 %

APPENDIX H: Example Geometry

OptiStruct solution from analysis 3

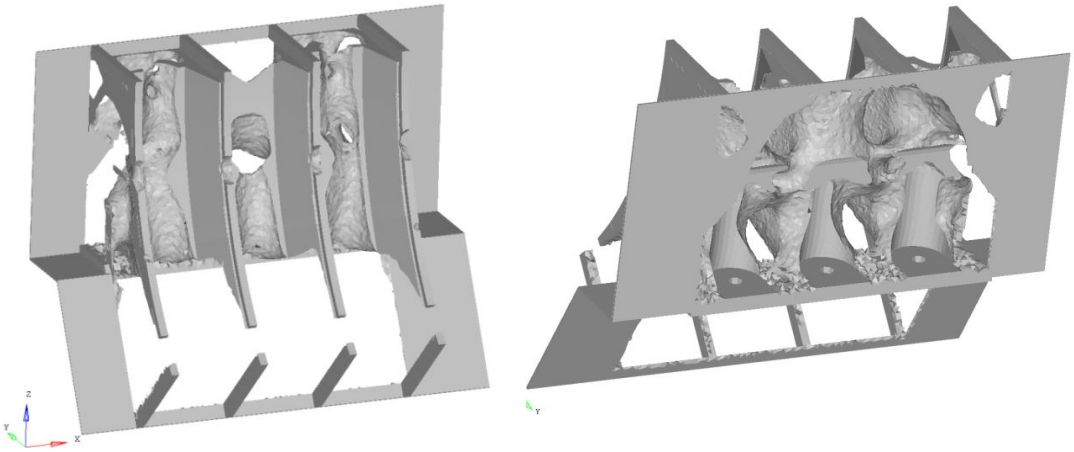

Example geometry reproduced in CAD

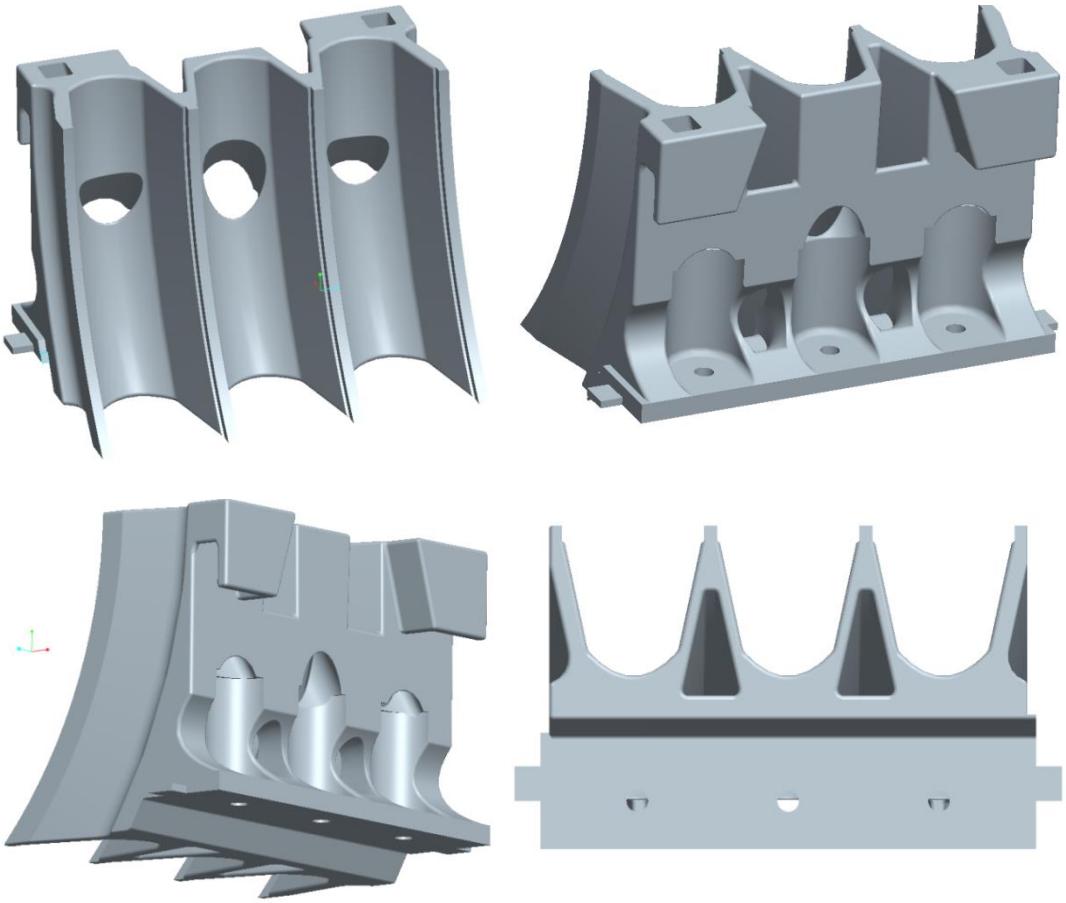

Figure 62. Example CAD-geometry based on the topology optimization result of analysis 3.